이학박사학위논문

Macroscopic Coherence in Quantum Mechanics: Quantification and Applications

양자 세계에서의 거시적 결맞음의 정량화 및 응용

2018년 2월

서울대학교 대학원
물리천문학부
권혁준

Macroscopic Coherence in Quantum Mechanics: Quantification and Applications

Hyukjoon Kwon

Supervised by

Professor **Hyunseok Jeong**

A Dissertation

Submitted to the Faculty of

Seoul National University

in Partial Fulfillment of

the Requirements for the Degree of

Doctor of Philosophy

Feb. 2018

Department of Physics and Astronomy

The Graduate School

Seoul National University

Abstract

Macroscopic Coherence in Quantum Mechanics: Quantification and Applications

Hyukjoon Kwon
Department of Physics and Astronomy
The Graduate School
Seoul National University

From the beginning of quantum mechanics, many physicists have raised the question whether the superposition principle can also be applied in the macroscopic regime. Quantum superposition between classically distinct states may occur unexpected phenomena such as Schrödinger's cat paradox, and it has attracted interests from both theoretical and experimental aspects. Recent developments in the field of quantum information science allow us to understand quantum coherence as a resource to perform nonclassical tasks, but how this quantum resource plays its role in the macroscopic regime has not been well uncovered yet. In this dissertation, we study quantification of macroscopic coherence in various physical systems based on quantum resource theory and investigate possible applications of macroscopic quantum states in both fundamental and technological aspects.

In order to quantify macroscopic coherence, the degree of coherence and physical size of the system should be considered at the same time. To this end, we suggest a weighted measure of coherence based on physical distance between quantum states. By introducing a cut-off function, the microscopic contribution of coherence can be ruled out then only coherence between macroscopically distinct states can be captured. Quantum state disturbance caused by imperfect measurements, or coarse-grained reference frames can be another way to quantify macroscopic coherence. At the same time, it can be the key to resolve why it is hard to see superposition between macroscopic objects. Both approaches fit in the resource theory of asymmetry that covariant operations cannot increase the degree of macroscopic coherence, and the connection between two different approaches is established. Using this framework, the degree of macroscopic coherence can be quantified for arbitrary physical systems, enabling us to investigate when quantum objects lose their nonclassical properties and experience a quantum-to-classical transition.

As a practical application of macroscopic coherence, we study a precise parameter estimation task, as known as quantum metrology. In particular, we focus on multi-mode optical fields in which macroscopic coherence can be captured by the negative Glauber–Sudarshan P-distribution. In this case, every pure nonclassical state can be directly utilized for multi-mode quadrature estimation tasks. Based on this observation, we develop the resource theory of nonclassicality, in which the negative P-function becomes a metrological resource that does not increase under linear optical elements.

In the fundamental point of view, we also show that hybrid entangle-

ment between particle-like (or quantum) and wave-like (or classical) states in optical fields can be used to observe the failure of local realism in quantum mechanics. Optical hybrid states which contain entanglement between polarization degree of freedom and continuous modes are shown to perform loop-hole free Bell-Clauser-Horne-Shimony-Holt inequality tests with imperfect photodetection, and their generation schemes are proposed as well.

Finally, we investigate another aspect of macroscopic coherence in many-body systems to reveal the role of coherence in quantum thermodynamics. We show that coherence can have two different roles in quantum thermodynamics. A certain type of coherence in many-body systems can be utilized to extract work deterministically while the other type of coherence can be interpreted as a clock resource. Interestingly, a trade-off relation between clock/work resources can be established in many-body quantum thermodynamics.

Keywords : Macroscopic coherence, Quantum metrology, Nonclassicality, Nonlocality, Quantum Thermodynamics

Student Number : 2012-20355

Contents

List of Figures

Chapter 1

Introduction

Quantum mechanics, originated from the wave-particle duality [1] has been one of the most successful theories describing microscopic systems, especially of the atomic scale. Based on quantum theory, we now understand the interference patterns in the double-slit experiment of single photons [2, 3] and electrons [4, 5] as the wave-like nature of particle being in *superposition* between different physical states. As quantum theory does not exclude superposition between even macroscopic objects, however, there can exist seemingly counter-intuitive situations which are well illustrated by the famous Schrödinger's cat paradox [6]. From the beginning of quantum mechanics, there have been numerous efforts to observe quantum interference of further macroscopic objects in various physical systems including atom [7–9], photon [10–15], optical cavity [16], and mechanical oscillator systems [17, 18]. In the double-slit experiment, interference of C_{60} molecules has been observed [19], and even organic molecules have been designed [20] and reported [21] to be in quantum superposition. Now many physicists believe that quantum superposition can exist between macroscopic objects, although it may take still a huge amount of time and efforts to generate a vivid superposition between literally alive and dead cat states.

Superposition in quantum mechanics can be further generalized into quantum coherence that is given by off-diagonal elements of a density ma-

trix with respect to physical states. For instance, if we describe Schrödinger's cat state as $|\Psi\rangle = |\mathrm{alive}\rangle + |\mathrm{dead}\rangle$, the off-diagonal terms $|\mathrm{alive}\rangle\langle\mathrm{dead}|$ and $|\mathrm{dead}\rangle\langle\mathrm{alive}|$ in the density matrix $\hat{\rho} = |\Psi\rangle\langle\Psi|$ refer to quantum coherence. These coherence terms definitely do not have classical counterparts that many quantum phenomena have been shown to emerge from this off-diagonal elements. In physical systems with the microscopic degree of freedom, such as single or two-qubit systems, we can characterize and quantify quantum coherence [22, 23] and correlations [24, 25], and its usefulness in quantum information processing such as quantum key distribution [26–28], computation [29–33], and communication [34–36] has been well verified. However, it is difficult to characterize the properties of coherence when the number of particles or the degree of Hilbert spaces increases, and practical applications of such coherences are not well studied yet.

A number of proposals have been made to quantify the size of a macroscopic superposition or the so-called "quantum macroscopicity" [37–54]. In 1980, Leggett who is one of the pioneers in this field defined a measure called "disconnectivity" [37] to quantify an effective size of macroscopic superposition, such as Greenberger-Horne-Zeilinger (GHZ) states based on genuine multipartite quantum correlations. Dür *et al*. [38] extended Leggett's work by investigating the effective size of the generalized GHZ states and Shimizu and Miyadera [41] suggested a measure of quantum macroscopicity based on correlations of local observables. In a different point of view, an interference-based measure [40] has been studied based on the sensitivity of quantum superposition for interferometric applications. Recently, quantum macroscopicity measures [44–46, 51] have been

suggested to quantify macroscopic quantum properties for general quantum states in an arbitrary physical system. Those measures are from different contexts, based on the phase space structures [44, 51], the quantum Fisher information [45], and the minimal extension of quantum theory [46], yet unified viewpoint has not been established. An axiomatic approach to quantum macroscopicity that uses a similar framework to that of coherence [22] has also been proposed [52], but it could be not sufficient for certain types of states [53].

Meanwhile, Leggett and Garg [55] have raised a fundamental question regarding macroscopic quantum superposition by introducing the concept of "macrorealism" to describe a classical (macroscopic) physical objects based on two postulates: *Macrorealism per se* and *Noninvasive measurability*. Leggett-Garg inequality [55] shows that quantum mechanical superposition between macroscopically distinct physical states can violate the bound given by the macrorealistic model, which is similar to the case of the violation of local hidden variable model by entangled quantum states [56]. The concept of macrorealism has been recently developed into no-signaling-in-time (NSIT) [57] in more rigorous ways.

In the previous discussion on Schrödinger's cat state, it is important to notice that macroscopic coherence between *alive* and *dead* cat should be distinguished from its statistical mixture $|\mathrm{alive}\rangle\langle\mathrm{alive}|+|\mathrm{dead}\rangle\langle\mathrm{dead}|$. Furthermore, coherence between macroscopic objects should lead to different emergent properties which should be distinguished from the accumulation of microscopic coherence [37], i.e., collecting coherences of individual electrons composing the cat would not become a superposition of alive/dead cat

states. Unfortunately, we cannot observe such Schrödinger's cat-like states in our real lives, and we also do not know much about how to characterize and utilize macroscopic quantum states generated in the laboratory. Based on this observation, it is natural to raise the following questions concerning macroscopic coherence: *1. "How can we quantify it?" 2. "Why it is hard to observe in our lives?" 3. "What can we do with it?"* This dissertation aims to study possible answers to these questions.

In Chapter 2 we review some basic concepts of coherence and introduce recent approaches of coherence and asymmetry using the framework of quantum resource theory. Adopting this concept, we study how to quantify macroscopic coherence in a consistent and physically acceptable way in Chapter 3. We suggest two different approaches of "weighted sum of coherence" and "disturbance by measurement" and verify the connection between them. This integrated viewpoint explains why it is hard to see such macroscopic coherence in the presence of thermal environment.

We introduce possible applications of macroscopic coherence in improving quantum technology and testing the foundation of physics. In Chapter 4 we illustrate how macroscopic coherence can be utilized for enhanced metrological tasks and introduce its connection to nonclassicality in multimode optical fields. We study another application of macroscopic coherence in Chapter 5, by investigating hybrid entanglement between microscopic and macroscopic (or classical) systems in optical fields. We propose a scheme to generate such hybrid entanglement and demonstrate how it can be useful to test the loop-hole free Bell inequality violation. In Chapter 6, we study the role of coherence in many-body systems which can be utilized

as work and clock resources in the thermodynamic viewpoint. Concluding remark are followed in Chapter. 7.

This dissertation is based on the following publications/preprints:

1. H. Kwon and H. Jeong, "Violation of the Bell–Clauser-Horne-Shimony-Holt inequality using imperfect photodetectors with optical hybrid states," Phys. Rev. A **88**, 052127 (2013).

2. H. Kwon and H. Jeong, "Generation of hybrid entanglement between a single-photon polarization qubit and a coherent state," Phys. Rev. A **91**, 012340 (2015).

3. H. Kwon, C.-Y. Park, K.-C. Tan, and and H. Jeong, "Disturbance-based measure of macroscopic coherence," New J. Phys. **19**, 043024 (2017).

4. H. Kwon, C.-Y Park, K.-C. Tan, D. Ahn, and H. Jeong, "Coherence, Asymmetry, and Quantum Macroscopicity", arXiv:1704.06469 (2017) (Accepted for publication in Phys. Rev. A).

5. H. Kwon, H. Jeong, D. Jennings, B. Yadin, and M. S. Kim, "Clock/work trade-off relation for coherence in quantum thermodynamics", arXiv: 1711.03395 (2017).

6. H. Jeong, M. Kang, and H. Kwon, "Characterizations and quantifications of macroscopic quantumness and its implementations using optical fields," Optics Communications **337**, 12 (2015).

7. A. Carlisle, H. Kwon, H. Jeong, A. Ferraro, and M. Paternostro, "Limitations of a measurement-assisted optomechanical route to quantum macroscopicity of superposition states," Phys. Rev. A **92**, 022123 (2015).

8. K.-C. Tan, H. Kwon, C.-Y. Park, and H. Jeong, "Unified view of quantum correlations and quantum coherence," Phys. Rev. A **94**, 022329 (2016).

9. K.-C. Tan, T. Volkoff, H. Kwon, and H. Jeong, "Quantifying the coherence between coherent states", Phys. Rev. Lett. **119**, 190405 (2017).

10. H. Kwon, K. C. Tan, T, Volkoff, and H. Jeong, "Nonclassicality of Light as a Quantifiable Resource for Quantum Metrology" (in preparation).

Chapter 2

Resource theory of quantum coherence and asymmetry

The contents of this chapter are largely based on Section II. and III. of [H. Kwon, C.-Y Park, K.-C. Tan, D. Ahn, and H. Jeong, "Coherence, Asymmetry, and Quantum Macroscopicity", arXiv:1704.06469] Ref. [58].

2.1 Introduction

In this Chapter, we study that quantum features can be quantified as a "resource" to perform nonclassical tasks. To this end, we introduce a framework of quantum resource theory which can be characterized by a set of *free states* and *free operations* for a given nonclassical task. *Free states* are the states which can be prepared without cost, thus cannot be utilized for a given nonclassical task. Then *free operations* can be defined as classical operations acting on quantum states, which maps every free state to another free state. In other words, a quantum resource cannot be generated by acting a free operation on free states. In order to quantify the amount of resources, we define *monotones* (sometimes called measures) which give zero values for *free states* and do not increase by *free operations*.

Entanglement theory [24, 25], which is the prototype of the quantum resource theory, is a good example to illustrate the structure of the theory.

Table 1: Various types of quantum resource theory

Resource theory	Incoherent operation	Incoherent state
Entanglement	LOCC	Separable state
Coherence	Incoherent operation	Incoherent state
Asymmetry	Covariant operation	Covariant state
Nonclassicality (in optics)	Linear optical map	Possitive P-function
Quantum Thermodynamics	Thermal operation	Gibbs state

In the resource theory of entanglement, free states and free operations are given by separable states and local operation and classical communications (LOCC), respectively. We can easily notice that entanglement cannot be generated from separable states and LOCC, which means that a separable state does not contain any entanglement resource. Moreover, we can quantify the degree of entanglement by measures such as the relative entropy of entanglement [59] and entanglement of formation [60], all of which do not increase by free operations, so-called entanglement monotones [24].

Recently, Baumgratz et al. [22] proposed a general framework to quantify quantum coherence with respect to a given set of preferred basis. As the essence of quantum phenomena comes from quantum superposition, or more generally quantum coherence between different physical states, it has been shown that "coherence theory" has a connection to entanglement [61, 62] and nonclassicality [33]. In this manner, one may say that "coherence" lies in the heart of quantum resource theories.

On the other hand, there are several different viewpoints to understand coherence in quantum states by which various types of quantum resource theory could be constructed based on nonclassical tasks in concern (see Ta-

ble 1 for some examples). In the remaining part of this chapter, we mainly focus on the resource theory of coherence and asymmetry with related measures. These measures can be used to quantify the degree of quantum macroscopicity in Chapter 3.

2.2 Quantifying quantum coherence

2.2.1 Incoherent states and incoherent operations

Coherence in quantum physics, in general, refers to the interference between different physical states. In the double-slit experiment, for example, each particle can be in superposition between its states passing the upper slit ($|\uparrow\rangle$) and the lower slit ($|\downarrow\rangle$) at the same time. More generally, if we take a set of orthogonal basis $\{|i\rangle\}$ we can express a quantum state in a density matrix form $\hat{\rho} = \sum_{i,j} \rho_{ij} |i\rangle \langle j|$. In this case, the off-diagonal terms ρ_{ij} with $i \neq j$ refer to coherence between different physical states $|i\rangle$ and $|j\rangle$.

Quantum coherence with respect to a given set of basis $\{|i\rangle\}$ has been recently studied in the viewpoint of resource theory [22, 23]. In the resource theory of coherence, a set of incoherent states $\mathcal{I}$ is given by quantum states which only contain diagonal terms, i.e., $\hat{\delta} = \sum_i p_i |i\rangle \langle i|$, where $p_i \geq 0$ and $\sum_i p_i = 1$. Then a set of incoherent operations $\mathcal{E}_{\mathrm{IC}}$ can be constructed by a quantum channel which maps every incoherent state to another incoherent state, i.e., $\mathcal{E}_{\mathrm{IC}}(\mathcal{I}) \subset \mathcal{I}$ [22]. More precisely, an incoherent operation can be characterized by Kraus operators as $\mathcal{E}_{\mathrm{IC}}(\hat{\rho}) = \sum_n \hat{K}_n \hat{\rho} \hat{K}_n^\dagger$, where $\hat{K}_n \mathcal{I} \hat{K}_n^\dagger \subseteq \mathcal{I}$ and $\sum_n \hat{K}_n^\dagger \hat{K}_n = \mathbb{1}$.

2.2.2 Measures of coherence

In order to quantify the amount of coherence in quantum states, we need a faithful measure of coherence, so-called a *coherence monotone*. The followings are the conditions that coherence monotone $\mathcal{C}(\hat{\rho})$ should satisfy [22].

(C1) $\mathcal{C}(\hat{\delta}) \geq 0$ and $\mathcal{C}(\hat{\delta}) = 0$ if and only if $\hat{\delta} \in \mathcal{I}$.

(C2a) (Weak monotonicity) $\mathcal{C}(\hat{\rho}) \geq \mathcal{C}(\mathcal{E}_{\mathrm{IC}}(\hat{\rho}))$ under a trace-preserving incoherent operation $\mathcal{E}$.

(C2b) (Strong monotonicity) $\mathcal{C}(\hat{\rho}) \geq \sum_n p_n \mathcal{C}(\hat{K}_n \hat{\rho} \hat{K}_n^\dagger / p_n)$, where $p_n = \mathrm{Tr}\hat{K}_n^\dagger \hat{\rho} \hat{K}$.

(C3) (Convexity) $\sum_i p_i \mathcal{C}(\hat{\rho}_i) \geq \mathcal{C}(\sum_i p_i \hat{\rho}_i)$.

(C1) condition verifies that a quantum state has coherence if and only if it is not in the diagonal form with respect to a given set of basis $\{|i\rangle\}$. (C2a) and (C2b) conditions show that the amount of coherence cannot be increased by trace preserving incoherent operations and selective incoherent operations on average, respectively. (C3) convexity guarantees that classical (statistical) mixing of quantum states does not increase the degree of coherence. Note that (C2b) is stronger condition since (C2b) together with (C3) leads to the weak monotonicity condition (C2a) [22].

Here, we introduce some examples of coherence monotones. First of all, we can add every off-diagonal element with respect to a given basis

$\{|i\rangle\}$. By doing this, we obtain the l_1-norm of coherence

$$\mathcal{C}_{l_1}(\hat{\rho}) = ||\hat{\rho} - \hat{\rho}_{\text{diag}}||_{l_1} = \sum_{i \neq j} |\rho_{ij}|,$$

where $\rho_{ij} = \langle i|\hat{\rho}\,|j\rangle$. The l_1-norm of coherence has been proven to be a coherence monotone satisfying all the conditions (C1)–(C3) [22]. Similarly, the l_2-norm of coherence may be defined as $\mathcal{C}_{l_2}(\hat{\rho}) = \sum_{i \neq j} |\rho_{ij}|^2$. However, this measure is not a valid coherence monotone since it does not satisfy (C2b) [22].

Another good way to quantify quantum coherence is using a distance function between quantum states, so-called a geometric measure of coherence. This type of coherence measures quantifies how far a state is apart from its closest incoherent state. Based on this concept, the relative entropy of coherence

$$\mathcal{C}_R(\hat{\rho}) := \min_{\hat{\delta} \in \mathcal{I}} S(\hat{\rho}||\hat{\delta}) = S(\hat{\rho}_{\text{diag}}) - S(\hat{\rho})$$

can be defined [22], where $\hat{\rho}_{\text{diag}} = \sum_i \rho_{ii}\,|i\rangle\,\langle i|$ and $S(\hat{\rho}||\hat{\tau}) = \text{Tr}(\hat{\rho}\log\hat{\rho} - \hat{\rho}\log\tau)$ is the quantum relative entropy. On the other hand, some of the geometric measures of coherence based on the Bures distance and the Hilbert-Schmidt norm have been found not to satisfy condition (C2b) [63]. Recently, another geometric measure

$$\mathcal{C}_F(\hat{\rho}) := 1 - \max_{\hat{\delta} \in \mathcal{I}} F(\hat{\rho}, \hat{\delta})$$

has been studied by observing the connection between entanglement and

coherence [64]. This measure has been proven to satisfy (C1)-(C3) [64], where $F(\hat{\rho},\hat{\tau}) = [\mathrm{Tr}\sqrt{\sqrt{\hat{\rho}}\hat{\tau}\sqrt{\hat{\rho}}}]^2$ is the fidelity between two quantum states $\hat{\rho}$ and $\hat{\tau}$.

In this dissertation, we introduce a new coherence measure based on the quantum affinity $A^2(\hat{\rho},\hat{\tau}) := [\mathrm{Tr}\sqrt{\hat{\rho}}\sqrt{\hat{\tau}}]^2$. It has been noticed that the quantum affinity and fidelity share similar information-theoretical properties [65]. Based on this observation, we define the affinity based measure of quantum coherence

$$\mathcal{C}_A(\hat{\rho}) = 1 - \max_{\hat{\delta}\in\mathcal{I}} A^2(\hat{\rho},\hat{\delta}). \tag{2.1}$$

Alternatively, we can express this measures in the following forms

$$\mathcal{C}_A(\hat{\rho}) = \sum_{i\neq j} |(\sqrt{\hat{\rho}})_{ij}|^2 = 1 - \sum_i (\sqrt{\hat{\rho}})^2_{ii}. \tag{2.2}$$

This can be shown as follows: Suppose that a incoherent state is given by $\hat{\delta} = \sum_i p_i |i\rangle\langle i|$. Then $A(\hat{\rho},\hat{\delta}) = \sum_i \sqrt{p_i}(\sqrt{\hat{\rho}})_{ii} \leq \sqrt{\sum_i p_i}\sqrt{\sum_i (\sqrt{\hat{\rho}})^2_{ii}} = \sqrt{\sum_i (\sqrt{\hat{\rho}})^2_{ii}}$ by the Cauchy-Schwartz inequality. The inequality is saturated when $p_i = (\sqrt{\hat{\rho}})^2_{ii}/\sum_i (\sqrt{\hat{\rho}})^2_{ii}$. Thus we have $\max_{\hat{\delta}\in\mathcal{I}} A(\hat{\rho},\hat{\delta})^2 = \sum_i (\sqrt{\hat{\rho}})^2_{ii} = 1 - \mathcal{C}_A(\hat{\rho})$.

These equivalent expressions show that measure $\mathcal{C}_A$ captures both properties from interference-based measures and geometric measures of coherence. An interesting remark is that even though the l_2-norm of coherence for $\hat{\rho}$ does not satisfy condition (C2b), the same measure for $\sqrt{\hat{\rho}}$ obeys all the condition (C1)–(C3). We also note that measure $\mathcal{C}_A$ is bounded between

0 and 1. The measure can be efficiently computable since the coherence of a quantum state in any given basis can be obtained by computing the diagonal elements of $\sqrt{\hat{\rho}}$. Finally, we verify that $\mathcal{C}_A$ is a proper measure of quantum coherence.

Theorem 1 (Affinity-based measure of coherence)**.** *With respect to a basis set* $\{|i\rangle\}$*,* $\mathcal{C}_A(\hat{\rho}) = 1 - \max_{\hat{\delta}\in\mathcal{I}} A^2(\hat{\rho}, \hat{\delta}) = \sum_{i\neq j} |(\sqrt{\hat{\rho}})_{ij}|^2$ *is a coherence monotone satisfying conditions (C1) – (C3).*

Proof: (C1) can be easily shown that $\mathcal{C}(\hat{\rho}) = 0$ *if and only if* $\hat{\rho}$ only contains diagonal terms. Note that $A(\hat{\rho}, \hat{\tau}) = 1$ *if and only if* $\hat{\rho} = \hat{\tau}$. (C2a) can be proven by using the property $A(\hat{\rho}, \hat{\tau}) \leq A(\mathcal{E}(\hat{\rho}), \mathcal{E}(\hat{\tau}))$ for any trace-preserving map $\mathcal{E}$. We then have $\mathcal{C}_A(\hat{\rho}) = 1 - A(\hat{\rho}, \hat{\delta}^*)^2 \geq 1 - A(\mathcal{E}_{\rm IC}(\hat{\rho}), \mathcal{E}_{\rm IC}(\hat{\delta}^*))^2 \geq 1 - \max_{\hat{\delta}\in\mathcal{I}} A(\mathcal{E}_{\rm IC}(\hat{\rho}), \hat{\delta})^2 = \mathcal{C}_A(\mathcal{E}_{\rm IC}(\hat{\rho}))$, where $\hat{\delta}^*$ maximizes $A(\hat{\rho}, \hat{\delta})$ for $\hat{\delta} \in \mathcal{I}$. (C2b) can be proven by showing $\sum_n p_n \mathcal{C}_A(\hat{K}_n \hat{\rho} \hat{K}_n^\dagger / p_n) \leq \mathcal{C}_A(\hat{\rho})$, for incoherent operator set $\{\hat{K}_n\}$. We first show that $A(\hat{\rho}, \hat{\tau}) \leq \sum_n A(\hat{K}_n \hat{\rho} \hat{K}_n^\dagger, \hat{K}_n \hat{\tau} \hat{K}_n^\dagger)$ for Kraus operators with $\sum_n \hat{K}_n^\dagger \hat{K}_n = \mathbb{1}$. A set of Kraus operators $\{\hat{K}\}$ can be expressed using ancillary state $\hat{\tau}_2$: $\hat{K}_n \hat{\rho} \hat{K}_n^\dagger = \mathrm{Tr}_2(\mathbb{1} \otimes \hat{\Pi}_n)\hat{U}(\hat{\rho} \otimes \hat{\tau}_2)\hat{U}^\dagger(\mathbb{1} \otimes \hat{\Pi}_n)$. Note that $A(\hat{\rho}, \hat{\sigma})$ is non-increasing under partial trace $A(\hat{\rho}_{12}, \hat{\sigma}_{12}) \leq A(\mathrm{Tr}_2\hat{\rho}_{12}, \mathrm{Tr}_2\hat{\sigma}_{12})$ and satisfies following properties for a set of projection operators $\{\hat{\Pi}_n\}$: $\sum_n A(\hat{\Pi}_n \hat{\rho} \hat{\Pi}_n, \hat{\Pi}_n \hat{\sigma} \hat{\Pi}_n) = A(\sum_n \hat{\Pi}_n \hat{\rho} \hat{\Pi}_n, \sum_n \hat{\Pi}_n \hat{\sigma} \hat{\Pi}_n)$.

Using these properties, we can show that

$$
\begin{aligned}
&\sum_n A(\hat{K}_n\hat{\rho}\hat{K}_n^\dagger, \hat{K}_n\hat{\sigma}\hat{K}_n^\dagger) \\
&= \sum_n A(\mathrm{Tr}_2(\mathbb{1}\otimes\hat{\Pi}_n)\hat{U}(\hat{\rho}\otimes\hat{\tau}_2)\hat{U}^\dagger(\mathbb{1}\otimes\hat{\Pi}_n), \mathrm{Tr}_2(\mathbb{1}\otimes\hat{\Pi}_n)\hat{U}(\hat{\sigma}\otimes\hat{\tau}_2)\hat{U}^\dagger(\mathbb{1}\otimes\hat{\Pi}_n)) \\
&\geq \sum_n A((\mathbb{1}\otimes\hat{\Pi}_n)\hat{U}(\hat{\rho}\otimes\hat{\tau}_2)\hat{U}^\dagger(\mathbb{1}\otimes\hat{\Pi}_n), (\mathbb{1}\otimes\hat{\Pi}_n)\hat{U}(\hat{\sigma}\otimes\hat{\tau}_2)\hat{U}^\dagger(\mathbb{1}\otimes\hat{\Pi}_n)) \\
&= A(\sum_n(\mathbb{1}\otimes\hat{\Pi}_n)\hat{U}(\hat{\rho}\otimes\hat{\tau}_2)\hat{U}^\dagger(\mathbb{1}\otimes\hat{\Pi}_n), \sum_n(\mathbb{1}\otimes\hat{\Pi}_n)\hat{U}(\hat{\sigma}\otimes\hat{\tau}_2)\hat{U}^\dagger(\mathbb{1}\otimes\hat{\Pi}_n)) \\
&\geq A(\hat{U}(\hat{\rho}\otimes\hat{\tau}_2)\hat{U}^\dagger, \hat{U}(\hat{\sigma}\otimes\hat{\tau}_2)\hat{U}^\dagger) \\
&= A(\hat{\rho}\otimes\hat{\tau}_2, \hat{\sigma}\otimes\hat{\tau}_2) \\
&= A(\hat{\rho},\hat{\sigma})A(\hat{\tau}_2,\hat{\tau}_2) \\
&= A(\hat{\rho},\hat{\sigma}).
\end{aligned}
\tag{2.3}
$$

We then have

$$
\begin{aligned}
\sum_n p_n \mathcal{C}_A(\hat{K}_n\hat{\rho}\hat{K}_n^\dagger/p_n) &= 1 - \sum_n p_n \max_{\hat{\delta}_n\in\mathcal{I}} A(\hat{K}_n\hat{\rho}\hat{K}_n^\dagger/p_n, \hat{\delta}_n)^2 \\
&\leq 1 - \sum_n A(\hat{K}_n\hat{\rho}\hat{K}_n^\dagger, \hat{K}_n\hat{\delta}^*\hat{K}_n^\dagger/q_n)^2 \\
&= 1 - \sum_n \frac{1}{q_n} A(\hat{K}_n\hat{\rho}\hat{K}_n^\dagger, \hat{K}_n\hat{\delta}^*\hat{K}_n^\dagger)^2 \\
&\leq 1 - \left[\sum_n A(\hat{K}_n\hat{\rho}\hat{K}_n^\dagger, \hat{K}_n\hat{\delta}^*\hat{K}_n^\dagger)\right]^2 \\
&\leq 1 - A(\hat{\rho},\hat{\delta}^*)^2 \\
&= \mathcal{C}_A(\hat{\rho}),
\end{aligned}
\tag{2.4}
$$

where $q_n = \mathrm{Tr}\hat{K}_n\hat{\delta}^*\hat{K}_n^\dagger$ and $\hat{\delta}^*$ gives the maximum value of $A(\hat{\rho},\hat{\delta})$ for $\hat{\delta}\in$

$\mathcal{I}$. Finally, (C3) can be proven by noticing that $\mathcal{C}_A(\hat{\rho}) = 1 - \sum_i (\sqrt{\hat{\rho}})_{ii}^2 = 1 - \sum_i \mathrm{Tr}\sqrt{\hat{\rho}}\hat{P}_i\sqrt{\hat{\rho}}\hat{P}_i$, where $\hat{P}_i = |i\rangle\langle i|$. According to Lieb's concavity theorem [66], $\mathrm{Tr}\sqrt{\hat{\rho}}\hat{P}_i\sqrt{\hat{\rho}}\hat{P}_i$ is concave in $\hat{\rho}$ for every i, which makes $\mathcal{C}_A(\hat{\rho})$ convex. □

2.3 Quantum coherence and asymmetry

In the resource theory of quantum coherence, a set of reference basis $\{|i\rangle\}$ does not have any restriction, and the degree of coherence can vary on this choice of basis. In order to construct a physically meaningful set of incoherent states, we can use one of the most fundamental concepts in physics, conservation laws. We call a physical system has a *symmetry* when its Lagrangian is invariant under a group operation, and then there exists a conserved quantity. For example, if the system has time-translation symmetry, then its energy becomes a conserved quantity. However, in quantum theory, different energy-eigenstates can be superposed then this kind of quantum states contains broken symmetry, which we call *asymmetry*. Independently from the resource theory of coherence, various studies have been done to quantify quantum coherence in the context of asymmetry [67–70] and to discover its applications including reference frame alignment [71], quantum metrology [72, 73], and quantum speed limits [74]. In this section, we study a general structure of asymmetry and how they are related to the resource theory of coherence.

2.3.1 Asymmetry and reference frame

The resource theory of asymmetry allows us to quantify the degree of symmetry breaking of a quantum state under a given group transformation [69, 70, 75]. Here, we consider a unitary group transformation in quantum mechanics acting on a quantum state $\hat{\rho}$

$$\mathcal{U}_x(\hat{\rho}) = \hat{U}_x \hat{\rho} \hat{U}_x^\dagger = e^{-ix\hat{L}} \hat{\rho} e^{ix\hat{L}}, \tag{2.5}$$

which is generated by a given observable $\hat{L}$ with real values of x. We can express the generator as $\hat{L} = \sum_i \lambda_i |i\rangle \langle i|$ using the eigen-decomposition, where λ_i assigns some physical quantities to the specific eigenstates $|i\rangle$. For example, when we choose $\hat{L}$ to be a Hamiltonian of the system, λ_i refers to an energy-eigenvalue, and the related group operation becomes a time translation. From the resource theoretical point of view, we can specify free states and free operations respect to this group translations $\hat{U}_x$. The free states can be defined as a state which does not change by any given group transformation generated by $\hat{L}$, i.e., $\mathcal{U}_x(\hat{\rho}) = \hat{\rho}$ for all x, so-called the translationally-covariant states. Then we define translationally-covariant operations as free operations, which satisfies

$$\mathcal{U}_x \circ \mathcal{E} = \mathcal{E} \circ \mathcal{U}_x$$

for every value of x [70, 75]. The measure of asymmetry $\mathcal{A}(\hat{\rho})$ can be defined to satisfy $\mathcal{A}(\hat{\rho}) = 0$ for translationally-covariant states and not to increase under translationally-covariant operations [67]. Some measures of

asymmetry including information-based measures [70, 75–77], the robustness of asymmetry [76], and the asymmetry-weight [77] have been studied. We introduce an interference-based measure of asymmetry, based on the discussion in the previous section.

Theorem 2 (Interference-based measure of asymmetry)**.** *For a given observable* $\hat{L} = \sum_i \lambda_i |i\rangle \langle i|$*,*

$$\mathcal{A}_A(\hat{\rho}) = \sum_{\lambda_i \neq \lambda_j} |(\sqrt{\hat{\rho}})_{ij}|^2 \tag{2.6}$$

is an asymmetry monotone with respect to $\hat{L}$*.*

Proof: For non-degenerate case (i.e. $\lambda_i \neq \lambda_j$ if and only if $i \neq j$), the proof is the same with Theorem 1. In the case of degeneracy, we write a free state $\hat{\sigma} = \sum_n p_n \hat{\sigma}_n = \sum_n p_n \sum_\lambda \lambda(n) |n, \lambda\rangle \langle n, \lambda|$, where each $\hat{\sigma}_n$ is translationally-covariant state and $\sum_\lambda \lambda(n) |n, \lambda\rangle \langle n, \lambda|$ is its eigndecomposition. Then we can follow the proof of Theorem. 1 if we can always choose a set of bases $\{|n, \lambda\rangle\}$ which gives

$$\mathcal{A}_A(\hat{\rho}) = 1 - \max_{\{p_n, \lambda(n), |n,\lambda\rangle\}} A^2(\hat{\rho}, \hat{\sigma}) = \sum_{\lambda_i \neq \lambda_j} |(\sqrt{\hat{\rho}})_{ij}|^2.$$

Now consider a projection $\hat{P}_n$ onto the states with $\lambda_i = n$. Using this projection, we can block-diagonalize $\sqrt{\hat{\rho}}$ and we can take eigendecomposition of each block $\hat{P}_n(\sqrt{\hat{\rho}})\hat{P}_n$ in order to obtain the desired free state. □

This measure quantifies the interference between the different eigenstates of $\hat{L}$, while excluding the contributions of the interference between

eigenstates with the same eigenvalues. Note that if an observable $\hat{L}$ has non-degenerate eigenvalues, the interference-based measure of asymmetry $\mathcal{A}_A$ coincides with the Affinity-based measure of coherence $\mathcal{C}_A$ with respect to the eigenbasis of the observable $\hat{L}$.

2.3.2 Modes of asymmetry

The asymmetry of quantum states could be further decomposed into individual modes of asymmetry [69]. We first note that every quantum state can be expressed in terms of the eigenbasis of $\hat{L} = \sum_i \lambda_i |i\rangle \langle i|$, and can be further decomposed into different modes of the eigenvalue spacing $\omega = \lambda_i - \lambda_j$.

$$\hat{\rho} = \sum_{i,j} \rho_{ij} |i\rangle \langle j| = \sum_{\omega \in \Omega} \hat{\rho}^{(\omega)}, \tag{2.7}$$

where $\hat{\rho}^{(\omega)} = \sum_{\lambda_i - \lambda_j = \omega} \rho_{ij} |i\rangle \langle j|$ and Ω is a set composed of every possible spacing between the eigenvalues (i.e. $\omega = \lambda_i - \lambda_j$) of the observable $\hat{L}$. This mode decomposition is useful to identify translationally-covariant states as an equivalent expression of $\hat{\rho} = \hat{\rho}^{(0)}$, for which coherence between the eigenstates of different eigenvalues do not exist [52, 69, 70]. We can also have an alternative expression of translationally-covariant operations as follows:

Proposition 1 (Covariant operations for modes of asymmetry)**.** *A quantum operation $\mathcal{E}$ is a translationally-covariant operation if and only if $\mathcal{E}$ satisfies $\mathcal{E}(\hat{\rho}^{(\omega)}) = \mathcal{E}(\hat{\rho})^{(\omega)}$ for every mode ω.*

Proof: We observe that $\mathcal{U}_x(\hat{\rho}) = e^{-i\hat{L}x}\hat{\rho}e^{i\hat{L}x} = \sum_{\omega\in\Omega} e^{-i\omega x}\hat{\rho}^{(\omega)}$ by taking eigenbases of the observable $\hat{L}$. Then we have

$$(\mathcal{E}\circ\mathcal{U}_x)(\hat{\rho}) = \mathcal{E}\left(\sum_{\omega\in\Omega} e^{-i\omega x}\hat{\rho}^{(\omega)}\right) = \sum_{\omega\in\Omega} e^{-i\omega x}\mathcal{E}\left(\hat{\rho}^{(\omega)}\right).$$

On the other hand, we have $(\mathcal{U}_x\circ\mathcal{E})(\hat{\rho}) = \sum_{\omega\in\Omega} e^{-i\omega x}\mathcal{E}(\hat{\rho})^{(\omega)}$. Two expressions are equal for translations $\mathcal{U}_x$ for all x if and only if $\mathcal{E}(\hat{\rho}^{(\omega)}) = \mathcal{E}(\hat{\rho})^{(\omega)}$ which completes the proof. □

Using modes of asymmetry, the degree of coherence stored within each mode ω can be individually quantified [69, 70]. The measure is given by

$$\mathcal{A}_{\rm tr}^{(\omega)}(\hat{\rho}) = \|\hat{\rho}^{(\omega)}\|_{\rm tr}, \tag{2.8}$$

where $\|\hat{X}\|_{\rm tr} = {\rm Tr}\sqrt{\hat{X}^\dagger\hat{X}}$ is the trace norm. Note that $\|\hat{\rho}^{(\omega)}\|_{\rm tr}$ is non-increasing under covariant operations for every ω [69]. Furthermore, it can be shown that any linear function of the modes forms a measure of asymmetry, i.e. $\left\|\sum_{\omega\in\Omega} c(\omega)\hat{\rho}^{(\omega)}\right\|_{\rm tr}$ is a measure of asymmetry for any complex function $c(\omega)$ [70].

We take similar approach using the previously suggested interference-based measure, by introducing a different type of mode decomposition and a measure based on a different norm, given by follows:

$$\mathcal{A}_{\rm HS}^{(\omega)}(\hat{\rho}) = \sum_{\lambda_i-\lambda_j=\omega} |(\sqrt{\hat{\rho}})_{ij}|^2 = \|\sqrt{\hat{\rho}}^{(\omega)}\|_{\rm HS}^2, \tag{2.9}$$

where $\|\hat{X}\|_{\rm HS} = [{\rm Tr}\hat{X}^\dagger\hat{X}]^{1/2}$ is the Hilbert-Schmidt norm.

For both measures $\mathcal{A}_{\rm tr}^{(\omega)}$ and $\mathcal{A}_{\rm HS}^{(\omega)}$, we observe that the total degree of asymmetry is given by the sum over ω with $\omega \neq 0$, i.e.

$$\mathcal{A}(\hat{\rho}) = \sum_{\omega \in \Omega - \{0\}} \mathcal{A}^{(\omega)}(\hat{\rho}), \tag{2.10}$$

which is non-increasing by covariant operations. In this case, we define each mode of coherence $A^{(\omega)}(\hat{\rho})$ as ω-coherence.

Unlike the measure based on the trace norm $\mathcal{A}_{\rm tr}$, however, some modes of $\mathcal{A}_{\rm HS}^{(\omega)}(\hat{\rho})$ can increase by covariant operations. We give an example of the case of increasing $\mathcal{A}_{\rm HS}^{(\omega)}(\hat{\rho})$ by a covariant operation. Consider quantum state $|\psi\rangle = (|0\rangle + |1\rangle + |2\rangle)/\sqrt{3}$ which can be express in the form of a density matrix,

$$\hat{\rho} = \frac{1}{3}\begin{pmatrix} 1 & 1 & 1 \\ 1 & 1 & 1 \\ 1 & 1 & 1 \end{pmatrix}. \tag{2.11}$$

Then we consider a partially-decohering map on $\omega = \pm 1$, which a is translationally-covariant operation. Under the operation, the state $\hat{\rho}$ evolves into

$$\Phi(\hat{\rho}) = \frac{1}{3}\begin{pmatrix} 1 & 0 & 1 \\ 0 & 1 & 0 \\ 1 & 0 & 1 \end{pmatrix}. \tag{2.12}$$

In this case, we can calculate each mode of coherences $\mathcal{A}_{\rm HS}^{(\omega)}$ for $\hat{\rho}$ and $\Phi(\hat{\rho})$, $\mathcal{A}_{\rm HS}^{(\pm 1)}(\hat{\rho}) = 2/9$ and $\mathcal{A}_{\rm HS}^{(\pm 1)}(\Phi(\hat{\rho})) = 0$, while $\mathcal{A}_{\rm HS}^{(\pm 2)}(\hat{\rho}) = 1/9$ and $\mathcal{A}_{\rm HS}^{(\pm 2)}(\Phi(\hat{\rho})) = 1/6$. Thus, for $\omega = 2$ we note that some modes of coherence

are increased by a translationally-covariant operation. Meanwhile, the total asymmetry does not increase under the partial decohering map: $\mathcal{A}_A(\rho) = \sum_{\omega\in\{\pm1\pm2\}} \mathcal{A}_{\mathrm{HS}}^{(\omega)}(\hat{\rho}) = 2/3$, while $\mathcal{A}_A(\Phi(\hat{\rho})) = \sum_{\omega\in\{\pm1\pm2\}} \mathcal{A}_{\mathrm{HS}}^{(\omega)}(\Phi(\hat{\rho})) = 1/3$.

2.4 Remarks

Until now, we have studied coherence and asymmetry in the viewpoint of quantum resource theory. Based on the concepts of *free states* and *free operations*, quantum coherence can be characterized as the amount of nonclassical resources contained in quantum states. Furthermore, we illustrate that asymmetry of quantum states can be considered as a resource for reference frame alignment task. These quantum resources can be quantified by a measure based on the quantum affinity with respect to the basis $\{|i\rangle\}$ an observable $\hat{L} = \sum_i \lambda_i |i\rangle\langle i|$. Moreover, we show that asymmetry of quantum states can be decomposed into modes given through the eigenvalue spacings $\omega = \lambda_i - \lambda_j$.

In the following Chapter 3, we discuss quantum macroscopicity by extending the resource theory of asymmetry and see that modes of asymmetry play an important role to quantify macroscopic coherence. Meanwhile, there are other types of resource theories based on different nonclassical tasks, as mentioned in the introduction of this chapter (Table. 1). In this dissertation, we additionally study two different types of resource theories, where both are connected to coherence and asymmetry. In Chapter 4, we introduce the resource theory of nonclassicality in optical fields which can be considered

as the extension of coherence theory to the continuous variable regimes. In Chapter 6, we show that a certain type of coherence in quantum thermodynamics is given by asymmetry with respect to energy eigenvalues of the system Hamiltonian when possible thermal operations are given by energy-preserving unitaries on a system coupled with a bath.

Chapter 3

Quantifying macroscopic coherence

The contents of this chapter are largely based on Section IV. and V. of [H. Kwon, C.-Y Park, K.-C. Tan, D. Ahn, and H Jeong, "Coherence, Asymmetry, and Quantum Macroscopicity", arXiv:1704.06469 (2017)] Ref. [58] and [H. Kwon, C.-Y. Park, K.-C. Tan, and H. Jeong, "Disturbance-based measure of macroscopic coherence," New J. Phys. **19**, 043024 (2017)] Ref. [53].

3.1 Introduction

Quantum theory is one of the most successful theories in physics. Base on the superposition principle, the theory describes properties of microscopic systems, such as atoms and electrons with extremely high precision. As illustrated in Schrödinger's cat paradox [6], however, the quantum theory could lead to some counter-intuitive situations since the theory does not exclude quantum superposition between objects in the macroscopic regime. From the beginning of quantum mechanics, many physicists questioned whether macroscopic superposition could exist, how would it look like, and why we cannot observe such macroscopic superposition in real lives.

Experimental efforts in various physical systems show that it is possible to superpose ever larger quantum systems [7–10, 16, 19], although it seems to have a long way to go to superpose "macroscopic" objects such

as alive/dead cats. In theory, on the other hand, it is an interesting issue to characterize macroscopic superposition and quantify the degree of macroscopic coherence with a generalized framework [37–52]. The main obstacle in this topic is that different physical systems have different properties, which makes difficult to construct a unified view of macroscopic quantum phenomena.

In this chapter, we study how to quantify quantum macroscopicity or macroscopic coherence in the viewpoint of coherence and asymmetry. We show that quantum macroscopicity could be quantified by taking account of (size of the system) and (degree of coherence) at the same time. Also, a scale parameter is introduced in order to exclude the accumulation of microscopic coherences, and then macroscopic coherence can be efficiently quantified. In another point of view, we take a different approach to quantify macroscopic coherence by measuring the disturbance of quantum states via coarse-grained measurements. This approach provides an operational meaning of macroscopic coherence, based on the relationship between the measurement precision and disturbance of the quantum state. Examples in N-particle spin systems and Bosonic systems are investigated to demonstrate the validity of these two approaches. We also establish the connection between two approaches and relate them to decoherence model which explains why a superposition between macroscopic objects cannot be observed in our real lives.

3.2 Properties of macroscopic quantum coherence

We first review some preliminary concepts regarding macroscopic quantum coherence. Let us consider a measurement observable described by a Hermitian operator $\hat{L} = \sum_i \lambda_i |i\rangle \langle i|$. The eigenstates of the observable $\hat{L}$ define a natural orthonormal basis $\{|i\rangle\}$, which can be used to quantify the amount of coherence in the system. Previous measures of quantum coherence [22, 64] quantify the degree of coherence contained in the quantum state with respect to the given basis $\{|i\rangle\}$. However, these measures give the same value for every superposition in the form of $|i\rangle + |j\rangle$, without any regard for physical measurement outcomes represented by components $|i\rangle$ and $|j\rangle$, which are λ_i and λ_j respectively. In other words, they did not consider how correctly $|i\rangle$ and $|j\rangle$ are discriminated by an actual measurement. In an attempt to quantify macroscopic quantum coherence, however, we should give some consideration to the outcomes of a physical measurement.

Recently, Yadin and Vedral [52] proposed a set of conditions that should be satisfied by a proper measure of macroscopic coherence. In their proposed resource theory of macroscopic coherence, the free operation $\mathcal{E}$ is characterized as completely positive trace-nonincreasing operations satisfying the condition $\mathcal{E}(\hat{\rho}^{(\omega)}) = \mathcal{E}(\hat{\rho})^{(\omega)}$, where $\hat{\rho}^{(\omega)} = \sum_{\lambda_i - \lambda_j = \omega} \rho_{ij} |i\rangle \langle j|$. Under such free operations, coherence terms $|i\rangle \langle j|$ with different modes $\omega = \lambda_i - \lambda_j$ cannot be mixed together, by which a physical distance of superposition $|\omega|$ cannot be increased freely, i.e. a transition from $|0\rangle + |1\rangle$ to $|0\rangle + |N\rangle$ is prohibited when $\lambda_1 \neq \lambda_N$. This type of free operations

has been previously studied in the context of asymmetry in a quantum state [67, 69, 75]. With respect to this set of free operations, the authors of [52] proposed that any reasonable measure of macroscopic quantum coherence $M(\hat{\rho})$ based on the resource theory should satisfy the following conditions:

(M1) $M(\hat{\rho}) \geq 0$ and $M(\hat{\rho}) = 0$ *if and only if* $\hat{\rho} = \hat{\rho}^{(0)}$.

(M2a) Non-increasing under any trace-preserving free operation, $M(\mathcal{E}(\hat{\rho})) \leq M(\hat{\rho})$.

(M2b) Non-increasing under any selective free operation, $\sum_\alpha p_\alpha M(\mathcal{E}_\alpha(\hat{\rho})/p_\alpha) \leq M(\hat{\rho})$ for $\mathcal{E} = \sum_\alpha \mathcal{E}_\alpha$, where $p_\alpha = \mathrm{Tr}\mathcal{E}_a(\hat{\rho})$.

(M3) Convexity, $M(\sum_i p_i \hat{\rho}_i) \leq \sum_i p_i M(\hat{\rho}_i)$.

(M4) $M(|i\rangle + |j\rangle) > M(|k\rangle + |l\rangle)$ if $|\lambda_i - \lambda_j| > |\lambda_k - \lambda_l|$.

Here, (M1) identifies free states which do not contain any macroscopic quantum coherence. (M2a) and (M2b) are required in a sense that one cannot increase macroscopic quantum coherence freely (i.e. by free operations), and often called weak and strong monotonicity conditions, respectively. The condition (M3) guarantees that macroscopic quantum coherence does not increase by mixing quantum states. Finally, condition (M4) is to quantify the macroscopic size of a superposition based on the distance between component states in terms of the difference between corresponding eigenvalues. This additional condition (M4) restricts the set of asymmetry monotones into a set of measures that discriminate macroscopic and microscopic superpositions. In this sense, the resource theory of [52] may be understood

as a type of an asymmetry (M1-M3) in addition to a size factor (M4). Yadin and Vedral [52] pointed out that among two general measures of quantum macroscopicity, one for bosonic systems [44] and the other for spin system [45], only the latter [45] based on the quantum Fisher information satisfies all the conditions (M1)–(M4). Known examples of measures that satisfy all these conditions are the quantum Fisher information and the Wigner-Yanase-Dyson skew information [52].

3.3 Asymmetry and macroscopic coherence

3.3.1 Macroscopic observables and covariant operations

A macroscopic physical system involves a large number of particles or modes. In order to quantify quantumness in a macroscopic system, it is natural to consider an observable, often called a *macroscopic observable* [78], representing some collective physical quantity of a composite system, such as a total Hamiltonian, angular momentum (or spin), and position/momentum. The choice of an appropriate observable depends on the character of the system and the physics in which we are interested.

We note that many of *macroscopic observables* are generators of the (collective) group transformations in the macroscopic system. For N-partite system, generators of this types of group transformations can be expressed as

$$\hat{L} = \sum_{n=1}^{N} \hat{L}^{(n)},$$

where $\hat{L}^{(n)}$ is a generator for each local party. For instance, the total Hamiltonian $\hat{H}_{\rm tot} = \sum_{n=1}^{N} \hat{H}^{(n)}$ gives rise to time translation $e^{-i\hat{H}_{\rm tot}t}$, total angular momentum $\vec{J}_{\rm tot} = \sum_{n=1}^{N} \vec{J}^{(n)}$ gives rise to rotation $e^{-i\theta\vec{n}\cdot\vec{J}_{\rm tot}}$ in a certain direction $\vec{n}$, and the center-of-mass position $\hat{x}_{\rm cm} = \sum_{n=1}^{N} \hat{x}^{(n)}/N$ or total momentum $\hat{p}_{\rm tot} = \sum_{n=1}^{N} \hat{p}^{(n)}$ translates a conjugate parameter $e^{-ip_0\hat{x}_{\rm cm}}$ or $e^{-ix_0\hat{p}_{\rm tot}}$, respectively. Moreover, the eigenvalue of collective generators $\hat{L}$ can be highly degenerate since they are given by the sum of eigenvalues of each local generator $\hat{L}^{(n)}$.

In this sense, it is natural to consider the asymmetry relative to some macroscopic observable, and its relationship to quantum macroscopicity. An attempt to relate microscopic and macroscopic coherence phenomena via the resource theoretic framework was proposed by Yadin and Vedral [52], by disallowing quantum operations that allow macroscopic coherence and microscopic coherence to be inter-converted. This is achieved by considering the modes of asymmetry via ω. In fact, we note by Proposition 1 in Chapter 2 that free operations in this framework of quantum macroscopicity are equivalent to translationally-covariant operations with respect to the given macroscopic observable. Especially, the quantum Fisher information and the Wigner-Yanase-Dyson skew information are measures of asymmetry that have been proven to satisfy the conditions to quantify quantum macroscopicity suggested in Ref. [52].

3.3.2 Weighted measures of asymmetry

Following the method of quantifying macroscopic quantum superposition within phase space presented in [44], we consider the characterization of

quantum macroscopicity by performing a sum of the form (effective size) $\times$ (degree of coherence) for every mode. In this scenario, the effective size of the coherence is supplied by the eigenvalue spacing ω of an observable $\hat{L}$ and the degree of coherence is given by the mode coherence(or asymmetry) for each ω.

As such, we introduce the following weighted sum of ω-coherence as a measure for quantifying quantum macroscopicity:

$$\mathcal{M}(\hat{\rho}) = \sum_{\omega \in \Omega} f(\omega) \mathcal{A}^{(\omega)}(\hat{\rho}) \tag{3.1}$$

by using a mode of asymmetry (or coherence) $\mathcal{A}^{(\omega)}$ studied in Chapter 2 and a given function $f(\omega)$ that characterizes the effective size of each mode ω.

In order for the measure to be consistent, we require that $f(\omega) = 0$ when $\omega = 0$ in order to ensure that $\mathcal{M}(\hat{\rho}) = 0$ when $\hat{\rho}$ is a translationally-covariant (i.e. free) state with respect to $\hat{L}$. For example, suppose we make a simple choice of $f(\omega) = \omega^2/2 = |\lambda_i - \lambda_j|^2/2$ for the ω-coherence measure $\mathcal{A}^{(\omega)}_{\mathrm{HS}}$. In this case, the weighted sum then gives rise to the Wigner-Yanse-Dyson skew information: $I_W(\hat{\rho}, \hat{L}) = -(1/2)\mathrm{Tr}[\sqrt{\hat{\rho}}, \hat{L}]^2$ [79] which has been pointed out as a potential candidate for measuring quantum coherence [80] and quantum macroscopicity [52]. Our approach then gives the skew information based measure of quantum macroscopicity with the interpretation of a weighted sum of mode coherences.

We generalize this concept by proposing the possible classes of weight functions $f(\omega)$ in order to construct consistent measures of macroscopicity via a weighted sum of ω-coherences.

Theorem 3 (Weighted measure of asymmetry for the Hilbert-Schmidt norm)**.** *Suppose* $f(\omega) = \omega^2 \int_{x\in\mathcal{X}} dx[\mathrm{sinc}(\omega x/2)]^2 g(x)$ *for* $g(x) \geq 0$ *and* $\mathcal{X} \subset \mathbb{R}$. *Then*

$$\mathcal{M}_{\mathrm{HS}}(\hat{\rho}) = \sum_{\omega\in\Omega^+} f(\omega)\mathcal{A}^{(\omega)}_{\mathrm{HS}}(\hat{\rho}) \tag{3.2}$$

is a convex measure and is a monotone under covariant operations, where Ω^+ *is the set of positive* $\omega \in \Omega$.

In order to prove this, we first show that the following construction is possible using the modes of asymmetry.

Proposition 2.

$$\sum_{\omega\in\Omega} \left(1 - e^{-i\omega x}\right) \mathcal{A}^{(\omega)}_{\mathrm{HS}}(\hat{\rho}) \tag{3.3}$$

is a convex measure and monotone under covariant operations for every x.

Proof: We note that the Hellinger distance $D_H(\hat{\rho},\hat{\tau})) = (1/2)\mathrm{Tr}(\sqrt{\hat{\rho}} - \sqrt{\hat{\tau}})^2 = 1 - \mathrm{Tr}\sqrt{\hat{\rho}}\sqrt{\hat{\tau}}$ between a quantum state $\hat{\rho}$ and its symmetric transformation $\mathcal{U}_x(\hat{\rho})$

$$D_H(\hat{\rho},\mathcal{U}_x(\hat{\rho})) = 1 - \mathrm{Tr}[\sqrt{\hat{\rho}}e^{-i\hat{L}x}\sqrt{\hat{\rho}}e^{i\hat{L}x}] \tag{3.4}$$

is a measure of asymmetry, i.e. convex and non-increasing under translationally-covariant operations [75] for any $x \in \mathbb{R}$. Then by direct expansion on the eigenbasis of $\hat{L}$, we get $D_H(\hat{\rho},\mathcal{U}_x(\hat{\rho})) = 1 - \sum_{i,j} |(\sqrt{\hat{\rho}})_{ij}|^2 e^{-i(\lambda_i-\lambda_j)x} = \sum_{\omega\in\Omega}(1 - e^{-i\omega x})\mathcal{A}^{(\omega)}_a(\hat{\rho})$. □

Now we prove the main theorem.

Proof: Note that $\mathcal{A}_{\rm HS}^{(-\omega)}(\hat{\rho}) = \mathcal{A}_{\rm HS}^{(\omega)}(\hat{\rho})$ by the hermicity of the density matrix, so the above quantity will always give rise to real values. To make this explicit, we may alternatively perform the sum over Ω^+, which is the set of positive ω in Ω. We then have

$$\sum_{\omega\in\Omega}(1-e^{-i\omega x})\mathcal{A}_{\rm HS}^{(\omega)}(\hat{\rho}) = x^2\sum_{\omega\in\Omega^+}\omega^2[{\rm sinc}(\omega x/2)]^2\mathcal{A}_{\rm HS}^{(\omega)}.$$

Then we not that the integration on x with multiplying a well-defined function $g(x)/x^2 \geq 0$,

$$\begin{aligned}&\int dx g(x)\sum_{\omega\in\Omega^+}\omega^2[{\rm sinc}(\omega x/2)]^2\mathcal{A}_{\rm HS}^{(\omega)}\\ &= \sum_{\omega\in\Omega^+}\omega^2\int dx[{\rm sinc}(\omega x/2)]^2 g(x)\mathcal{A}_{\rm HS}^{(\omega)}\end{aligned}$$

does not change the monotonicity and convexity. Finally by defining $f(\omega) = \omega^2\int dx[{\rm sinc}(\omega x/2)]^2 g(x)$, $\mathcal{M}_{\rm HS}(\hat{\rho}) = \sum_{\omega\in\Omega^+} f(\omega)\mathcal{A}_{\rm HS}^{(\omega)}(\hat{\rho})$ becomes a convex measure, which is monotone under covariant operations. □

The above construction generalizes the Wigner-Yanase-Dyson skew information based measure $I_W(\hat{\rho},\hat{L})$, which can be retrieved by choosing $g(x) = \delta(x)$, where $\delta(x)$ is the Dirac-delta function. In this case $f(\omega) = \omega^2$.

A quantum macroscopicity measure based on the trace norm can also be constructed as follows, again by considering the sum over modes of the form (effective size) $\times$ (degree of coherence):

Theorem 4 (Weighted measure of asymmetry for the trace norm)**.** *For* $f(\omega) \geq$

0 *for all* ω *and* $f(0) = 0$*,*

$$\mathcal{M}_{\mathrm{tr}}(\hat{\rho}) = \sum_{\omega \in \Omega^{+}} f(\omega) \mathcal{A}_{\mathrm{tr}}^{(\omega)}(\hat{\rho}) \tag{3.5}$$

is a convex measure and monotone under covariant operations.

The proof is straightforward from the fact that $\mathcal{A}_{\mathrm{tr}}^{(\omega)}(\hat{\rho})$ is convex and monotone under covariant operations for every ω, and $f(\omega)$ is a non-negative function. Similarly, we may take $f(\omega) = \omega^2$ to construct a measure of quantum macroscopicity based on the trace norm, $\mathcal{M}_{\mathrm{tr}}(\hat{\rho}) = \sum_{\omega \in \Omega^{+}} \omega^2 ||\hat{\rho}^{(\omega)}||_{\mathrm{tr}}$.

3.3.3 Ruling out microscopic coherences: Scaled measure of coherence

In previous section, we have discussed the weighted measure of ω-coherence using some weight function $f(\omega)$. To quantify "macroscopic" coherence of quantum states, we additionally require to impose an ordering between different eigenvalue spacings ω. To this end, we may take the effective size $f(\omega)$ to be *monotonically increasing when* ω *increases*.

An important requirement for consistent quantum macroscopicity measures is that *products of many microscopic superpositions should be distinguished from genuine superpositions of macroscopically distinct states [37]*. Examples of such accumulation of microscopic coherences are Bose-Einstein condensates and superconductivity. In this sense, the conditions for quantum macroscopicity suggested in Ref. [52] may not be sufficient because there exist measures satisfying them that can give rise to higher degrees of macroscopicity for product states $\hat{\rho}^{\otimes n}$ than the GHZ type en-

tangled states when the former is a simple accumulation of coherence between microscopic states, while the latter superposes macroscopically distinct states [53]. This leads to an additional condition that proper weight functions for macroscopic coherence measure should satisfy.

Here, we introduce a particular class of weight functions, parametrized by the scaling parameter σ, that will enable us to distinguish GHZ states from product states. We call this a *scaled* measure of quantum coherence based on the Hilbert-Schmidt norm, which cuts off the microscopic contribution to coherence by introducing a scale σ.

Definition 1 (Scaled measure of quantum coherence)**.** *For a given scale parameter $\sigma > 0$, the scaled measure of quantum coherence is defined as*

$$\mathcal{M}_\sigma(\hat{\rho}) = \sum_{\omega\in\Omega} \left[1 - e^{-\frac{\omega^2}{8\sigma^2}}\right] \mathcal{A}_{\mathrm{HS}}^{(\omega)}(\hat{\rho}). \tag{3.6}$$

It can be shown that the scaled measure $\mathcal{M}_\sigma$ is non-increasing under translationally-covariant operations by applying Theorem. 3 with $g(x) = x^2(\sqrt{\pi}\tau)^{-1}e^{-x^2/\tau^2}$ and taking $\tau = (\sqrt{2}\sigma)^{-1}$. The scale parameter σ determines an effective cutoff of the weight. To see this, note that for $\omega \lesssim \sigma$, the weight $1 - \exp[-\omega^2/(8\sigma^2)]$ is relatively small compared to the case of $\omega \gtrsim \sigma$. This cutoff may be used to exclude microscopic coherence. In the limit where there is no cutoff imposed, i.e., $\sigma \to 0$, the scaled measure of coherence becomes $\mathcal{M}_\sigma(\hat{\rho}) \to \mathcal{A}_A(\hat{\rho})$, which is the standard "unweighted" measure of asymmetry studied in Chapter 2.

This measure can also be interpreted as the deviation of a quantum state

for a fuzzy reference frame [81, 82]. Note that

$$M_\sigma(\hat{\rho}) = \int D_H(\hat{\rho}, \mathcal{U}_x(\hat{\rho})) \frac{1}{\sqrt{\pi}\tau} e^{-x^2/\tau^2} dx,$$

so the scaled measure of coherence has the interpretation of the average Hellinger distance $D_H(\hat{\rho}, \mathcal{U}_x(\hat{\rho})) = (1/2)\mathrm{Tr}\left[\sqrt{\hat{\rho}} - \sqrt{\mathcal{U}_x(\hat{\rho})}\right]^2$ generated by a group transformation $\mathcal{U}_x$ over the broadening by the Gaussian distribution, when the alignment of the reference frame is imperfect.

The scaled measure of coherence is also related to the measurement process with a finite precision [82, 83] onto the eigenbasis of the macroscopic observable. For the given observable $\hat{L} = \sum_i \lambda_i |i\rangle \langle i|$, the Gaussian smoothing of the projections $\hat{P}_i = |i\rangle \langle i|$ are given by $\hat{P}_i \to \hat{Q}_x^\sigma = \sum_i \sqrt{q_i^\sigma(x)} \hat{P}_i$, where $q_i^\sigma(x) = (\sqrt{2\pi}\sigma)^{-1} e^{-(x-\lambda_i)^2/(2\sigma^2)}$ with the domain $x \in (-\infty, \infty)$. In this case, the effect of the imperfect measurement process $\Phi_\sigma(\hat{\rho}) = \int dx \hat{Q}_x^\sigma \hat{\rho} \hat{Q}_x^{\sigma\dagger}$ can be captured via the measurement-induced disturbance suggested in Ref. [53, 82], which gives the lower bound of the scaled measure of coherence,

$$\frac{1}{2} D_B(\hat{\rho}, \Phi_\sigma(\hat{\rho})) \leq \mathcal{M}_\sigma(\hat{\rho}) \leq 1 - e^{-\frac{I_W(\hat{\rho}, \hat{L})}{4\sigma^2}}, \tag{3.7}$$

where $D_B(\hat{\rho}, \hat{\tau}) = 2 - 2\sqrt{F(\hat{\rho}, \hat{\tau})}$ is the Bures distance. In the following section, we will see that $D_B(\hat{\rho}, \Phi_\sigma(\hat{\rho}))$ itself becomes a valid measure of quantum macroscopicity. The bounds in (3.7) can be proven as follows:

Proof: Using the relation between the fidelity and the affinity [65], we note that

$$\frac{1}{2}D_B(\hat{\rho}, \Phi_\sigma(\hat{\rho})) \leq D_H(\hat{\rho}, \Phi_\sigma(\hat{\rho})). \tag{3.8}$$

The first inequality of Eq. (3.7) then can be proved by

$$\begin{aligned}
D_H(\hat{\rho}, \Phi_\sigma(\hat{\rho})) &= 1 - \mathrm{Tr}\sqrt{\hat{\rho}}\sqrt{\int dx \hat{Q}_x^\sigma \hat{\rho} \hat{Q}_x^{\sigma\dagger}} \\
&\leq 1 - \int dx \mathrm{Tr}\sqrt{\hat{\rho}}\hat{Q}_x^\sigma\sqrt{\hat{\rho}}\hat{Q}_x^{\sigma\dagger} \\
&= 1 - \sum_{i,j}\int dx \sqrt{q_i^\sigma(x)q_j^\sigma(x)}\mathrm{Tr}\sqrt{\hat{\rho}}\hat{P}_i\sqrt{\hat{\rho}}\hat{P}_j \\
&= 1 - \sum_{i,j} e^{-\frac{(\lambda_i-\lambda_j)^2}{8\sigma^2}}\mathrm{Tr}\sqrt{\hat{\rho}}\hat{P}_i\sqrt{\hat{\rho}}\hat{P}_j \\
&= \sum_{\omega\in\Omega}\left[1 - e^{-\frac{\omega^2}{8\sigma^2}}\right]\sum_{\lambda_i-\lambda_j=\omega}\mathrm{Tr}\sqrt{\hat{\rho}}\hat{P}_i\sqrt{\hat{\rho}}\hat{P}_j \\
&= \mathcal{M}_\sigma(\hat{\rho}),
\end{aligned} \tag{3.9}$$

where the inequality comes from operator Jensen's inequality [84] and noting that $\hat{Q}_x^\sigma = \hat{Q}_x^{\sigma\dagger}$ is unital operators. Also note that $\int dx\sqrt{q_i^\sigma(x)q_j^\sigma(x)} = \exp[-(\lambda_i-\lambda_j)^2/(8\sigma^2)]$ for $q_i^\sigma(x) = (\sqrt{2\pi}\sigma)^{-1}e^{-(x-\lambda_i)^2/(2\sigma^2)}$ and

$$\sum_{\lambda_i-\lambda_j=\omega}\mathrm{Tr}\sqrt{\hat{\rho}}\hat{P}_i\sqrt{\hat{\rho}}\hat{P}_j = \sum_{\lambda_i-\lambda_j=\omega}|(\sqrt{\hat{\rho}})_{ij}|^2 = \mathcal{A}_{\mathrm{HS}}^{(\omega)}(\hat{\rho}).$$

The second inequality holds by Jensen's inequality

$$\begin{aligned}\mathcal{M}_\sigma(\hat{\rho}) &= \sum_{\omega\in\Omega}\left[1-e^{-\frac{\omega^2}{8\sigma^2}}\right]\mathcal{A}_{\rm HS}^{(\omega)}(\hat{\rho}) \\ &\leq 1-e^{-\sum_{\omega\in\Omega}\frac{\omega^2}{8\sigma^2}\mathcal{A}_{\rm HS}^{(\omega)}(\hat{\rho})} \\ &= 1-e^{-\frac{I_W(\hat{\rho},\hat{L})}{4\sigma^2}},\end{aligned} \tag{3.10}$$

where $1-e^{-\frac{\omega^2}{8\sigma^2}}$ is a concave function of ω^2. □

It is important to note that the skew information I_W is additive for a product state $\otimes_{n=1}^N\hat{\rho}_n$ with respect to a collective operator $\sum_{n=1}^N\hat{L}^{(n)}$, i.e., $I_W(\otimes_{n=1}^N\hat{\rho}_n,\sum_{n=1}^N\hat{L}^{(n)})=\sum_{n=1}^N I_W(\hat{\rho}_n,\hat{L}^{(n)})\leq NL_{\max}^2/4$, where $L_{\max}$ is the maximum among the eigenvalue differences of $\hat{L}^{(n)}$. Then the upper bound of (3.7) becomes

$$\mathcal{M}_\sigma(\otimes_{n=1}^N\hat{\rho}_n)\leq 1-\exp[-NL_{\max}^2/(4\sigma)^2)]. \tag{3.11}$$

If we take the cutoff to be $\sigma=\sqrt{N\log N}$, we have $\lim_{N\to\infty}\mathcal{M}_\sigma(\otimes_{n=1}^N\hat{\rho}_n)\to 0$, regardless of the local state $\hat{\rho}_n$ when $L_{\max}$ is bounded by a finite value. Consequently, by the convexity of $\mathcal{M}_\sigma$, *microscopic coherences contained in any separable multi-partite state are ruled out for the cutoff* $\sigma=\sqrt{N\log N}$ *in the large particle limit of* $N\gg 1$. The bound (3.7) might be also be useful for the direct detection of quantum macroscopicity in laboratories with finite precision measurements [82].

We also show that a general form of a scaling function can be chosen such that $\mathcal{M}_\sigma(\hat{\rho})=\sum_{\omega\in\Omega}f(\omega^2/\sigma^2)\mathcal{A}_{\rm HS}^{(\omega)}(\hat{\rho})$ is an asymmetry monotone for a concave function $f(x)\geq 0$ that is monotonically increasing with $x\geq 0$

and $f(0) = 0$. In this case, by taking a collective observable $\sum_{n=1}^{N} \hat{L}^{(n)}$ and the cutoff $\sigma = \sqrt{N \log N}$, we can rule out microscopic coherences from every separable state $\hat{\rho}_{\rm sep} = \sum_i p_i \otimes_{n=1}^{N} \hat{\rho}_n^i$ in N-partite systems because

$$\begin{aligned}
\mathcal{M}_\sigma(\hat{\rho}_{\rm sep}) &\leq \sum_i p_i \mathcal{M}_\sigma(\otimes_{n=1}^{N} \hat{\rho}_n^i) \\
&= \sum_i p_i f\left(\frac{\sum_{\omega \in \Omega} \omega^2 \mathcal{A}_{\rm HS}^{(\omega)}(\otimes_{n=1}^{N} \hat{\rho}_n^i)}{N \log N} \right) \\
&= \sum_i p_i f\left(\frac{2 I_W(\otimes_{n=1}^{N} \hat{\rho}_n^i, \sum_{n=1}^{N} \hat{L}^{(n)})}{N \log N} \right) \\
&\leq f\left(\frac{L_{\rm max}^2}{2 \log N} \right)
\end{aligned} \tag{3.12}$$

becomes zero when $N \to \infty$ for a bounded $L_{\rm max}$.

3.3.4 Application to N-partite spin-$1/2$ systems

In this section, we investigate macroscopic coherence of an N-partite spin state with respect to the total spin on z-axis $\hat{S}_z = \sum_{n=1}^{N} \hat{s}_z^{(n)}$, where $\hat{s}_z^{(n)} = \mathbb{1}_1 \otimes \mathbb{1}_2 \otimes \cdots \otimes \mathbb{1}_{n-1} \otimes \hat{s}_z \otimes \mathbb{1}_{n+1} \otimes \cdots \otimes \mathbb{1}_N$ is the local spin observable. Then $\hat{S}_z$ has an eigenvalue spectrum $\{-N/2, -N/2+1, \cdots, N/2-1, N/2\}$ and the maximum difference between eigenvalues is $\omega_{\rm max} = N$.

In order to test the consistency of our measure, we first compare a general type of product states in N-particles spin system,

$$|\theta, \phi\rangle = (\cos(\theta/2)\,|0\rangle + \sin(\theta/2) e^{i\phi}\,|1\rangle)^{\otimes N},$$

so-called a spin coherent state, with a generalized GHZ state

$$|\psi_{\rm GHZ}\rangle = \cos(\theta/2)\,|0\rangle^{\otimes N} + \sin(\theta/2)e^{i\phi}\,|1\rangle^{\otimes N}$$

for $\theta \in [0,\pi]$ and $\phi \in [0,2\pi]$. Each mode of asymmetry for the spin coherent state is then given by

$$\begin{aligned}
\mathcal{A}^{(\omega)}_{\rm tr}(|\theta,\phi\rangle) &= \sum_{k=\omega}^{N} \sqrt{\binom{N}{k}\binom{N}{k-w}} \cos^{2N-2k+\omega}(\theta/2)\sin^{2k-\omega}(\theta/2) \\
&\approx \frac{1}{2}\exp\left[-\frac{\omega^2}{2N\sin^2\theta}\right]\mathrm{erfc}\left(\frac{\omega-2N\sin^2(\theta/2)}{\sqrt{2N\sin^2\theta}}\right), \\
\mathcal{A}^{(\omega)}_{\rm HS}(|\theta,\phi\rangle) &= \sum_{k=\omega}^{N} \binom{N}{k}\binom{N}{k-w} \cos^{2(2N-2k+\omega)}(\theta/2)\sin^{2(2k-\omega)}(\theta/2) \\
&\approx \frac{1}{2\sqrt{\pi N\sin^2\theta}}\exp\left[-\frac{\omega^2}{N\sin^2\theta}\right]\mathrm{erfc}\left(\frac{\omega-2N\sin^2(\theta/2)}{\sqrt{N\sin^2\theta}}\right),
\end{aligned}$$

respectively, where $\mathrm{erfc}(x) = (2/\sqrt{\pi})\int_x^\infty e^{-t^2}dt$ is the complementary error function and the approximations are given when $N \gg 1$ using the normal approximation of binomial distributions.

When we take the weight function $f(\omega) = \omega^2$ for the both measures, we have $\mathcal{M}_{\rm tr}(|\theta,\phi\rangle) \approx \sqrt{\pi/2}N^{3/2}\sin^3\theta \propto N^{3/2}$ and $\mathcal{M}_{\rm HS}(|\theta,\phi\rangle) \approx (1/4)N\sin^2\theta \propto N$ for a large number of N. On the other hand, for the GHZ state $|\psi_{\rm GHZ}\rangle$, each mode of asymmetry is given by $\mathcal{A}^{(\omega)}_1(|\psi_{\rm GHZ}\rangle) = (1/2)\sin\theta(\delta_{N,\omega}+\delta_{N,-\omega})$ and $\mathcal{A}^{(\omega)}_{HS}(|\psi_{\rm GHZ}\rangle) = (1/4)\sin^2\theta(\delta_{N,\omega}+\delta_{N,-\omega})$, respectively. In the case of $f(\omega) = \omega^2$, both weighted measures are given by $\mathcal{M}_{\rm tr}(|\psi_{\rm GHZ}\rangle) = (1/2)N^2\sin\theta$ and $\mathcal{M}_{\rm HS}(|\psi_{\rm GHZ}\rangle) = (1/4)N^2\sin^2\theta$, which both scale with N^2. Figure 1 (a) and (b) show that the product state

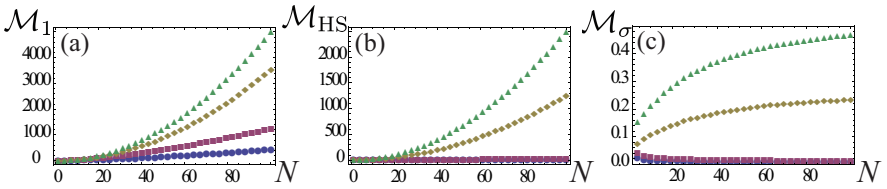

Figure 1: The degree of quantum macroscopcity for spin coherent states $|\theta,\phi\rangle$ and GHZ-states $|\psi_{\rm GHZ}\rangle$ based on the weighted measures of (a) l_1 norm ($\mathcal{M}_1$) and (b) Hilbert-Schmidt norm ($\mathcal{M}_{\rm HS}$) and (c) the scaled measure of coherence ($\mathcal{M}_\sigma$) for $\sigma = \sqrt{N\log N}$. Square symbols and circular symbols refer to the coherent states with $(\theta,\phi) = (\pi/2, 0)$, and $(\theta,\phi) = (\pi/4, 0)$, respectively. Triangular symbols and diamond symbols refer to the GHZ-states with $\theta = \pi/2$, and $\theta = \pi/4$, respectively.

and the GHZ state scales differently on the number of particles N, microscopic coherence in the product state can be distinguished from macroscopic coherence in the GHZ-state. Thus, for both measures, the choice of weight function $f(\omega) = \omega^2$ passes the basic consistency check, and they may be considered appropriate candidates for quantifying quantum macroscopicity, as GHZ states always have a larger macroscopicity than product states in the macroscopic limit.

We can also adapt the scaled measure of quantum coherence $\mathcal{M}_\sigma$ for the states discussed above. The scaled measure of coherence for a spin coherent state $|\theta,\phi\rangle$ is given by

$$\mathcal{M}_\sigma(|\theta,\phi\rangle) \approx 1 - \frac{1}{\sqrt{1 + (N\sin^2\theta/(8\sigma^2))}}.$$

Note that every spin coherent state $|\theta,\phi\rangle$ are separable thus the macroscopcity tends to $\mathcal{M}_\sigma(|\theta,\phi\rangle) \to 0$ for a large value of $N \gg 1$ by Eq. (3.11) when $\sigma = \sqrt{N\log N}$. Figure 1 (c) demonstrates how the product of microscopic

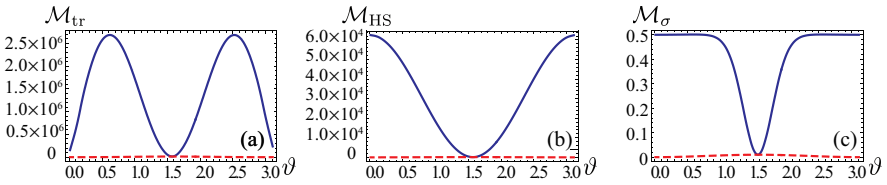

Figure 2: The degree of quantum macroscopcity for the product state $|0\rangle^{\otimes N}$ (dashed lines) and the GHZ-state $|0\rangle^{\otimes N} + |1\rangle^{\otimes N}$ (solid lines) with respect to the total spin measurement $\hat{S}_{\vec{n}}$ for different $\vec{n} = (\sin\vartheta\sin\varphi, \sin\vartheta\cos\varphi, \cos\vartheta)$. The weighted measures of (a) the trace norm ($\mathcal{M}_{\rm tr}$) and (b) the Hilbert-Schmidt norm ($\mathcal{M}_{\rm HS}$) and (c) the scaled measure of coherence ($\mathcal{M}_{\sigma}$) for $\sigma = \sqrt{N\log N}$ are evaluated for $N = 500$. All the measures do not depend on φ.

coherence in a spin coherent state $|\theta, \phi\rangle$ behaves differently from that of the GHZ-state $|\psi_{\rm GHZ}\rangle$ by taking the cutoff $\sigma = \sqrt{N\log N}$. On the other hand, the scaled measure of coherence for GHZ-state is given by

$$\mathcal{M}_{\sigma}(|\psi_{\rm GHZ}\rangle) = (1/2)\sin^2\theta(1 - \exp[-N^2/(8\sigma^2)]).$$

Thus, even if we take $\sigma = \sqrt{N\log N}$, the macroscopic coherence of the GHZ state $\mathcal{M}_{\sigma}(|\psi_{\rm GHZ}\rangle)$ gives the larger value of for the larger value of N (see Fig. 1). This can be interpreted as the evidence of genuine macroscopic coherence in the N-partite spin system.

Quantum macroscopicity measures could be investigated for a general product state $|\psi_{\rm prod}\rangle = \otimes_{i=1}^{N}|\psi_i\rangle$, where $|\psi_i\rangle = \cos(\theta_i/2)|0\rangle + \sin(\theta_i/2)e^{i\phi_i}|1\rangle$ with general total spin measurement $\hat{S}_{\vec{n}} = \vec{n}\cdot\vec{S}$ with $\vec{n} = (\sin\vartheta\cos\varphi, \sin\vartheta\sin\varphi, \cos\vartheta)$ and $\vec{S} := (\hat{S}_x, \hat{S}_y, \hat{S}_z)$. In this case, the Hilbert-Schmidt norm based measure with the choice of weight function $f(\omega) = \omega^2$ is $\mathcal{M}_{\rm HS}(|\psi_{\rm prod}\rangle) = \sum_{i=1}^{N}{\rm Var}(|\psi_i\rangle, \hat{s}_{\vec{n}}^{(i)}) = (1/4)\sum_{i=1}^{N}\sin^2\Theta_i$,

where Θ_i is an angle between two vectors $\vec{m}_i = (\sin\theta_i \cos\phi_i, \sin\theta_i \sin\phi_i, \cos\theta_i)$ and $\vec{n}$. The scaled measure of coherence for every product state $\mathcal{M}_\sigma(|\psi_{\rm prod}\rangle)$ vanishes by choosing the scale parameter $\sigma = \sqrt{N \log N}$ when $N \gg 1$ by Eq. (3.11).

On the other hand, quantum macroscopicity of the GHZ state $|\psi_{\rm GHZ}\rangle$ may scale differently depending on the choice of the measurement basis. The trace norm based measure for the GHZ state tends to oscillate by changing measurement axis $\vec{n}$ which gives the highest value for $\vartheta \approx \pi/4$. The Hilbert-Schmidt norm based measure of the GHZ state is given by

$$\mathcal{M}_{\rm HS}(|\psi_{\rm GHZ}\rangle) = (1/4)N^2 \sin^2\theta \cos^2\vartheta + (N/4)\sin^2\vartheta$$

for $N > 2$. Thus, quantum macroscopicity measures for the GHZ-state give significantly larger values than those for product states unless ϑ is near $\pi/2$. When choosing the measurement axis $\hat{S}_x$ ($\vartheta = \pi/2,\ \varphi = 0$), however, quantum macroscopicity of the GHZ-state cannot be discriminated from product states since both states contain small degrees of coherence between distinct eigenstates of $\hat{S}_x$ with $\omega \propto N$ which vanishes when $N \gg 1$.

The scaled measure of coherence shows the similar behavior with the other two measures, but it seems more robust against the choice of the measurement basis $\vec{n}$. Especially, in the limit of the large system size $N \gg 1$, the scaled measure of coherence for the GHZ-state is given by $\mathcal{M}_\sigma(|\psi_{\rm GHZ}\rangle) \approx 0.5$ except for the narrow region near $\vartheta = \pi/2$ while $\mathcal{M}_\sigma(|\psi_{\rm prod}\rangle) = 0$ for product states. The difference of quantum macroscopicity between the product state $|0\rangle^{\otimes N}$ and the GHZ-state $|0\rangle^{\otimes N} + |1\rangle^{\otimes N}$ is shown in Fig. 2

with respect to the total spin measurement axis $\vec{n}$.

3.3.5 Decoherence effect

In this section, we study how decoherence affects macroscopic coherence of the N-particle spin system. We analyze the degree of macroscopic coherence when the system experience a decoherence channel given by the following Lindblad form,

$$\mathcal{L}(\hat{\rho}) = \frac{d\hat{\rho}}{d\tau} = \hat{A}\hat{\rho}\hat{A}^{\dagger} - \frac{1}{2}(\hat{A}^{\dagger}\hat{A}\hat{\rho} + \hat{\rho}\hat{A}^{\dagger}\hat{A}). \tag{3.13}$$

We first analyze the case of the depolarizing channel when $\hat{A} = \hat{S}_z$. In this case, the GHZ-state $|\psi_{\rm GHZ}\rangle$ evolves into

$$\begin{aligned}\hat{\rho}_{\rm GHZ}(\tau) = \cos^2(\theta/2)(|0\rangle\langle 0|)^{\otimes N} + \sin^2(\theta/2)(|1\rangle\langle 1|)^{\otimes N} \\ + \frac{\sin\theta}{2}e^{-\frac{N^2\tau}{2}}(e^{-i\phi}(|0\rangle\langle 1|)^{\otimes N} + e^{i\phi}(|1\rangle\langle 0|)^{\otimes N}),\end{aligned}$$

after time τ. Note that the off-diagonal terms experience the exponential decay $\exp[-N^2\tau/2]$ and the macroscopicity of the GHZ-state rapidly degrades under the depolarizing channel.

We also discuss the dissipation channel described in the Lindblad form Eq. (3.13) by taking $\hat{A} = \hat{S}_-$, where $\hat{S}_{\pm} = \sum_{n=1}^{N} \hat{s}_{\pm}^{(n)}$ are collective ladder operators given by the sum of ladder operators for each local party $\hat{s}_{\pm}^{(n)} = \hat{s}_x^{(n)} \pm i\hat{s}_y^{(n)}$.

Figure 3 demonstrates that macroscopic coherence is fragile under the both dephasing and dissipation channels. These results imply that extremely noisless environment is required in order to generate and manipulate quan-

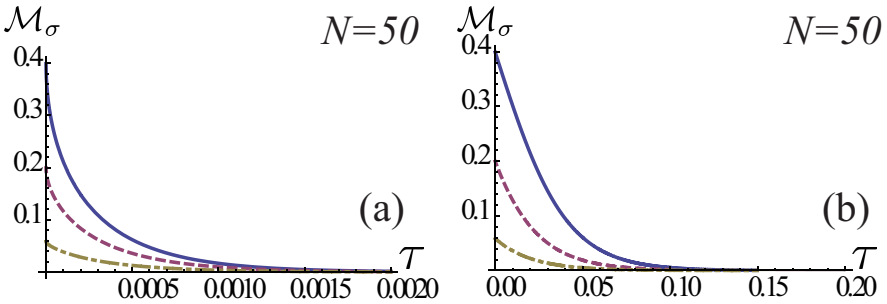

Figure 3: Decay of the scaled measure of quantum macroscopcity when the initial state is given by the pure GHZ-states $|\psi_{\rm GHZ}\rangle = \cos(\theta/2)\,|0\rangle^{\otimes N} + \sin(\theta/2)\,|1\rangle^{\otimes N}$. The number of the particle is given by $N = 50$. Both (a) the dephasing channel $\hat{A} = \hat{S}_z$ and (b) the dissipation channel $\hat{A} = \hat{S}_-$ lead to the rapid decay of macroscopic coherence, even starting with the superposition $|0\rangle^{\otimes N} + |1\rangle^{\otimes N}$ ($\theta = \pi/2$). For the both figures, solid lines refer to $\theta = \pi/2$, dashed lines refer to $\theta = \pi/4$, and dot-dashed lines refer to $\theta = \pi/8$.

tum states while preserving macroscopic quantum coherence. We also note that the degree of macroscopic coherence decays faster under the dephsing channel than the dissipation channel for a given characteristic time τ.

3.4 Disturbance-based measure of macroscopic coherence

In this section, we study a different type of quantum macroscopicity measures based on the state disturbance induced by a coarse-grained measurement. We show that a family of disturbance-based measures, one of which has already appeared in the previous section satisfies the criteria of macroscopic coherence [52]. In some cases, however, the criteria in Ref. [52] cannot yield consistent results without additional constraints. This problem is overcome by introducing coarse-graining of the measurement depending on the system size. We prove an inequality which relates the Wigner-Yanase-Dyson skew information (and consequently, the quantum Fisher information) and the state disturbance induced by coarse-grained measurement, from which we argue that an appropriate limit to yield a consistent measure is the classical limit. We further show that our concept of quantum macroscopicity corrsponds to the fragility of a quantum state under a certain type of decoherence. Our operational viewpoint on quantum macroscopicity allows one to effectively identify the quantum coherence between the macroscopically-separated components of a superposition. This approach can be applied to both spin and bosonic systems, and we present several examples that lead to reasonable results in this section.

3.4.1 Macroscopic coherence and coarse-grained measurement

Based on the previous discussions, we may say that macroscopic coherence is coherence of a quantum superposition between two macroscopically distinct states. In other words, the component states of the superposition are supposed to yield two distinct outcomes when a measurement on a macroscopic scale is performed. We discuss the concept of a coarse-grained measurement [78, 83, 85] introduced in the previous section further to describe such a macroscopic measurement with respect to an observable $\hat{L} = \sum_i \lambda_i |i\rangle \langle i|$. We remind that a *coarse grained measurement* is defined to be the following set of Kraus operators:

$$\hat{Q}_x^\sigma = \sum_i \sqrt{q_i^\sigma(x)}\, |i\rangle \langle i|. \tag{3.14}$$

with some smoothing function $q_i^\sigma(x)$ depending on the measurement outcome λ_i and the smoothing parameter σ. In the previous section, we have introduced a coarse-grained measurement that has a Gaussian smoothing function

$$q_i^\sigma(x) = \frac{1}{\sqrt{2\pi}\sigma} e^{-\frac{(\lambda_i - x)^2}{2\sigma^2}},$$

where x is a continuous variable over the real line, as done in the previous section. The smoothing function $q_i^\sigma(x)$ is centered around measurement outcome λ_i. The standard deviation σ determines the level of precision of the measurement and therefore quantifies the amount of coarse graining of the measurement. One may interpret the above measurement as an inter-

action with the needle of a measuring apparatus that returns a normal distribution about the position a_i when the system is in the space projected by $\hat{P}_i = |i\rangle\langle i|$. If $\sigma \to 0$, the measurement process becomes projective, while an increasing σ implies an increasingly imprecise measurement process. One may verify that $\int_{-\infty}^{\infty} \hat{Q}_x^{\sigma\dagger}\hat{Q}_x^{\sigma}dx = \mathbb{1}$ for any $\sigma > 0$ so it is indeed a valid positive-operator valued measurement (POVM). In such a case, the post measurement state is given by $\Phi_\sigma(\hat{\rho}) = \int_{-\infty}^{\infty} dx \hat{Q}_x^{\sigma}\hat{\rho}\hat{Q}_x^{\sigma\dagger} = \sum_{\omega\in\Omega} e^{-\omega^2/(8\sigma^2)}\hat{\rho}^{(\omega)}$, where $\Omega = \{\lambda_i - \lambda_j\}$ is a set of the spacing between the eigenvalues of the observable $\hat{L} = \sum_i \lambda_i |i\rangle\langle i|$.

There have been studies on quantifiers of the size of a superposition based on the distinguishability between two components states with a finite measurement precision [43, 47]. Reference [47] suggested a measure of the size of macroscopic superpositions by quantifying the amount of noise that can be tolerated by a coarse-grained photon number measurement. Applications of these measures, however, are limited only to pure states and it is required to choose a specific decomposition (such as $|A\rangle + |B\rangle$) that represents the superposition. Here, we show that the quantum state disturbance caused by a coarse-grained measurement naturally leads to measures of macroscopic coherence that are applicable to arbitrary forms of states and that satisfy all conditions (M1)–(M4).

When one performs a non-selective projective (i.e. precise) measurement on the state with the given measurement basis set, all coherence terms between eigenstates of the different measurement outcomes will vanish. However, when a coarse-grained measurement is performed, certain coherence terms may survive depending on the precision of the measurement. It is

therefore reasonable to expect that at a certain level of the measurement precision, only macroscopic coherence will be disturbed by the measurement process. Towards this end, we propose the disturbance of the quantum state induced by the coarse grained measurement process as a natural measure of macroscopic quantum coherence.

In order to quantify quantum macroscopicity by quantum state disturbance, we will employ distance measures $D(\hat{\rho}, \hat{\tau})$ between quantum states $\hat{\rho}$ and $\hat{\tau}$ that satisfy the following set of conditions.

(D1) $D(\hat{\rho}, \hat{\tau}) \geq 0$, where the equality is saturated if and only if $\hat{\rho} = \hat{\tau}$

(D2) Unitary invariance: $D(\hat{U}\hat{\rho}\hat{U}^{\dagger}, \hat{U}\hat{\tau}\hat{U}^{\dagger}) = D(\hat{\rho}, \hat{\tau})$.

(D3a) Contractivity under a completely positive trace-preserving map $\mathcal{E}$, $D(\hat{\rho}, \hat{\tau}) \geq D(\mathcal{E}(\hat{\rho}), \mathcal{E}(\hat{\tau}))$ (Note that $\mathcal{E}$ is not necessarily a free operation).

(D3b) $D(\hat{\rho}, \hat{\tau}) \geq \sum_{\alpha} p_{\alpha} D(\mathcal{E}_{\alpha}(\hat{\rho})/p_{\alpha}, \mathcal{E}_{\alpha}(\hat{\tau})/p_{\alpha})$, when $p_{\alpha} = \mathrm{Tr}\mathcal{E}_{\alpha}(\hat{\rho}) = \mathrm{Tr}\mathcal{E}_{\alpha}(\hat{\sigma})$ and $\sum_{\alpha} \mathcal{E}_{\alpha} = \mathcal{E}$. (Note that $\mathcal{E}_{\alpha}$ is not necessarily a free operation).

(D4) Joint convexity : $D(\sum_i p_i \hat{\rho}_i, \sum_i p_i \hat{\tau}_i) \leq \sum_i p_i D(\hat{\rho}_i, \hat{\tau}_i)$.

Remarkably, despite starting from considerably different physical arguments, the following theorem shows that the measurement disturbance satisfies the set of conditions proposed by Yadin and Vedral [52].

Theorem 5 (Disturbance-based measure of macroscopic quantum coherence)**.** *For any coarse-grained measurement process Φ_σ with $\sigma > 0$,*

$$M_\sigma(\hat{\rho}) := D(\hat{\rho}, \Phi_\sigma(\hat{\rho})) \tag{3.15}$$

satisfies (M1) – (M4) when the distance measure $D(\hat{\rho}, \hat{\tau})$ satisfies (D1) – (D4).

Details and proofs can be found in the Appendix. Theorem 5 allows us to define a new family of macroscopic quantum coherence measures parametrized by the measurement precision σ. In the special case of $\sigma = 0$, this type of measure becomes a measure of coherence with respect to the eigenbasis $\{|i\rangle\}$ of the observable, suggested in [86], but does not satisfy (M4) anymore. The Bures distance $D_B(\hat{\rho}, \hat{\tau}) = 2 - 2\sqrt{\mathcal{F}(\hat{\rho}, \hat{\tau})}$ defined in terms of the fidelity between quantum states $\mathcal{F}(\hat{\rho}, \hat{\tau}) = [\mathrm{Tr}\sqrt{\sqrt{\hat{\rho}}\hat{\tau}\sqrt{\hat{\rho}}}]^2$ and the quantum relative entropy defined by $S(\hat{\rho}||\hat{\tau}) = \mathrm{Tr}\hat{\rho}\ln\hat{\rho} - \mathrm{Tr}\hat{\rho}\ln\hat{\tau}$ are good examples satisfying all the conditions (D1) – (D4). For the rest of the section, we focus on the the measure based on the Bures distance, $M_\sigma^B(\hat{\rho}) = D_B(\hat{\rho}, \Phi_\sigma(\hat{\rho}))$.

However, we observe that the disturbance-based measure $M_\sigma(\hat{\rho})$ with certain values of σ may lead to unreasonable conclusions even when it satisfies all the conditions in [52]. The following example shows that a product of microscopic superpositions has a larger value of M_σ than the Greenberger–Horne–-Zeilinger(GHZ)-state when σ is sufficiently small. This is contrary to our understanding and previous results [44, 45, 51] that the latter state is clearly in a macroscopic superposition while the former is not.

Consider a magnetization measurement on a system of N spin-$1/2$ particles, of the same type studied by Poulin [78]. The measurement is defined by a Hermitian operator $\hat{L} = \sum_{i=1}^{N} \hat{s}_z^{(i)}$ where $s_z^{(i)} := \hat{\sigma}_z/2$ and $\hat{\sigma}_z$ is the standard Pauli Z operator. The observable $\hat{L}$ represents a collective measurement of the overall spins rather than addressing each individual spin. We compare the values of quantum macroscopicity measure $M(\hat{\rho})$ between two different quantum states, a product state $\hat{\rho}_{\rm p}^N = \left|\Psi_{\rm p}^N\right\rangle \left\langle\Psi_{\rm p}^N\right|$ with $\left|\Psi_{\rm p}^N\right\rangle = (\cos\theta\,|0\rangle + \sin\theta\,|1\rangle)^{\otimes N}$ and the GHZ-state $\hat{\rho}_{\rm GHZ}^N = \left|\Psi_{\rm GHZ}^N\right\rangle \left\langle\Psi_{\rm GHZ}^N\right|$ with $\left|\Psi_{\rm GHZ}^N\right\rangle = 2^{-1/2}\left(|0\rangle^{\otimes N} + |1\rangle^{\otimes N}\right)$. The state $\hat{\rho}_{\rm p}^N$ is a product of microscopic superpositions (between $|0\rangle$ and $|1\rangle$) and does not contain long range coherence between the spins in the system. Moreover, $\hat{\rho}_{\rm p}^N$ is a kind of a spin coherent state and its classicality has been studied in Refs. [83, 87]. On the other hand, $\hat{\rho}_{\rm GHZ}^N$ could be a typical model of Schrödinger's cat state that two components of the superposition give maximally different outcomes (all spin up, all spin down), leading to a large variance for the observable $\hat{L}$. Also it contains multipartite quantum correlation between the spins in the system [88].

In order to compare the quantum macroscpicity $M_\sigma^B(\hat{\rho})$, we first evaluate the fidelity between the pre- and post-measurement states. The fidelity for the product state $\hat{\rho}_{\rm p}^N$ is given by

$$\mathcal{F}(\hat{\rho}_{\rm p}^N, \Phi_\sigma(\hat{\rho}_{\rm p}^N)) \approx \frac{1}{\sqrt{1 + N\sin^2(2\theta)/(8\sigma^2)}}$$

using the approximation of the binomial distribution to the normal distribution for $N \gg 1$. On the other hand, in the case of the GHZ-state $\hat{\rho}_{\rm GHZ}^N$, we

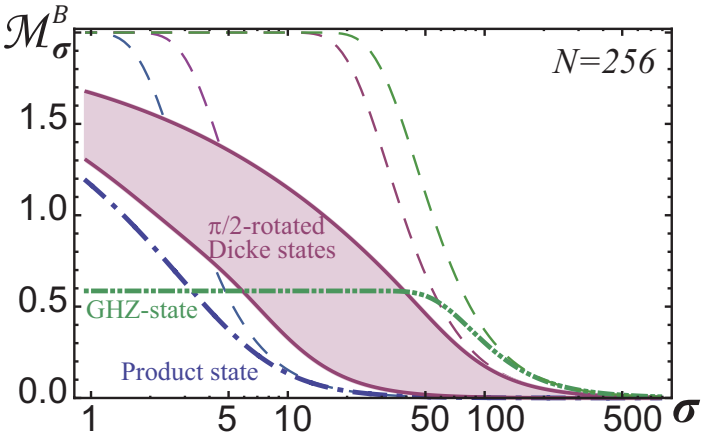

Figure 4: Disturbance-based coherence M_σ^B for measuring total magnetization of N spin-1/2 system with $N = 256$. A product state (dot-dashed line), a GHZ-state (double-dot-dashed line), and $\pi/2$-rotated Dicke states (solid lines) are investigated. Upper line on rotated Dicke states (shaded region) refers to $k = N/2$, while lower line refers to $k = 1$. Dashed lines refer to the bound given by Eq. 3.17.

have

$$\mathcal{F}(\hat{\rho}^N_{\rm GHZ}, \Phi_\sigma(\hat{\rho}^N_{\rm GHZ})) = \frac{1}{2}\left(1 + e^{-\frac{N^2}{8\sigma^2}}\right).$$

Note that for small enough values of $\sigma \ll 1$, $M_\sigma(\hat{\rho}^N_{\rm p})$ tends to the maximum value of 2 for the product state, while $M_\sigma(\hat{\rho}^N_{\rm GHZ})$ is $2 - \sqrt{2} \approx 0.586$ for the GHZ state (see Fig. 4). This suggests that an accumulation (i.e., direct product) of microscopic superposition is more macroscopically-quantum than a pure superposition of two macroscopically distinct states. The result clearly demonstrates that the conditions proposed in [52] are not sufficient to prescribe a completely consistent measure of macroscopic coherence.

3.4.2 Quantum state disturbance and macroscopic coherence

In order to overcome the issues described in the previous section, we revisit to the basic premise of macroscopic quantumness. As far back as Schrödinger [6], a system is said to be macroscopic quantum when each state constructing superposition is distinguished directly by a classical measurement. In metrology, it is well known that the limit of a classical measurement is given by $\sigma \propto \sqrt{N}$ for N-particle systems, and quantum resources are necessary to achieve higher efficiencies [72,73]. Previous studies of coarse-grained measurement similarly argued that the condition $\sigma \gg \sqrt{N}$ allows macroscopic observables to be considered classical [78, 83].

The following theorem relating our disturbance-based measure $M_\sigma^B(\hat{\rho})$ to the Wigner-Yanase-Dyson skew information $I_W(\hat{\rho}, \hat{L}) = (-1/2)\mathrm{Tr}[\sqrt{\hat{\rho}}, \hat{L}]^2$ further reinforces our argument.

Theorem 6. *Coarse-grained measurement disturbance $M_\sigma^B(\hat{\rho})$ is lower bounded by Wigner-Yanase-Dyson skew information $I_W(\hat{\rho}, \hat{L})$,*

$$M_\sigma^B(\hat{\rho}) \leq 2\left(1 - e^{-\frac{I_W(\hat{\rho},\hat{L})}{4\sigma^2}}\right). \tag{3.16}$$

For a pure state $|\psi\rangle$, we have

$$M_\sigma^B(|\psi\rangle) \leq 2\left(1 - e^{-\frac{\mathrm{Var}_{|\psi\rangle}(\hat{L})}{8\sigma^2}}\right), \tag{3.17}$$

where $\mathrm{Var}_{|\psi\rangle}(\hat{L}) = \langle\psi|\hat{L}^2|\psi\rangle - \langle\psi|\hat{L}|\psi\rangle^2$ is the variance of the observable $\hat{L}$, which is identical to $I_W(|\psi\rangle\langle\psi|, \hat{L})$ for a pure state.

In the case of mixed states, the proof is already given in the previous section by Eq. (3.7) since $M_\sigma^B(\hat{\rho}) = D_B(\hat{\rho}, \Phi_\sigma(\hat{\rho}))$. Thus prove the second inequality of Theorem 2 for pure quantum states.

Proof: In order to prove the upper bound of $M_\sigma^B(\hat{\rho}) = 2-2\sqrt{\mathcal{F}(\hat{\rho}, \Phi_\sigma(\hat{\rho}))}$, we show the lower bound of the fidelity $\sqrt{\mathcal{F}(\hat{\rho}, \Phi_\sigma(\hat{\rho}))}$. Note that when one of the states are pure, the fidelity is given by $\mathcal{F}(|\psi\rangle\langle\psi|, \hat{\sigma}) = \langle\psi|\hat{\sigma}|\psi\rangle$. Then, we have for the coarse-grained measurement process,

$$\begin{aligned}
\mathcal{F}(|\psi\rangle\langle\psi|, \Phi_\sigma(|\psi\rangle\langle\psi|)) &= \int_{-\infty}^{\infty} dx \langle\psi|\hat{Q}_x^\sigma|\psi\rangle\langle\psi|\hat{Q}_x^\sigma|\psi\rangle \\
&= \sum_{i,j} \exp\left[-\frac{(\lambda_i - \lambda_j)^2}{8\sigma^2}\right] \langle\psi|i\rangle\langle i|\psi\rangle\langle\psi|j\rangle\langle j|\psi\rangle \\
&\geq \exp\left[-\frac{\sum_{i,j}(\lambda_i - \lambda_j)^2 |\langle\psi|i\rangle|^2 |\langle\psi|j\rangle|^2}{8\sigma^2}\right].
\end{aligned} \tag{3.18}$$

Note that $|\langle\psi|i\rangle|^2$ is the probability of getting outcome a_i, thus $\sum_{i,j}(\lambda_i - \lambda_j)^2|\langle\psi|i\rangle|^2|\langle\psi|j\rangle|^2 = 2\mathrm{Var}_{|\psi\rangle}(\hat{L})$, then we finally get $\sqrt{\mathcal{F}(\hat{\rho}, \Phi_\sigma(\hat{\rho}))} \geq \exp[-\mathrm{Var}_{|\psi\rangle}(\hat{L})/(8\sigma^2)]$. □

The above inequality reflects the intuition that the more precise the measurements and the more coherence present within the system, the more the measurement will disturb the quantum state.

A previous study [45] argued that scaling of the quantum Fisher information with the number of particles N characterizes whether a N-particle system is macroscopically quantum. Moreover, the Wigner-Yanase-Dyson skew information is a closely related with the quantum Fisher information

due to the following relation [65]

$$4I_W(\hat{\rho}, \hat{L}) \leq I_F(\hat{\rho}, \hat{L}) \leq 8I_W(\hat{\rho}, \hat{L}), \tag{3.19}$$

where the quantum Fisher information is given by $I_F(\hat{\rho}, \hat{L}) = 2\sum_{i \neq j}(\mu_i - \mu_j)^2/(\mu_i + \mu_j)|\langle\psi_i|\hat{L}|\psi_j\rangle|^2$ for eigendecomposition of $\hat{\rho} = \sum_i \mu_i |\psi_i\rangle \langle\psi_i|$. We then note that the inequality (3.16) relates our measure to the previous suggested measure of quantum macroscopicity based on the quantum Fisher information [45]. According to [45], quantum states with $I_F(\hat{\rho}, \hat{L}) = O(N^1)$ can be interpreted as classical(or at least microscopic quantum) while the states with $I_F(\hat{\rho}, \hat{L}) = O(N^2)$ may be considered macroscopic quantum.

It is worth mentioning that a similar inequality was recently derived in a separate study of macrorealism based on the Leggett-Garg inequality [82] as

$$\sqrt{\mathcal{F}(\hat{\rho}, \Phi_\sigma(\hat{\rho}))} \geq B_F = e^{-\frac{I_F(\hat{\rho}, \hat{L})}{32\sigma^2}} - \mathrm{erfc}\left(\frac{\sqrt{2}\pi\sigma}{\sqrt{I_F(\hat{\rho}, \hat{L})}}\right) \tag{3.20}$$

while the inequality Eq. (3.16) can be expressed as $\sqrt{\mathcal{F}(\hat{\rho}, \Phi_\sigma(\hat{\rho}))} \geq B_W = e^{-\frac{I_W(\hat{\rho}, \hat{L})}{4\sigma^2}}$. We point out that the bounds B_F give negative values when $I_F/\sigma^2 \geq 37.806$, which leads to the trivial bound $B_F < 0 \leq \sqrt{\mathcal{F}(\hat{\rho}, \Phi_\sigma(\hat{\rho}))}$, while our bound B_W is positive for any I_W and σ. In the case of a pure state $|\psi\rangle$, the bound given by Eq. (3.17) is always tighter than the bound Eq. (3.20) given by the quantum Fisher information, since $I_F(|\psi\rangle, \hat{L}) = 4\mathrm{Var}_{|\psi\rangle}(\hat{L})$. In the case of a mixed state, the bound B_F seems tighter than

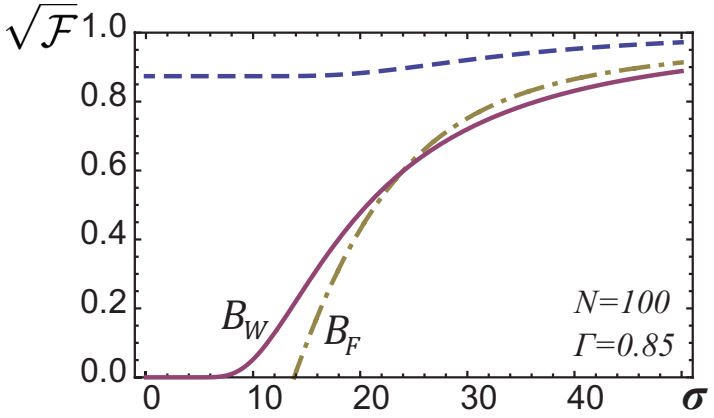

Figure 5: Comparison between the lower bounds B_F(dot-dashed line) and B_W(solid line) of the fidelity $\sqrt{\mathcal{F}}$(dashed line) for the decohered GHZ-state $\hat{\rho}_\Gamma^N$ with $N = 100$ and $\Gamma = 0.85$.

B_W when σ is large. However, in some regions of small σ, B_W could be tighter than B_F.

We compare two different lower bounds of the fidelity between pre- and post measurement states, $\sqrt{\mathcal{F}(\hat{\rho}, \Phi_\sigma(\hat{\rho}))} \geq B_{F(W)}$ where $B_F = e^{-\frac{I_F(\hat{\rho},\hat{L})}{32\sigma^2}} - \mathrm{erfc}\left(\frac{\sqrt{2}\pi\sigma}{\sqrt{I_F(\hat{\rho},\hat{L})}}\right)$ [82] and $B_W = e^{-\frac{I_W(\hat{\rho},\hat{L})}{4\sigma^2}}$, respectively. We evaluate both the bounds for a decohered GHZ-state in a spin system given by

$$\hat{\rho}_\Gamma^N = \frac{1}{2}\left(|0\rangle\langle 0| + |N\rangle\langle N| + \Gamma(|0\rangle\langle N| + |N\rangle\langle 0|)\right), \tag{3.21}$$

where $0 \leq \Gamma \leq 1$. The quantum Fisher information and Wigner-Yanase-Dyson skew information are given by $I_F(\hat{\rho}_\Gamma^N, \hat{L}) = N^2\Gamma^2$ and $I_W(\hat{\rho}_\Gamma^N, \hat{L}) = \frac{N^2}{4}(1-\sqrt{1-\Gamma^2})$, respectively. When the coarse-grain parameter σ is large, the second term of B_F becomes negligible and B_F gives a tighter bound than B_W (note that $I_F \leq I_W$ for any Γ). On the other hand, if the coarse-

grain parameter σ is relatively small compared to I_F and I_W, the second term of B_F has a significant value while the first term becomes small. Thus, there is some value of σ where the two bounds, B_F and B_W, meet as described in Fig. 5. When the state is pure ($\Gamma = 1$), we can use the bound Eq. (3.17), and our bound given by $\sqrt{\mathcal{F}(\hat{\rho}, \Phi_\sigma(\hat{\rho}))} \geq B = e^{-\frac{\mathrm{Var}_{|\psi\rangle}(\hat{L})}{8\sigma^2}} = e^{-\frac{N^2}{32\sigma^2}}$ is always tighter than $B_F = e^{-\frac{N^2}{32\sigma^2}} - \mathrm{erfc}\left(\frac{\sqrt{2}\pi\sigma}{N^2}\right)$.

3.4.3 Examples in spin and bosonic systems

Theorem 6 naturally manifests itself in the disturbance-based measure. Provided the level of coarse graining is chosen to be $\sigma \propto \sqrt{N}$, a state with $I_W(\hat{\rho}, \hat{L}) = O(N^1)$ will result in a measurement disturbance close to zero. For example, the macroscopic coherence for a product of microscopic quantum states $\hat{\rho}^{\otimes N}$ is close to zero according to our measure, since the Wigner-Yanase-Dyson skew information scales with the order of $O(N)$. In contrast, a non-classical skew information $I_W(\hat{\rho}, \hat{L}) = O(N^2)$, for example in the case of a GHZ state, allows the measure $M^B_\sigma(\hat{\rho})$ to reach its maximum value of 2 for $N \gg 1$. This observation allows us to circumvent the inconsistency observed in the previous section. We will therefore impose the classical limit $\sigma = \sqrt{N}$ as the appropriate level of coarse graining for our disturbance based measure.

Another example in the spin system is a rotated Dicke state given by $\hat{R}_{\theta,\phi}\,|N,k\rangle$, where $|N,k\rangle = \binom{N}{k}^{-1/2} \sum_P P(|\underbrace{0\cdots0}_{N-k}\underbrace{1\cdots1}_{k}\rangle)$ is a sum over all all symmetric permutations P, and $\hat{R}_{\theta,\phi} = e^{\xi \hat{J}_+ - \xi^* \hat{J}_-}$ is the rotation operator with $\hat{J}_\pm = \sum_{i=1}^N (\sigma_x^{(i)} \pm i\sigma_y^{(i)})$ and $\xi = \theta e^{i\phi}/2$. In the case of

$\theta = \pi/2$ and $\phi = 0$, the macroscopic coherence of the state depends on the excitation number k. Such a state becomes a product state when $k = 0$ or $k = N$.

Figure 4 compares the behavior of M_σ^B between rotated Dicke, GHZ and product states for varying levels of the coarse graining parameter σ. We also observe that at the classical limit of $\sigma = \sqrt{N}$, rotated Dicke states with excitation number $k \approx N/2$ result in higher levels of macroscopic coherence M_σ^B than the GHZ-state. This property does not persist however, if we were to continue decreasing the amount of measurement precision (i.e. increase σ). For a sufficiently large σ, the GHZ-state tends to have the highest level of macroscopic coherence among all the states considered. Our disturbance-based measure appears to capture ideas from both the more general quantum coherence measures given by [22] and the macroscopic coherence measures based on the variance of the observable [44, 45, 48, 80] since it encodes information about *how many states are currently in superposition* as well as *how far apart these superposed states are* with respect to the given measurement observable and the measurement precision σ.

We also apply the disturbance-based measure to bosonic systems described by the annihilation operator $\hat{a}$ and the creation operator $\hat{a}^\dagger$. Since a bosonic system can contain many particles in a single mode, the system may be considered macroscopic when the mean particle number $\bar{n} = \langle \hat{a}^\dagger \hat{a} \rangle$ is large. In this case, the particle number $\hat{n} = \hat{a}^\dagger \hat{a}$ and the quadrature $\hat{X}_\theta = (e^{-i\theta}\hat{a} + e^{i\theta}\hat{a}^\dagger)/\sqrt{2}$ are natural candidates for measurement observables. We now consider the value of M_σ^B with respect to an X-quadrature

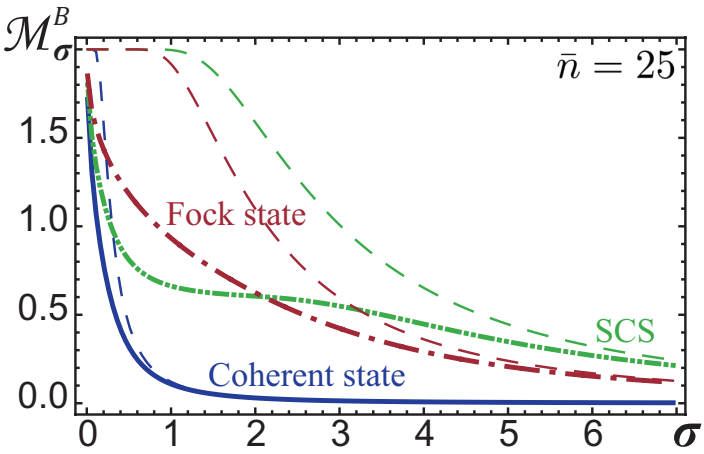

Figure 6: Disturbance-based coherence measure M_σ^B for quadrature measurement for bosonic system with the same mean particle number $\bar{n} = 25$. A Fock state (dot-dashed line), a superposition of coherent states (double-dot-dashed line), and a coherent state (solid line) are investigated. Dashed lines refer to the bound given by Eq. (3.17).

measurement $\hat{X} = (\hat{a}+\hat{a}^\dagger)/\sqrt{2}$. Figure 6 shows the disturbance-based measure M_σ^B for typical states of a bosonic system. Again, we see that for small values of σ, a bosonic coherent state $|\alpha\rangle$ contains non-trivial macroscopic quantumness, which are not in agreement with our understanding. However, M_σ^B rapidly decreases with σ and becomes essentially zero at the imposed classical limit of $\sigma \approx 1$. This makes sense when we note that bosonic coherent states are the most classical states among all pure states [89, 90] and the classical measurement is based on electric (or magnetic) fields which are proportional to $\hat{X}_\theta$. In the case of the $\hat{X}$ measurement for coherent states, the noise is given by $\mathrm{Var}(\hat{X}) = 1/2$, while the signal is given by $\langle\hat{X}\rangle \sim \sqrt{\bar{n}}$. Then the signal to noise ratio $\langle\hat{X}\rangle/\sqrt{\mathrm{Var}(\hat{X})}$ scales by $\sqrt{\bar{n}}$ which corresponds to the measuring of the magnetization $\hat{M}$ for the spin system with

spin coherent states, $\langle\hat{M}\rangle/\sqrt{\mathrm{Var}(\hat{M})} \propto \sqrt{N}$. Based on this, the noise corresponding to the bosonic system, $\sigma \sim \sqrt{\mathrm{Var}(\hat{X})} \sim 1$, would be a proper choice of the classical limit.

We also evaluate the values of M_σ^B for a superposition of coherent states (SCS) $|\alpha\rangle + |-\alpha\rangle$ and the Fock state $|n\rangle$. In the phase space, the distance between two bosonic coherent states, $|\alpha\rangle$ and $|-\alpha\rangle$, becomes greater when amplitude α becomes larger. The two coherent states can then be distinguishable by a "classical-like" measurement such as a homodyne detection with a large degree of imprecision. Thus, a SCS for $\alpha \gg 1$ is often exemplified as a typical example of a macroscopic superposition and even called a Schrödinger cat state. It may not be immediately clear whether Fock states $|n\rangle$ are macroscopic superpositions. However, in the coherent state representation, a Fock state of $n \gg 1$ can also be understood as a superposition of many coherent states where the coherent states are far separate in the phase space. So, they may be possible candidates for macroscopic superpositions when $n \gg 1$.

In comparison to coherent states, a SCS and the Fock state give nontrivial values of M_σ^B at the classical limit of σ (see Fig. 6). All these observations are compatible with the common expectation that coherent states are classical, while SCS and the Fock states are considered macroscopically quantum.

3.4.4 Connection to a decoherence model

Decoherence in a particular basis can be regarded as a measurement performed by the environment [91]. Based on this concept, we may consider a connection between the quantum macroscopicity measure in the present work and the fragility of a quantum state by a certain type of decoherence. We show that a coarse-grained measurement of observable $\hat{L}$ can be equivalently modeled by a decoherence process under linear coupling between the system observable $\hat{L}$ and the environment operator $\hat{p}_E$. After time t, the initial state of the system $\hat{\rho}_0$ evolves into

$$\hat{\rho}(t) = \mathrm{Tr}_E e^{-ig\hat{L}\hat{p}_E t} \left(\hat{\rho}_0 \otimes \hat{\tau}_E\right) e^{ig\hat{L}\hat{p}_E t}, \tag{3.22}$$

where $\hat{\tau}_E$ is the initial state of the environment and g is a coupling constant. By taking the eigenstates of $\hat{p}_E$ to be $|p\rangle$ with continuous variable p, we get

$$\hat{\rho}(t) = \sum_{\omega\in\Omega} \hat{\rho}_0^{(\omega)} \left[\int dp e^{-i(gt)p\delta} \langle p|\hat{\tau}_E\,|p\rangle\right]. \tag{3.23}$$

Now we choose the environment state to have $\langle p|\hat{\tau}_E\,|p\rangle \propto e^{-\mu^2 p^2}$ so that $\hat{\rho}(t) = \sum_{\omega\in\Omega} \hat{\rho}_0^{(\omega)} e^{-\frac{(gt)^2\omega^2}{4\mu^2}}$. In this case, the state distance between the initial and final states $D(\hat{\rho}_0, \hat{\rho}(t))$, which indicates the fragility of the initial quantum state under this kind of decoherence, is exactly the state disturbance $M_\sigma(\hat{\rho}_0)$ caused by a coarse-grained measurement for the corresponding value of $\sigma = \mu/(\sqrt{2}gt)$.

For example, we suppose that the environment is in a thermal state $\hat{\tau}_E = e^{-\beta\hat{H}_E}/Z_E$, where $Z_E = \mathrm{Tr}e^{-\beta\hat{H}_E}$ and $\beta = (k_B T)^{-1}$ is an inverse

temperature. For simplicity, we further assume that the thermal bath is a single-mode harmonic oscillator with hamiltonian $\hat{H}_E = \hbar\omega_0 \left(\hat{a}_E^\dagger \hat{a}_E + \frac{1}{2}\right)$ and the coupling with the system is given by the momentum operator, $\hat{p}_E = (\hat{a}_E - \hat{a}_E^\dagger)/(\sqrt{2}i)$. In this case, we have $\langle p|\hat{\tau}_E|q\rangle \propto \exp[-\tanh(\beta\omega_0/2)\hat{p}_E^2]$, and $\tanh(\beta\omega_0/2)/(g^2t^2)$ corresponds to $2\sigma^2$ in the coarse-grained measurement. We then see that large values of σ correspond to short decoherence times, weak coupling and/or low bath temperatures. In other words, a quantum state with a large value of $M_\sigma(\hat{\rho})$ for the classical limit of σ is easily decohered by a thermal environment. This result is consistent with the previous research [92] that macroscopic coherence is fragile under decoherence effects even if a bath is in the low temperature.

3.4.5 Appendix: Proof of Theorem 5

Proof: (M1) Note that $M_\sigma(\hat{\rho}) = D(\hat{\rho}, \Phi_\sigma(\hat{\rho})) = 0$ if and only if $\hat{\rho} = \Phi_\sigma(\hat{\rho})$. This is only achieved when Φ_σ is given by a convex sum of projections $\hat{P}_n = \sum_{\lambda_i=n} |i\rangle\langle i|$, thus this condition can be achieved when $\hat{\rho} = \hat{\rho}^{(0)}$.

(M2a) By using Proposition. 1, we show that

$$\begin{aligned} M_\sigma(\mathcal{E}(\hat{\rho})) &= D(\mathcal{E}(\hat{\rho}), (\Phi_\sigma \circ \mathcal{E})(\hat{\rho})) \\ &= D(\mathcal{E}(\hat{\rho}), (\mathcal{E} \circ \Phi_\sigma)(\hat{\rho})) \\ &\leq D(\hat{\rho}, \Phi_\sigma(\hat{\rho})) \\ &= M_\sigma(\hat{\rho}) \end{aligned} \tag{3.24}$$

for trace-preserving free operation $\mathcal{E}$.

(M2b) Similarly, by using Proposition. 1 and the condition (D3b), we show that

$$\begin{aligned}\sum_{\alpha} p_\alpha M_\sigma(\mathcal{E}_\alpha(\hat{\rho})/p_\alpha) &= \sum_{\alpha} p_\alpha D(\mathcal{E}_\alpha(\hat{\rho})/p_\alpha, \Phi_\sigma(\mathcal{E}_\alpha(\hat{\rho})/p_\alpha)) \\ &= \sum_{\alpha} p_\alpha D(\mathcal{E}_\alpha(\hat{\rho})/p_\alpha, \mathcal{E}_\alpha(\Phi_\sigma(\hat{\rho}))/p_\alpha) \\ &\leq D(\hat{\rho}, \Phi_\sigma(\hat{\rho})) \\ &= M_\sigma(\hat{\rho}),\end{aligned} \tag{3.25}$$

where $\mathrm{Tr}\mathcal{E}_\alpha(\Phi_\sigma(\hat{\rho})) = \mathrm{Tr}\Phi_\sigma(\mathcal{E}_\alpha(\hat{\rho})) = \mathrm{Tr}\mathcal{E}_\alpha(\hat{\rho}) = p_\alpha$, since Φ_σ is a trace preserving map.

(M3) Convexity can be directly proven by using joint convexity of the distance measure,

$$\begin{aligned}M_\sigma\left(\sum_i p_i\hat{\rho}_i\right) &= D\left(\sum_i p_i\hat{\rho}_i, \Phi_\sigma(\sum_i p_i\hat{\rho}_i)\right) \\ &= D\left(\sum_i p_i\hat{\rho}_i, \sum_i p_i\Phi_\sigma(\hat{\rho}_i)\right) \\ &\leq \sum_i p_i D(\hat{\rho}_i, \Phi_\sigma(\hat{\rho}_i)) \\ &= \sum_i p_i M_\sigma(\hat{\rho}_i).\end{aligned}$$

(M4) Now we prove that there is an ordering of M between two states $|\psi_0\rangle = (|i\rangle + |j\rangle)/\sqrt{2}$ and $|\psi_1\rangle = (|k\rangle + |l\rangle)/\sqrt{2}$, i.e. $M(|\psi_0\rangle) > M(|\psi_1\rangle)$ in the case of $|\lambda_i - \lambda_j| > |a_k - a_l|$. Note that we can always choose the unitary operation $\hat{U}$, which transforms the bases $|k\rangle \to |i\rangle$ and $|l\rangle \to |j\rangle$. Then

in $\{|i\rangle, |j\rangle\}$ basis, we can write the states, $\hat{\rho}_0 = |\psi_0\rangle\langle\psi_0| = \frac{1}{2}\begin{pmatrix} 1 & 1 \\ 1 & 1 \end{pmatrix}$, $\Phi_\sigma(\hat{\rho}_0) = \frac{1}{2}\begin{pmatrix} 1 & K \\ K & 1 \end{pmatrix}$, $\hat{U}\hat{\rho}_1\hat{U}^\dagger = \hat{\rho}_0$, and $\hat{U}\Phi_\sigma(\hat{\rho}_1)\hat{U}^\dagger = \frac{1}{2}\begin{pmatrix} 1 & J \\ J & 1 \end{pmatrix}$, where $K = e^{-(\lambda_i-\lambda_j)^2/(8\sigma^2)}$ and $J = e^{-(\lambda_k-\lambda_l)^2/(8\sigma^2)}$, respectively. Since $|\lambda_i - \lambda_j| > |\lambda_k - \lambda_l|$, $0 \le K < J \le 1$ for any $\sigma > 0$, then we can choose $0 < \lambda = \frac{1-J}{1-K} < 1$ such that $\hat{U}\Phi_\sigma(\hat{\rho}_1)\hat{U}^\dagger = \lambda\Phi_\sigma(\hat{\rho}_0) + (1-\lambda)\hat{\rho}_0$. Then by the unitary invariance and joint convexity of the distance measure D, we have

$$\begin{aligned} M(\hat{\rho}_1) &= D(\hat{\rho}_1, \Phi_\sigma(\hat{\rho}_1)) \\ &= D(\hat{U}\hat{\rho}_1\hat{U}^\dagger, \hat{U}\Phi_\sigma(\hat{\rho}_1)\hat{U}^\dagger) \\ &= D(\lambda\hat{\rho}_0 + (1-\lambda)\hat{\rho}_0, \lambda\Phi_\sigma(\hat{\rho}_0) + (1-\lambda)\hat{\rho}_0) \\ &\le \lambda D(\hat{\rho}_0, \Phi_\sigma(\hat{\rho}_0)) + (1-\lambda)D(\hat{\rho}_0, \hat{\rho}_0) \\ &= \lambda D(\hat{\rho}_0, \Phi_\sigma(\hat{\rho}_0)) \\ &< D(\hat{\rho}_0, \Phi_\sigma(\hat{\rho}_0)) \\ &= M(\hat{\rho}_0), \end{aligned} \tag{3.26}$$

which completes the proof. □

We also note that if a distance measure $D(\hat{\rho}, \hat{\sigma})$ satisfies all conditions (D1)–(D4) without the property (D3b), the macroscopicity measure $M_\sigma(\hat{\rho}) = D(\hat{\rho}, \Phi_\sigma(\hat{\rho}))$ based on D satisfies (M1)–(M4) except (M2b).

In the case of the Bures distance, $D_B(\hat{\rho}, \hat{\sigma}) = 2 - 2\sqrt{\mathcal{F}(\hat{\rho}, \hat{\sigma})}$, (D1), (D2), (D3a), and (D4) can be easily proven by using the properties of the

fidelity [93]. We can also prove the condition (D3b) by follows.

$$\begin{aligned}
&\sum_\alpha p_\alpha D_B(\mathcal{E}_\alpha(\hat{\rho})/p_\alpha, \mathcal{E}_\alpha(\hat{\sigma})/p_\alpha) \\
&\qquad = 2\sum_\alpha p_\alpha \left(1 - \sqrt{\mathcal{F}(\mathcal{E}_\alpha(\hat{\rho})/p_\alpha, \mathcal{E}_\alpha(\hat{\sigma})/p_\alpha)}\right) \\
&\qquad = 2\left(1 - \sum_\alpha \sqrt{\mathcal{F}(\mathcal{E}_\alpha(\hat{\rho}), \mathcal{E}_\alpha(\hat{\sigma}))}\right),
\end{aligned} \tag{3.27}$$

by using $\sqrt{\mathcal{F}(\hat{\rho}/p, \hat{\sigma}/p)} = \sqrt{\mathcal{F}(\hat{\rho}, \hat{\sigma})}/p$. In order to complete the proof, we prove that $\sqrt{\mathcal{F}(\hat{\rho}, \hat{\sigma})} \leq \sum_\alpha \sqrt{\mathcal{F}(\mathcal{E}_\alpha(\hat{\rho}), \mathcal{E}_\alpha(\hat{\sigma}))}$ when $\sum_\alpha \mathcal{E}_\alpha = \mathcal{E}$. Note that $\mathcal{E}_\alpha(\hat{\rho})$ can be expressed using ancillary state $\hat{\tau}_2$: $\mathcal{E}_\alpha(\hat{\rho}) = \mathrm{Tr}_2(\mathbb{1} \otimes \hat{\Pi}_\alpha)\hat{U}(\hat{\rho} \otimes \hat{\tau}_2)\hat{U}^\dagger(\mathbb{1} \otimes \hat{\Pi}_\alpha)$. Note that fidelity is non-decreasing under partial trace $\sqrt{\mathcal{F}(\hat{\rho}_{12}, \hat{\sigma}_{12})} \leq \sqrt{\mathcal{F}(\mathrm{Tr}_2\hat{\rho}_{12}, \mathrm{Tr}_2\hat{\sigma}_{12})}$ and satisfies following properties for a set of projection operators $\{\hat{\Pi}_n\}$: $\sum_n \sqrt{\mathcal{F}(\hat{\Pi}_n\hat{\rho}\hat{\Pi}_n, \hat{\Pi}_n\hat{\sigma}\hat{\Pi}_n)} = \sqrt{\mathcal{F}(\sum_n \hat{\Pi}_n\hat{\rho}\hat{\Pi}_n, \sum_n \hat{\Pi}_n\hat{\sigma}\hat{\Pi}_n)}$. Using these properties we can show that $\sum_\alpha \sqrt{\mathcal{F}(\mathcal{E}_\alpha(\hat{\rho}), \mathcal{E}_\alpha(\hat{\sigma}))} \geq \sqrt{\mathcal{F}(\hat{U}(\hat{\rho} \otimes \hat{\tau}_2)\hat{U}^\dagger, \hat{U}(\hat{\sigma} \otimes \hat{\tau}_2)\hat{U}^\dagger)} = \sqrt{\mathcal{F}(\hat{\rho}, \hat{\sigma})}$, since fidelity is invariant under unitary operations.

The conditions (D1)–(D4) for the relative entropy $S(\hat{\rho}||\hat{\sigma})$ can be proved similarly. (D1), (D2), (D3a), and (D4) directly comes from the elementary properties of relative entropy [93]. (D3b) can be proved by noting that $\sum_\alpha p_\alpha S(\mathcal{E}_\alpha(\hat{\rho})/p_\alpha||\mathcal{E}_\alpha(\hat{\sigma})/p_\alpha) = \sum_\alpha S(\mathcal{E}_\alpha(\hat{\rho})||\mathcal{E}_\alpha(\hat{\sigma}))$. Then (D3b) can be proved a same argument above by using $\sum_n S(\hat{\Pi}_n\hat{\rho}\hat{\Pi}_n||\hat{\Pi}_n\hat{\sigma}\hat{\Pi}_n) = S(\sum_n \hat{\Pi}_n\hat{\rho}\hat{\Pi}_n||\sum_n \hat{\Pi}_n\hat{\sigma}\hat{\Pi}_n)$.

3.5 Remarks

To conclude, we have pointed out that quantum macroscopicity could be considered via the asymmetry with respect to some macroscopic observable, which generates a collective group transformation on the total system. We have suggested two different types of measures to quantify quantum macroscopicity in general physical systems.

Weighted measures of macroscopic coherence can be constructed based on the observation that multiple modes of ω contribute differently to the coherence as the system size gets larger. From this viewpoint, we define a class of quantum macroscopicity measures characterized by a sum of the form (effective size) $\times$ (degree of coherence) for all the modes of ω. Through this, we demonstrate that many macroscopic measures of coherence may be related to the total coherence of a system via a simple weighted sum.

We also discuss how it is desirable to exclude microscopic superpositions in order to implement a proper measure of macroscopic coherence, which is not guaranteed simply by the conditions proposed in Ref. [52] as shown in Ref. [53]. We then show how one may introduce a cutoff for microscopic superpositions, leading what we call a scaled measure of coherence where the coherence for each mode is differently weighted by appropriately choosing a scaling parameter σ, which may be interpreted as a fuzziness in measurement reference frame. This scaled measure can thus rule out microscopic superpositions by virtue of the fact that they are not detectable for a given degree of fuzziness. In this way, the measure assures that only the coherence between macroscopically distinct states is considered. We then

compared the degree of macroscopic coherence of a product state and a GHZ-state in N-particle spin systems. Microscopic coherences in a product state are effectively suppressed by introducing the cutoff $\sigma = \sqrt{N \log N}$, and we have demonstrated that degree of macroscopic coherence in the GHZ state is easily decayed by decoherence.

Another type of measures to quantify quantum macroscopicity is given by disturbance-based measures under coarse-grained measurements. This argument stems from physical grounds that a precise measurement will affect all the coherence present in the system, while a sufficiently imprecise measurement will affect only the portion of the coherence between classically distinct states. We demonstrated that our disturbance-based measure satisfies a series of properties to quantify macroscopic coherence laid out in [52]. In the process, we pointed out that conditions for macroscopic coherence proposed in [52] is insufficient to yield consistent results without additional constraints. This inconsistency can be overcome by fixing the level of coarse-graining to an appropriate classical limit. We also demonstrated an inequality relating the measurement-induced disturbance and the Wigner-Yanase-Dyson skew information and argued that this kind of classical limit is necessary to produce a reliable measure of macroscopic coherence. Furthermore, we establish the direct connection between the disturbance-based quantum macroscopicity measure and the fragility of a quantum state under decoherence.

We emphasize that the disturbance-based measure provides an operational point of view on macroscopic quantumness that can be quantified by the degree of disturbance throughout the measurement of a given im-

precision. The imprecision of the measurement allows us to focus on the coherence between macroscopically distinct states by blurring the interference below the measurement resolution. We can thus identify whether the quantum state is in a macroscopic superposition by investigating the state disturbance throughout the measurement only with a macroscopic resolution. As we have demonstrated for both spin and bosonic systems, our approach is not limited to a specific quantum system but can be applied to arbitrary macroscopic observables and quantum systems with large particle numbers.

Moreover, the arguments presented in this chapter are not limited to any particular system, but may also be applied to any general macroscopic observable $\hat{L}$ for any macroscopic, composite systems. We expect that the viewpoint concerning the state disturbance induced by coarse-grained measurement may lead to greater insights on macroscopic quantum effects and coherence.

Chapter 4

Macroscopic coherence in optical fields as a resource for quantum metrology

The contents of this chapter are largely based on [H. Kwon, K. C. Tan, T, Volkoff, and H. Jeong, "Nonclassicality of Light as a Quantifiable Resource for Quantum Metrology" (in preparation).].

4.1 Introduction

The differences between classical and quantum physics have long been a fruitful area of physical research. In recent decades, developments in the area of quantum information have managed to introduce renewed impetus in the the study of such differences, primarily because such differences between classical and nonclassical theories can be exploited to perform useful informational tasks [27, 35, 94–97], but also because the quantum information perspective have led to a proliferation of new techniques that simultaneously allows more light to be shed on age old questions.

One of the promising application in quantum optics is the parameter estimation task beyond classical limit, as known as quantum metrology [72, 73]. For example, in the phase estimation task, the precision using classical

states of light is bounded by the standard quantum limit, by using coherent states as probe and reference fields. In this case, one can achieve a estimation precision with the shot-noise limit, proportional to the mean photon number in the field. On the other hand, if we have nonclassical resources of light, such as squeezed states [98, 99], NOON states [100–102], or superposition of coherent states [103–105], we can further achieve the Heisenberg limit, which is proportional to the square of the mean photon number [72]. Even when the noise-environment contaminates the states, it has been studied that we can attain a better precision than the one that classical resources allows [106].

In this chapter, we show that nonclassical states in optical fields can be utilized as the parameter estimation task for displacement. Furthermore, we demonstrate that every multi-mode pure nonclassical state with negative Glauber-Sudarshan P distribution provides metrological enhancement over all classical states when estimating the parameter generated by collective quadrature operators. Moreover, we show that this metrological power can quantify the degree of nonclassicality for a general mixed state. Based on this concept, we establish the resource theory of nonclassicality in multi-mode optical fields, which is monotone under linear optical elements, including phase-shift, beam-splitter, and displacement operators. Our results can be applied to nonclassicality detection and high-precision force sensing tasks. Finally, we discuss that this nonclassicality is related to the macroscopic coherence in optical fields.

4.2 Quantum metrology and quantum Fisher information

Consider a situation to estimated the parameter ϕ generated by an observable $\hat{L}$ in quantum system. For instance, the phase in quantum optical fields are obtained by taking $\hat{L} = \hat{n}$, where $\hat{n}$ is the number operator. In a general situation, a given quantum state with an initial state $\hat{\rho}_0$ evolves into

$$\hat{\rho}_\phi = e^{-i\phi\hat{L}}\hat{\rho}_0 e^{i\phi\hat{L}}.$$

Then, we can consider an estimator $\hat{\phi}$ in order to guess the actual value of ϕ. In this case, precision of the estimation is defined as $(\Delta\phi)^2 := \langle(\hat{\phi} - \phi)^2\rangle$. The fundamental limitation of the precision is given by the so-called quantum Carmér Rao bound [107]

$$(\Delta\phi)^2 \geq \frac{1}{I_F(\hat{\rho}, \hat{L})},$$

where $I_F(\hat{\rho}, \hat{L}) = 2\sum_{i,j} \frac{(\lambda_i - \lambda_j)^2}{\lambda_i + \lambda_j} |\langle i|\hat{L}\,|j\rangle\,|^2$ is the quantum Fisher information with respect to an observable $\hat{A}$ when the eigenvalues and eigenstates of $\hat{\rho}$ are given by λ_i and $|i\rangle$, respectively. The quantum Fisher information has been also studied in quantum information theory to quantify multi-partite entanglement [108–110] and macroscopic quantum coherence [54] based on the usefulness of a quantum state for metrological tasks beyond the classical limit.

In this chapter, we focus on the parameter estimation of θ for a unitary

dynamics generated by a collective quadrature observable. To illustrate the situation briefly, we give an example in a single-mode case with one of the quadrature operators given by $\hat{X} = (\hat{a} + \hat{a}^\dagger)/\sqrt{2}$, where $\hat{a}$ is an bosonic annihilation operator. Under the unitary dynamics generated by this quadrature operator $\hat{X}$, an initial quantum state $\hat{\rho}_0$ evolves into

$$\hat{\rho}_\theta = e^{-i\theta\hat{X}}\hat{\rho}_0 e^{i\theta\hat{X}}.$$

If we estimate the parameter θ using $\hat{\rho}_\theta$, a tight bound for the variance of the estimator $(\Delta\theta)^2$ is given by

$$(\Delta\theta)^2 \geq \frac{1}{I_F(\hat{\rho}_0, \hat{X})}, \tag{4.1}$$

which is the quantum Cramér Rao bound with respect to the parameter estimation of θ generated by $\hat{X}$.

4.3 Nonclassicality in multi-mode optical fields as a resource for high-precision parameter estimation

In light fields, the general nonclassicality could be defined as the positivity of Glauber-Sudarshan P representation [111]. A multi-mode optical field is described by using a set of bosonic operators $\{\hat{a}_n\}$, where $\hat{a}_n$ is the annihilation operator in n-th mode. Generally, a N-mode optical state $\hat{\rho}$ in a Hilbert

space $\mathcal{H}$ is said to be classical when it has representation

$$\hat{\rho} = \frac{1}{\pi^N} \int d^{2N}\boldsymbol{\alpha} P(\boldsymbol{\alpha}) \left|\boldsymbol{\alpha}\right\rangle \left\langle\boldsymbol{\alpha}\right|$$

with positive $P(\boldsymbol{\alpha})$, where $d^{2N}\boldsymbol{\alpha} = d^2\alpha_1 d^2\alpha_2 \cdots d^2\alpha_N$ $\left|\boldsymbol{\alpha}\right\rangle = \left|\alpha_1\right\rangle \otimes \left|\alpha_2\right\rangle \otimes \cdots \otimes \left|\alpha_N\right\rangle$. The set of coherent states

$$\left|\alpha_n\right\rangle = e^{-\frac{|\alpha_n|^2}{2}} \sum_{m=0}^{\infty} \frac{\alpha_n^m}{\sqrt{m!}} \left|m\right\rangle$$

thus forms the basis for classical light [112]. In order to characterize and quantify non-classically for optical states, various approaches including, distance based measures [113, 114], the nonclassicality depth [115], entanglement potential [116–118], characteristic function methods [119], and operational approaches [120, 121] have been suggested.

In a more recent development, it was demonstrated that the nonclassicality of light fields may be characterized [122] using the language of the resource theory of coherence [22], suggesting that nonclassical light and coherence are identical resources. Emerging from this characterization is the so-called resource theory of linear optics, which is perhaps the most natural set of "classical" optical operations that can be performed in the laboratory. With this recent formalization of a resource theory to characterize light fields, one may therefore expect to find quantifiers of nonclassicality with operational or other physical significance, paralleling the developments in entanglement and coherence theory.

In this section, we show that nonclassicality of an optical quantum state

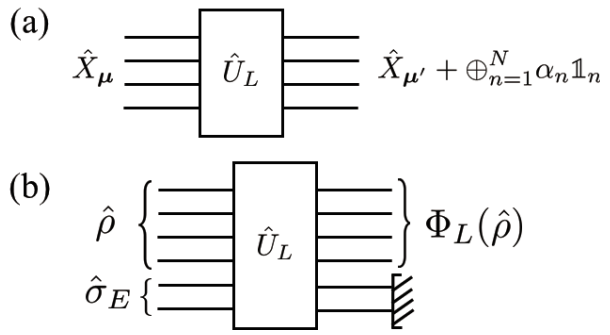

Figure 7: (a) Linear optical unitary and (b) linear optical map.

can be understood as a resource for high-precision parameter estimation tasks. To this end, we introduce the optimal and mean metrological powers based on the quantum Fisher information and demonstrate that these measures fit into the resource theory of nonclassicality suggested in Ref. [122] for both single-mode and multi-mode optical states.

4.3.1 Linear optical map and nonclassicality criteria

In order to construct a resource theory of nonclassicality, we introduce a set of free operations as follows: We first define a general N-mode bosonic operator $\hat{a}_{\boldsymbol{\mu}} = \sum_{n=1}^{N} \mu_n \hat{a}_n$ with complex values $\mu_n = \mathrm{Re}[\mu_n] + i\mathrm{Im}[\mu_n]$, and $\boldsymbol{\mu} = (\mathrm{Re}[\mu_1], -\mathrm{Im}[\mu_1], \mathrm{Re}[\mu_2], -\mathrm{Im}[\mu_2], \cdots, \mathrm{Re}[\mu_N], -\mathrm{Im}[\mu_N])^T$ to be a real $2N$-dimensional unit vector satisfying $||\boldsymbol{\mu}||^2 := \sum_{n=1}^{N} |\mu_n|^2 = 1$. Consequently, a general collective quadrature operator in an N-mode optical system is given by $\hat{X}_{\boldsymbol{\mu}} = (\hat{a}_{\boldsymbol{\mu}} + \hat{a}_{\boldsymbol{\mu}}^{\dagger})/\sqrt{2}$. Then following Ref. [122], we define multi-dimensional linear optical unitary operations to be $\hat{U}_L$, which transforms $\hat{a}_{\boldsymbol{\mu}}$ into $\hat{a}_{\boldsymbol{\mu}'} + \oplus_{n=1}^{N} \alpha_n \mathbb{1}_n$, satisfying the condition $||\boldsymbol{\mu}||^2 =$

$||\boldsymbol{\mu}'||^2$, and α_n is some complex number and $\mathbb{1}_n$ is the identity operator on the nth mode. Additionally, these operations could be realized by the Hamiltonian in a form $\hat{H} = \sum_{n=1}^{N} A_n \hat{a}_n + \sum_{n=1}^{N} A_n^* \hat{a}_n^\dagger + \sum_{n,m=1}^{N} B_{nm} \hat{a}_n^\dagger \hat{a}_m$, with complex values of A_n and B_{nm} satisfying $B_{nm} = B_{mn}^*$, which can be implemented by only using local phase shifters, displacement, and beam splitter operations.

Using linear optical unitary operations, we define a linear optical map

$$\Phi_L(\hat{\rho}_A) = \mathrm{Tr}_E(\hat{U}_L \hat{\rho}_A \otimes \hat{\sigma}_E \hat{U}_L^\dagger),$$

where $\hat{\sigma}_E$ is a classical state. We also define a selective linear operation by a set of Kraus operators $\{\hat{K}_i\}$ satisfying $\sum_i \hat{K}_i^\dagger \hat{K}_i = \mathbb{1}$ when there exists $\hat{U}_L$ and classical ancilla $\sigma_{EE'}$ and some set of orthogonal vectors $\{|i\rangle_{E'}\}$ such that $\mathrm{Tr}_E(\hat{U}_L \hat{\rho}_A \otimes \hat{\sigma}_{EE'} \hat{U}_L^\dagger) = \sum_i p_i \hat{\rho}_A^i \otimes |i\rangle_{E'} \langle i|$ for some density matrices $\hat{\rho}_A^i$, where $p_i \hat{\rho}_A^i := \hat{K}_i \hat{\rho}_A \hat{K}_i^\dagger$ and $p_i := \mathrm{Tr}(\hat{K}_i \hat{\rho}_A \hat{K}_i^\dagger)$. Base on these linear optical maps, following conditions that nonclassicality measure should satisfy have been proposed [122] :

(Q1) $\mathcal{Q}(\hat{\rho}) = 0$ *if and only if* $\hat{\rho}$ is classical.

(Q2) (a) (Weak monotonicity) $\mathcal{Q}$ is monotonically decreasing under linear optical operations Φ_L, i.e. $\mathcal{Q}(\hat{\rho}_A) \geq \mathcal{Q}(\Phi_L(\hat{\rho}_A))$.

(b) (Strong monotonicity) $\mathcal{Q}$ is non-increasing under a selective linear optical operations on average, i.e. $\mathcal{Q}(\hat{\rho}) \geq \sum_i p_i \mathcal{Q}(\hat{\rho}_i)$ where $p_i := \mathrm{Tr}(\hat{K}_i^\dagger \hat{K}_i \hat{\rho})$ and $\hat{\rho}_i := (\hat{K}_i \hat{\rho} \hat{K}_i^\dagger)/p_i$.

(Q3) $\mathcal{Q}$ is convex, i.e. $\mathcal{Q}(\sum_i p_i \hat{\rho}_i) \leq \sum_i p_i \mathcal{Q}(\hat{\rho}_i)$.

4.3.2 Metrological power of light

In order to quantify nonclassicality in optical fields, we focus on the parameter estimation of θ for a unitary dynamics generated by a collective quadrature observable $\hat{X}_{\boldsymbol{\mu}}$. Under the unitary dynamics, an initial quantum state $\hat{\rho}_0$ evolves into

$$\hat{\rho}_{\theta,\boldsymbol{\mu}} = e^{-i\theta\hat{X}_{\boldsymbol{\mu}}}\hat{\rho}_0 e^{i\theta\hat{X}_{\boldsymbol{\mu}}}.$$

If we estimate the parameter θ using $\hat{\rho}_{\theta,\boldsymbol{\mu}}$, a tight bound for the variance of the estimator $(\Delta\theta)^2_{\boldsymbol{\mu}}$ is given by

$$(\Delta\theta)^2_{\boldsymbol{\mu}} \geq \frac{1}{I_F(\hat{\rho}_0, \hat{X}_{\boldsymbol{\mu}})} = \frac{1}{\boldsymbol{\mu}^T \mathbf{F} \boldsymbol{\mu}}, \tag{4.2}$$

which is the so-called the quantum Cramér Rao bound. This can be derived by using the decomposition

$$\hat{X}_{\boldsymbol{\mu}} = \sum_{n=1}^{N}\left(\frac{\mu_n \hat{a}_n + \mu_n^* \hat{a}_n^\dagger}{\sqrt{2}}\right) = \sum_{n=1}^{N}\left(\mathrm{Re}[\mu_n]\hat{X}^{(2n-1)} - \mathrm{Im}[\mu_n]\hat{X}^{(2n)}\right),$$

where $\hat{X}^{(2n-1)} = (\hat{a}_n + \hat{a}_n^\dagger)/\sqrt{2}$ and $\hat{X}^{(2n)} = (\hat{a}_n - \hat{a}_n^\dagger)/(\sqrt{2}i)$ are the local quadrature operators. We then get

$$\begin{aligned} I_F(\hat{\rho}, \hat{X}_{\boldsymbol{\mu}}) &= 2\sum_{i,j}\frac{(\lambda_i - \lambda_j)^2}{\lambda_i + \lambda_j}|\langle i|\sum_{n=1}^{N}\left(\mathrm{Re}[\mu_n]\hat{X}^{(2n-1)} - \mathrm{Im}[\mu_n]\hat{X}^{(2n)}\right)|j\rangle\,|^2 \\ &= (\mathrm{Re}[\mu_1], -\mathrm{Im}[\mu_1], \cdots, \mathrm{Re}[\mu_N], -\mathrm{Im}[\mu_N]) \cdot \{F_{mn}(\hat{\rho})\} \\ &\quad \cdot (\mathrm{Re}[\mu_1], -\mathrm{Im}[\mu_1], \cdots, \mathrm{Re}[\mu_N], -\mathrm{Im}[\mu_N])^T \\ &= \boldsymbol{\mu}^T \boldsymbol{F} \boldsymbol{\mu}, \end{aligned}$$

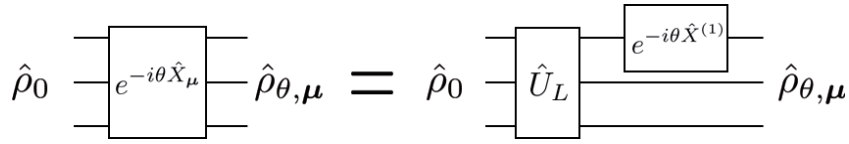

Figure 8: Quantum metrology for a collective quadrature and a single quadrature operator.

where $\boldsymbol{F}$ is a real symmetric $2N \times 2N$ matrix

$$F_{mn}(\hat{\rho}) := 2\sum_{i,j} \frac{(\lambda_i - \lambda_j)^2}{\lambda_i + \lambda_j} \langle i|\hat{X}^{(m)}\,|j\rangle\,\langle j|\hat{X}^{(n)}\,|i\rangle$$

so-called the quantum Fisher information matrix.

For a multi-mode coherent state $|\boldsymbol{\alpha}\rangle$, the quantum Fisher information is given by $I_F(|\boldsymbol{\alpha}\rangle\,, \hat{X}_{\boldsymbol{\mu}}) = 2$ for any $\boldsymbol{\mu}$. Then by the convexity of the quantum Fisher information, the minimum variance of the estimator $(\Delta\theta)^2$ achieved from any classical state is lower bounded by $I_F(|\boldsymbol{\alpha}\rangle\,, \hat{X}_{\boldsymbol{\mu}})^{-1} = 1/2$, which we call the standard quantum limit. As such, a quantum state $\hat{\rho}$ with the quantum Fisher information $I_F(\hat{\rho}, \hat{X}_{\boldsymbol{\mu}})$ larger than 2 will outperform all classical states for metrological tasks associated with the dynamics of a collective quadrature observable $\hat{X}_{\boldsymbol{\mu}}$. We also observe that quantum estimation tasks of the parameter generated by a collective quadrature observable are equivalent to estimating the parameter generated by a quadrature observable for a single mode up to a linear optical unitary operation. In other words, one can always find an optical linear unitary operator $\hat{U}_L$ such that $\hat{U}_L e^{-i\theta\hat{X}_{\boldsymbol{\mu}}}\hat{U}_L^{\dagger} = e^{-i\theta\hat{X}^{(k)}}$ for any given $k \in \{1, 2, \cdots, 2N\}$ (See Fig. 8). Also, a displacement operation in any mode does not change the value of the quantum Fisher information with respect to $\hat{X}_{\boldsymbol{\mu}}$.

Consequently, $\max_{\boldsymbol{\mu}\in\mathcal{S}} \boldsymbol{\mu}^T \boldsymbol{F} \boldsymbol{\mu} = \lambda_{\max}(\boldsymbol{F})$ leads to Eq, (4.3). Also, Eq. (4.4) can be derived using $\int_{\mathcal{S}} \frac{d^{2N}\boldsymbol{\mu}}{\mathrm{Vol}(\mathcal{S})} (\boldsymbol{\mu}^T \boldsymbol{F} \boldsymbol{\mu}) = \frac{1}{2N} \mathrm{Tr}(\boldsymbol{F})$, since $\boldsymbol{F}$ is a real symmetric matrix.

Based on this observation, we introduce two different measures to quantify the metrological power of multi-mode optical fields. First, one may optimize the metrological power with respect to the quadrature among all possible parametrizations $\boldsymbol{\mu}$.

$$\mathcal{P}_{\mathrm{opt}}(\hat{\rho}) := \frac{1}{2} \max_{\boldsymbol{\mu}\in\mathcal{S}} I_F(\hat{\rho}, \hat{X}_{\boldsymbol{\mu}}) = \frac{\lambda_{\max}(\mathbf{F})}{2}, \tag{4.3}$$

where $\mathcal{S} = \{\boldsymbol{\mu} | \sum_{n=1}^{N} |\mu_n|^2 = 1\}$ and $\lambda_{\max}(\mathbf{F})$ is the maximum eigenvalue of $\boldsymbol{F}$. This quantifies the maximum sensitivity of estimating θ, $\min_{\boldsymbol{\mu}\in\mathcal{S}} (\Delta\theta)^2_{\boldsymbol{\mu}} = \left[\max_{\boldsymbol{\mu}\in\mathcal{S}} \boldsymbol{\mu}^T \boldsymbol{F} \boldsymbol{\mu}\right]^{-1} = (2\mathcal{P}_{\mathrm{opt}})^{-1}$, which can be obtained by first performing some linear optical unitary operation $\hat{U}_L$, followed by estimating θ with respect to the single mode generator $\hat{X}^{(1)}$. We may also define the mean metrological power over all such parametrizations $\boldsymbol{\mu}$,

$$\mathcal{P}_{\mathrm{mean}}(\hat{\rho}) := \frac{1}{2} \int_{\mathcal{S}} \frac{d^{2N}\boldsymbol{\mu}}{\mathrm{Vol}(\mathcal{S})} I_F(\hat{\rho}, \hat{X}_{\boldsymbol{\mu}}) = \frac{\mathrm{Tr}(\mathbf{F})}{4N}, \tag{4.4}$$

where $d^{2N}\boldsymbol{\mu} = d^2\mu_1 d^2\mu_2 \cdots d^2\mu_N$ and $\mathrm{Vol}(\mathcal{S}) = \int_{\mathcal{S}} d^{2N}\boldsymbol{\mu} = 2\pi^N/(N-1)!$. Normalization factors for both Eqs. (4.3) and (4.4) are chosen to such that the metrological power of coherent states to be 1. Especially for $\mathcal{P}_{\mathrm{mean}}$ this normalization corresponds to (2 times) the standard quantum limit for displacement estimation achievable by coherent states in N independent sensors, i.e., N optical modes. Now we prove following properties of the

metrological powers:

Proposition 3 (Metrological power of light)**.**

1. *For a pure state $|\psi\rangle$, $\mathcal{P}(|\psi\rangle) \geq 1$, where equality holds if and only if $|\psi\rangle$ is a coherent state $|\boldsymbol{\alpha}\rangle$. For a mixed state $\hat{\rho}$, $\mathcal{P}(\hat{\rho}) \leq 1$ when $\hat{\rho}$ is classical.*

2. *Linear optical unitaries do not change the metrological power, i.e. $\mathcal{P}(\hat{U}_L\hat{\rho}\hat{U}_L^\dagger) = \mathcal{P}(\hat{\rho})$.*

3. *Combining two optical fields A and B cannot increase the overall metrological power, i.e. $\mathcal{P}(\hat{U}_L(\hat{\rho}_A\otimes\hat{\sigma}_B)\hat{U}_L^\dagger) \leq \max\{\mathcal{P}(\hat{\rho}_A), \mathcal{P}(\hat{\sigma}_B)\}$, regardless of the number of modes in each field.*

We use the notation $\mathcal{P}$ when describing both $\mathcal{P}_{\text{opt}}$ and $\mathcal{P}_{\text{mean}}$ for simplicity. All technical proofs in this chapter are presented in Appendix. It is important to notice from Proposition 3 that *"a pure quantum state outperforms all classical states in the metrological power if and only if the state is non-classical (i.e., contains negative P distribution)."*

4.3.3 Quantifying nonclassicality via metrological power

Based on the above definitions, we introduce the following measure of non-classicality for multi-mode optical states. For a pure state $|\psi\rangle$ in bosonic systems, we define

$$\mathcal{C}(|\psi\rangle) := \mathcal{P}_{\text{mean}}(|\psi\rangle) - 1 \tag{4.5}$$

as a non-classality measure. Then we extend this measure to quantify non-classicality of any mixed state by taking convex roof of $\mathcal{C}$:

$$\mathcal{Q}(\hat{\rho}) := \min_{\{p_i, |\psi_i\rangle\}} \sum_i p_i \mathcal{C}(|\psi_i\rangle), \tag{4.6}$$

where $\{p_i, |\psi_i\rangle\}$ is a pure state decomposition of $\hat{\rho}$ satisfying $\hat{\rho} = \sum_i p_i |\psi_i\rangle \langle\psi_i|$ with $p_i \geq 0$ and $|\psi_i\rangle$. The following is a key result of this chapter.

Theorem 7. *$\mathcal{Q}$ is a nonclassicality measure, satisfying the conditions (Q1)–(Q3).*

We note that the value of nonclassicality is bounded from above by $\mathcal{Q}(\hat{\rho}) \leq 2\bar{n}$, where $\bar{n} = \mathrm{Tr}\left[\sum_{n=1}^{N} \hat{a}_n^\dagger \hat{a}_n \hat{\rho}\right]$ is the mean photon number.

In many general, the convex roof construction is complicated to compute. In such cases, the optimal metrological power $\mathcal{P}_{\mathrm{opt}}$ can be considered as another option to quantify nonclassicality,

$$\mathcal{M}(\hat{\rho}) = \max\left\{\mathcal{P}_{\mathrm{opt}}(\hat{\rho}) - 1, 0\right\}. \tag{4.7}$$

However, there is a compromise since this nonclassicality measure is not faithful, so it does not strictly satisfy the conditions for a nonclassicality measure which was previously defined. Nonetheless, it still has many useful properties.

Theorem 8. *The nonclassicality quantifier $\mathcal{M}$ satisfies following properties:*

1. $\mathcal{M}(\hat{\rho}) = 0$ *if $\hat{\rho}$ is classical,*

2. *$\mathcal{M}$ is invariant under linear optical unitaries $\hat{U}_L$ and weakly monotone under linear optical maps,*

3. *$\mathcal{M}$ is convex,*

4. *Multiple copies of the same state do not increase $\mathcal{M}$, i.e. $\mathcal{M}(\hat{\rho}^{\otimes M}) = \mathcal{M}(\hat{\rho})$. More generally, $\mathcal{M}(\hat{\rho}_A \otimes \hat{\sigma}_B) = \max\{\mathcal{M}(\hat{\rho}_A), \mathcal{M}(\hat{\sigma}_B)\}$.*

Therefore, this quantifier can witness nonclassicality, since any state with non-zero $\mathcal{M}$ is nonclassical. Although $\mathcal{M}(\hat{\rho}) = 0$ does not guarantee that $\hat{\rho}$ is classical in general, this type of measure is easier to calculate especially for Gaussian states. In particular, $\mathcal{M}(\hat{\rho}) = 0$ is also sufficient condition for single-mode Gaussian states to be classical, i.e. the measrure is faithful over single mode Gaussian states. We also observe that the last property in Theorem 8 fulfills one of the proposed requirements that is necessary to quantify the genuine quantum macroscopicity: the accumulation microscopic quantum coherence should be distinguished from the genuine macroscopic coherence present in states such as GHZ-states [37]. Similar quantum macroscopicity measures for optical systems have been proposed in Ref. [123, 124] that are also based on the quantum Fisher information, for instance the quantity $\max_{\vec{\phi}} I_F(\hat{\rho}, \hat{X}_{\vec{\phi}})/N$ using the sum of quadratures $\hat{X}_{\vec{\phi}} = \sum_{n=1}^{N} \hat{X}_{\phi_n}^{(n)}$, where $\hat{X}_{\phi_n}^{(n)} = \cos\phi_n \hat{X}^{(n)} + \sin\phi_n \hat{P}^{(n)}$ and $\vec{\phi} = (\phi_1, \phi_2, \cdots, \phi_N)^T$. In this case, however, we point out that a linear bosonic map can increase the measure, since $\hat{X}_{\vec{\phi}}$ in general does not transform in a covariant way, i.e. $\hat{U}_L^\dagger \hat{X}_{\vec{\phi}} \hat{U}_L \neq \hat{X}_{\vec{\phi}'}$. Thus, measures of this type do not fit into the resource theoretical description under linear optical maps, although it may capture many properties of macroscopic coherence.

4.3.4 Examples and applications

We demonstrate that well-known non-classical optical states such as Fock states $|n\rangle$, NOON-states $|N\rangle|0\rangle + |0\rangle|N\rangle$, and optical cat states $|\alpha\rangle + |-\alpha\rangle$ all achieve $\mathcal{Q} = 2\bar{n}$ which is the maximal allowed value for a given mean photon number. Also, a decohered cat state $\hat{\rho}_\Gamma = |\alpha\rangle\langle\alpha| + |-\alpha\rangle\langle-\alpha| + \Gamma(|\alpha\rangle\langle-\alpha| + |-\alpha\rangle\langle\alpha|)$ is non-classical unless $\Gamma = 0$, and also $\mathcal{M}(\hat{\rho}) > 0$ for non-zero $\Gamma > 0$, i.e., $\mathcal{M}$ is a faithful nonclassicality measure for decohered cat states. Due to the invariance under linear optical unitary operations, we can also compare the quantum macroscopicity between an entangled coherent state $|\alpha\rangle_1|\alpha\rangle_2 + |-\alpha\rangle_1|-\alpha\rangle_2$ and an optical cat state $|\alpha\rangle + |-\alpha\rangle$. Note that we can convert the entangled coherent state into $(|\sqrt{2}\alpha\rangle_1 + |-\sqrt{2}\alpha\rangle_1)|0\rangle_2$ using a $50:50$ beam splitter. As such, the degree of nonclassicality in terms of $\mathcal{M}$ for the entangled coherent state is equivalent with an optical cat state with an amplitude $\sqrt{2}\alpha$.

We also apply our result to Gaussian states. A single-mode Gaussian state can be represented as $\hat{\rho}_G = \hat{D}(\alpha)\hat{S}(\xi)\hat{\tau}\hat{S}^\dagger(\xi)\hat{D}^\dagger(\alpha)$, by using a squeezing operation $\hat{S}(\xi) = \exp\left[-\xi\hat{a}^{\dagger 2}/2 + \xi^*\hat{a}^2/2\right]$ and a displacement operation $\hat{D}(\alpha) = \exp\left[\alpha\hat{a}^\dagger - \alpha^*\hat{a}\right]$ on a thermal state $\hat{\tau} = \sum_n \bar{n}_{\rm th}^n/(1+\bar{n}_{\rm th})^{n+1}|n\rangle\langle n|$ with the mean photon number $\bar{n}_{\rm th}$. Among single-mode Guassian states, a pure displaced squeezed state $\hat{D}(\alpha)\hat{S}(\xi)|0\rangle$ gives the maximum nonclassicality $\mathcal{C} = 2\bar{n}$. The optimal metrological power is given by $\mathcal{M}(\hat{\rho}_G) = \max\{\exp(2r)/(2\bar{n}_{\rm th}+1) - 1, 0\}$, which depends on the mean photon number of the thermal state $\bar{n}_{\rm th}$ and the squeezing parameter $r = |\xi|$. Note that a single-mode Gaussian state is classical (i.e., has a pos-

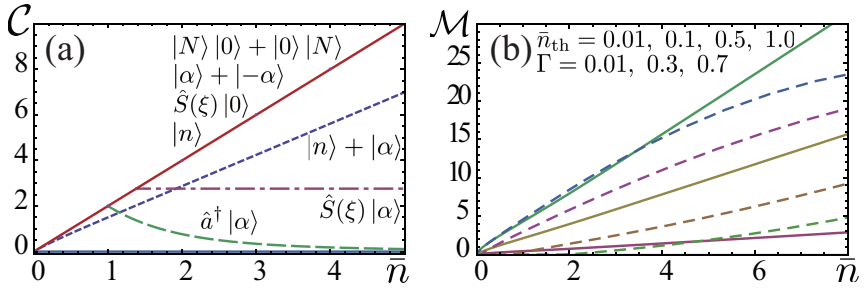

Figure 9: Nonclassicality vs. mean photon number $\bar{n}$. (a) $\mathcal{C}$ gives the maximum value $2\bar{n}$ (solid line) for NOON states $|N\rangle|0\rangle + |0\rangle|N\rangle$, cat states $|\alpha\rangle + |-\alpha\rangle$, squeezed vacuum states $\hat{S}(\xi)|0\rangle$, and Fock states $|n\rangle$. Also, superposition between Fock state and coherent state $|n\rangle + |\alpha\rangle$ with $n = |\alpha|^2$ (dotted line), squeezed coherent states $\hat{S}(\xi)|\alpha\rangle$ for $\xi = 1.0$ (dot-dashed line), and photon-added coherent states $\hat{a}^\dagger|\alpha\rangle$ (dashed line) are evaluated. (b) Nonclassicality quantifier $\mathcal{M}$ for decohered cat states $\hat{\rho}_\Gamma$ (solid lines) and squeezed thermal states $\hat{S}(\xi)\hat{\tau}\hat{S}^\dagger(\xi)$ (dashed lines). Decoherence factors and mean photon numbers in thermal states are given by $\Gamma = 0.01,\ 0.3,\ 0.7$ and $\bar{n}_{\rm th} = 0.01,\ 0.1,\ 0.5,\ 1.0$, respectively (both starting from above).

itive P-representation) when $r_c \leq (1/2)\log(2\bar{n}_{\rm th}+1)$. Thus, *the optimal metrological power $\mathcal{M}(\hat{\rho}_G)$ is zero if and only if a single-mode Gaussian state $\hat{\rho}_G$ is classical.*

We also provide an example of two mode squeezed states $\hat{\rho}_{\rm TM} = \hat{S}_{\rm TM}(\zeta)|00\rangle_{12}$, where $\hat{S}_{\rm TM}(\zeta) = \exp\left[-\zeta\hat{a}_1^\dagger\hat{a}_2^\dagger + \zeta^*\hat{a}_1\hat{a}_2\right]$. For this example, local quadrature operator measurements do not appear to have any quantum advantage over classical states since the local states are thermal states. On the other hand, a two mode squeezed state can be converted into the product of two single-mode squeezed states via a linear optical unitary by using the $50:50$ beam splitter, $\hat{U}_{\rm BS}\hat{S}_{\rm TM}(\zeta)\hat{U}_{\rm BS}^\dagger = \hat{S}_1(\zeta)\otimes\hat{S}_2(\zeta)$. As such, the nonclassicality of the two mode squeezed state and two single-mode squeezed states, have the same metrological power. More generally,

for any multi-mode Gaussian state $\hat{\rho}_{(\boldsymbol{V},\boldsymbol{d})}$ can be parametrized by the covariance matrix $\boldsymbol{V}$ and the displacement $\boldsymbol{d}$, with its characteristic function $\chi(\boldsymbol{\xi}) = \mathrm{Tr}[\hat{D}(\boldsymbol{\xi})\hat{\rho}_{(\boldsymbol{V},\boldsymbol{d})}] = e^{-\frac{1}{2}\boldsymbol{\xi}^T\boldsymbol{V}\boldsymbol{\xi}+\boldsymbol{\xi}^T\boldsymbol{d}}$. Then there exists the sympletic matrix $\boldsymbol{S}$ such that $\boldsymbol{V} = \boldsymbol{S}(\boldsymbol{V}^{\oplus})\boldsymbol{S}^T$, where $\boldsymbol{V}^{\oplus} = \oplus_{n=1}^{N}\nu_n\mathbb{1}_n$ with $\boldsymbol{S}\boldsymbol{\Omega}\boldsymbol{S}^T = \boldsymbol{\Omega}$ for a block matrix $\boldsymbol{\Omega} = \begin{pmatrix} 0 & 1 \\ -1 & 0 \end{pmatrix} \otimes \mathbb{1}_{N\times N}$. Using the fact that every sympletic operation S has corresponding multi-mode unitary operation $\hat{U}_{\boldsymbol{S}}$ (not necessarily be a linear optical map), we can express the state as follows:

$$\hat{\rho}_{(\boldsymbol{V},\boldsymbol{d})} = \hat{U}_{\boldsymbol{S}}\left(\otimes_{n=1}^{N}\hat{\tau}_n\right)\hat{U}_{\boldsymbol{S}}^{\dagger},$$

where $\hat{\tau}_n$ is a thermal state of n-th mode with mean-photon number $(\nu_n - 1)/2$. Then the quantum Fisher information with respect to $\hat{X}_{\boldsymbol{\mu}}$ is given by

$$I_F(\hat{\rho}_{(\boldsymbol{V},\boldsymbol{d})}, \hat{X}_{\boldsymbol{\mu}}) = I_F(\hat{U}_{\boldsymbol{S}}\left(\oplus_{n=1}^{N}\hat{\tau}_n\right)\hat{U}_{\boldsymbol{S}}^{\dagger}, \hat{X}_{\boldsymbol{\mu}}) = I_F(\otimes_{n=1}^{N}\hat{\tau}_n, \hat{U}_{\boldsymbol{S}}^{\dagger}\hat{X}_{\boldsymbol{\mu}}\hat{U}_{\boldsymbol{S}}).$$

It is important to note that $\hat{U}_{\boldsymbol{S}}^{\dagger}\hat{X}_{\boldsymbol{\mu}}\hat{U}_{\boldsymbol{S}} = \hat{X}_{\tilde{\boldsymbol{\mu}}}$, where $\tilde{\boldsymbol{\mu}} = (\boldsymbol{S}^{-1})^T\boldsymbol{\mu}$, where $||\tilde{\boldsymbol{\mu}}||^2 \neq 1$ in general.

Moreover, the quantum Fisher information matrix for a multi-mode thermal state is given by $\boldsymbol{F}(\otimes_{n=1}^{N}\hat{\tau}_n) = 2\oplus_{n=1}^{N}\nu_n^{-1}\mathbb{1}_n = 2(\boldsymbol{V}^{\oplus})^{-1} = 2\boldsymbol{S}^T\boldsymbol{V}^{-1}\boldsymbol{S}$. Using the expression of Eq. (4.2), we get

$$\begin{aligned} I_F(\hat{\rho}_{(\boldsymbol{V},\boldsymbol{d})}, \hat{X}_{\boldsymbol{\mu}}) &= 2((\boldsymbol{S}^{-1})^T\boldsymbol{\mu})^T\boldsymbol{F}(\otimes_{n=1}^{N}\hat{\tau}_n)(\boldsymbol{S}^{-1})^T\boldsymbol{\mu} \\ &= 2\boldsymbol{\mu}^T(\boldsymbol{S}^{-1}\boldsymbol{S}^T\boldsymbol{V}^{-1}\boldsymbol{S}(\boldsymbol{S}^{-1})^T)\boldsymbol{\mu}. \end{aligned}$$

We then obtain the following closed form formula:

$$\mathcal{M}(\hat{\rho}_{(\boldsymbol{V},\boldsymbol{d})}) = \max\{\lambda_{\max}\left[\boldsymbol{S}^{-1}\boldsymbol{S}^{T}\boldsymbol{V}^{-1}\boldsymbol{S}(\boldsymbol{S}^{-1})^{T}\right] - 1, 0\}. \tag{4.8}$$

in terms of $\boldsymbol{V}$ and $\boldsymbol{S}$.

Based on our result, nonclassicality can be detected in the laboratory by accessing quantum Fisher information with respect to a collective quadrature observables $\hat{X}_{\boldsymbol{\mu}}$. It has been suggested in Ref. [82] that one can estimate the value of quantum Fisher information by the following lower bound $\mathcal{M}(\hat{\rho}) \geq 2\theta^{-1}\arccos^2 B_{\Omega} - 1$, where $B_{\Omega} = \sum_m \sqrt{p_m q_m}$ with $q_m = \mathrm{Tr}[\hat{\Omega}_m\hat{\rho}]$ and $q_m = \mathrm{Tr}[\hat{\Omega}_m e^{-i\theta\hat{X}_{\boldsymbol{\mu}}}\hat{\rho}e^{i\theta\hat{X}_{\boldsymbol{\mu}}}]$ for a generalized measurement given by a set of positive operators $\{\hat{\Omega}_m\}$. Moreover, we can adopt the quadrature measurement $\hat{X}^{(n)}_{\phi_n} = (\hat{a}_n e^{-i\phi_n} + \hat{a}_n^{\dagger}e^{i\phi_n})/\sqrt{2}$ on each mode which can be realized by the local homodyne-detection. Note that the unitary evolution generated by $\hat{X}_{\boldsymbol{\mu}}$ is in fact just a a multi-mode displacement operation, $e^{-i\theta\hat{X}_{\boldsymbol{\mu}}} = \otimes_{i=n}^{N}\hat{D}_n(-i\theta\mu_n^*/\sqrt{2})$, where $\hat{D}_n$ are displacement operators on n-th mode. This observation leads to $B_{\Omega} = \int d^N\boldsymbol{x}\sqrt{p(\boldsymbol{x})p(\boldsymbol{x}-\boldsymbol{\chi}\theta)}$, where $p(\boldsymbol{x})$ is a probability distribution for multi-mode quadratures $\boldsymbol{x} = (x_1^{\phi_1}, x_2^{\phi_2}, \cdots, x_N^{\phi_N})^T$ and $\boldsymbol{\chi} = (\chi_1, \chi_2, \cdots, \chi_N)^T$ with $\chi_n = \mathrm{Re}[\mu_n]\sin\phi_n + \mathrm{Im}[\mu_n]\cos\phi_n$. For the limiting case of $\theta \to 0$,

$$\mathcal{M}(\hat{\rho}) \geq \max_{\boldsymbol{\mu}\in S}\left[\lim_{\theta\to 0}\frac{2\arccos^2 B_{\Omega}}{\theta^2}\right] - 1 = \frac{\lambda_{\max}[\boldsymbol{G}]}{2} - 1, \tag{4.9}$$

where $\boldsymbol{G}$ is a $2N \times 2N$ real matrix with

$$G_{kl} = \int d^N \boldsymbol{x} p(\boldsymbol{x})^{-1} \frac{\partial p(\boldsymbol{x})}{\partial x_n^{\phi_n}} \frac{\partial p(\boldsymbol{x})}{\partial x_m^{\phi_m}} \times \begin{cases} \sin\phi_n & (k = 2n-1) \\ -\cos\phi_n & (k = 2n) \end{cases} \begin{cases} \sin\phi_m & (l = 2n-1) \\ -\cos\phi_m & (l = 2n) \end{cases}.$$

Therefore, only the probability distribution for a multi-mode quadrature observable is required to detect the nonclassicality of optical fields. Even in the case of a limited measurement precision, Eq. (6) of Ref. [82] or Theorem 2 of Ref. [53] can be adopted to estimate the value of $\mathcal{M}$.

In practical sense, the following metrological procedure can be applied to a displacement sensing task. Note that estimation of the parameter θ generated by a collective quadrature operators $e^{-i\theta\hat{X}_{\boldsymbol{\mu}}}$ is identical to a displacement sensing task for $\otimes_{n=1}^{N}\hat{D}_i(-i\theta\mu_n^*/\sqrt{2})$. In this task, the nonclassicality of a cavity field becomes a useful resource for a precise force-sensing. In linearized optomechanical systems, the interaction Hamiltonian is given by $\hat{H}_{\rm int}^{(\rm lin)} = -\hbar g_0\sqrt{\bar{n}_{\rm cav}}(\delta\hat{a}^\dagger + \delta\hat{a})(\hat{b} + \hat{b}^\dagger)$, where g_0 is the coupling strength, $\bar{n}_{\rm cav}$ is the mean photon number in cavity, and $\hat{a}$ and $\hat{b}$ are annihilation operators for the cavity and the mechanical mode, respectively. $\delta\hat{a}$ denotes the fluctuation from the average coherent field $\hat{a} = \bar{\alpha} + \delta\hat{a}$ with $\bar{\alpha} = \langle\hat{a}\rangle$ [125, 126]. When the position of the mirror $\hat{x} = (\hat{b} + \hat{b}^\dagger)/\sqrt{2}$ is considered classical, its deviation δx, generated for example by an external force, is captured as a displacement $\hat{D}(i\hbar g_0\sqrt{\bar{n}_{\rm cav}}\delta x/2)$ on the cavity field. Thus, higher degree of nonclassicality $\mathcal{M}$ in the cavity field might be an important resource for high resolution force-sensing tasks.

4.3.5 Appendix

4.3.5.1 Proof for Proposition 3

Proof: We first show that $\mathcal{P}(|\psi\rangle) \geq 1$. Taking a collective quadrature observable $\hat{X}_{\boldsymbol{\mu}}$ and its conjugate operator $\hat{P}_{\boldsymbol{\mu}} = (\hat{a}_{\boldsymbol{\mu}} - \hat{a}^{\dagger}_{\boldsymbol{\mu}})/(\sqrt{2}i) = \hat{X}_{\tilde{\boldsymbol{\mu}}}$, with $\tilde{\mu}_n = -i\mu_n$ for every n. Then, we note that $[\hat{X}_{\boldsymbol{\mu}}, \hat{P}_{\boldsymbol{\mu}}] = i$. Then we have

$$\begin{aligned}
\mathrm{Var}(\psi, \hat{X}_{\boldsymbol{\mu}}) + \mathrm{Var}(\psi, \hat{P}_{\boldsymbol{\mu}}) &\geq 2\sqrt{\mathrm{Var}(\psi, \hat{X}_{\boldsymbol{\mu}})\mathrm{Var}(\psi, \hat{P}_{\boldsymbol{\mu}})} \\
&\geq |\langle [\hat{X}_{\boldsymbol{\mu}}, \hat{P}_{\boldsymbol{\mu}}] \rangle| \\
&= 1,
\end{aligned}$$

where the second inequality is the Heisenberg uncertainty relation. Then, using the fact that $I_F(|\psi\rangle, \hat{X}_{\boldsymbol{\mu}}) = 4\mathrm{Var}(\psi, \hat{X}_{\boldsymbol{\mu}})$,

$$\begin{aligned}
\mathcal{P}_{\mathrm{opt}}(|\psi\rangle) &= \frac{1}{2} \max_{\boldsymbol{\mu} \in \mathcal{S}} I_F(|\psi\rangle, \hat{X}_{\boldsymbol{\mu}}) \\
&\geq \frac{1}{4} \left[I_F(|\psi\rangle, \hat{X}_{\boldsymbol{\mu}}) + I_F(|\psi\rangle, \hat{P}_{\boldsymbol{\mu}}) \right] \\
&= \mathrm{Var}(\psi, \hat{X}_{\boldsymbol{\mu}}) + \mathrm{Var}(\psi, \hat{P}_{\boldsymbol{\mu}}) \geq 1,
\end{aligned}$$

and

$$\begin{aligned}
\mathcal{P}_{\mathrm{mean}}(|\psi\rangle) &= \frac{1}{2} \int_{\mathcal{S}} \frac{d^{2N}\boldsymbol{\mu}}{\mathrm{Vol}(\mathcal{S})} I_F(|\psi\rangle, \hat{X}_{\boldsymbol{\mu}}) \\
&= \frac{1}{4} \left[\int_{\mathcal{S}} \frac{d^{2N}\boldsymbol{\mu}}{\mathrm{Vol}(\mathcal{S})} I_F(|\psi\rangle, \hat{X}_{\boldsymbol{\mu}}) + \int_{\mathcal{S}} \frac{d^{2N}\tilde{\boldsymbol{\mu}}}{\mathrm{Vol}(\mathcal{S})} I_F(|\psi\rangle, \hat{X}_{\tilde{\boldsymbol{\mu}}}) \right] \\
&= \int_{\mathcal{S}} \frac{d^{2N}\boldsymbol{\mu}}{\mathrm{Vol}(\mathcal{S})} \left[\mathrm{Var}(\psi, \hat{X}_{\boldsymbol{\mu}}) + \mathrm{Var}(\psi, \hat{P}_{\boldsymbol{\mu}}) \right] \\
&\geq 1,
\end{aligned}$$

since $d^{2N}\boldsymbol{\mu} = d^{2N}\tilde{\boldsymbol{\mu}}$ when integrating over $\mathcal{S}$.

We now show that the equality holds *if and only if* $|\psi\rangle$ is a coherent state. Note that $\mathcal{P}_{\rm opt}(|\psi\rangle) = 1$ or $\mathcal{P}_{\rm mean}(|\psi\rangle) = 1$ is equivalent with the condition $(1/2)I_F(|\psi\rangle, \hat{X}_{\boldsymbol{\mu}}) = 1$ for any $\boldsymbol{\mu} \in \mathcal{S}$. Then the "*if*" part can be verified by directly showing that for any coherent state $|\boldsymbol{\alpha}\rangle = |\alpha_1\alpha_2\cdots\alpha_N\rangle$.

$$\begin{aligned}\frac{1}{2}I_F(|\boldsymbol{\alpha}\rangle, \hat{X}_{\boldsymbol{\mu}}) &= \frac{1}{2}I_F(|\alpha_1\alpha_2\cdots\alpha_N\rangle, \sum_{n=1}^{N}\left(\mu_n\hat{a}_n + \mu_n^*\hat{a}_n^\dagger\right)/\sqrt{2}) \\ &= \frac{1}{2}\sum_{n=1}^{N}|\mu_n|^2 I_F(|\alpha_n\rangle\langle\alpha_n|, \hat{X}_{\boldsymbol{\mu}_n}) \\ &= 1,\end{aligned}$$

where $\hat{X}_{\boldsymbol{\mu}_n} = |\mu_n|^{-1}(\mu_n\hat{a}_n + \mu_n^*\hat{a}_n^\dagger)/\sqrt{2}$ is a single-mode quadrature operator of the n-th mode. We used the fact that the quantum Fisher information of any quadrature observable $\hat{x}_\theta = (\hat{a}e^{-i\theta} + \hat{a}^\dagger e^{i\theta})/\sqrt{2}$ is given by $I_F(|\alpha\rangle\langle\alpha|, \hat{x}_\theta) = 2$ for any single-mode coherent state $|\alpha\rangle$.

The "*only if*" part can be proved as follows. The N-mode pure optical state $|\psi\rangle$ can be decomposed into one selected mode and remaining modes, $|\psi\rangle = \sum_j \sqrt{\lambda_j}|\phi_j^{(1)}\rangle|\phi_j^{(2\cdots N)}\rangle$, by the Schmidt decomposition. Then we

note that

$$
\begin{aligned}
&\mathrm{Var}(\psi, \hat{X}^{(1)}) + \mathrm{Var}(\psi, \hat{X}^{(2)}) \\
&= \sum_j \lambda_j \left[\langle \phi_j^{(1)} | \hat{x}_1^2 | \phi_j^{(1)} \rangle + \langle \phi_j^{(1)} | \hat{p}_1^2 | \phi_j^{(1)} \rangle \right] \\
&\quad - \left[\sum_j \langle \phi_j^{(1)} | \hat{x}_1 | \phi_j^{(1)} \rangle \right]^2 - \left[\sum_j \langle \phi_j^{(1)} | \hat{p}_1 | \phi_j^{(1)} \rangle \right]^2 \\
&\geq \sum_j \lambda_j \left[\mathrm{Var}(\phi_j^{(1)}, \hat{x}_1) + \mathrm{Var}(\phi_j^{(1)}, \hat{p}_1) \right] \\
&\geq 1,
\end{aligned}
$$

where $\hat{x}_1 = (\hat{a}_1 + \hat{a}_1^\dagger)/\sqrt{2}$ and $\hat{p}_1 = (\hat{a}_1 - \hat{a}_1^\dagger)/\sqrt{2i}$ are quadrature operators on the first mode. The first inequality saturates only if every $\langle \phi_j^{(1)} | \hat{x}_1 | \phi_j^{(1)} \rangle$ gives the same value and $\langle \phi_j^{(1)} | \hat{p}_1 | \phi_j^{(1)} \rangle$ also gives the same value for all j ($\langle \phi_j^{(1)} | \hat{x}_1 | \phi_j^{(1)} \rangle$ and $\langle \phi_j^{(1)} | \hat{p}_1 | \phi_j^{(1)} \rangle$ are not necessarily to be the same). The second inequality is the Heisenberg uncertainty and only coherent state $|\phi_j^{(1)}\rangle = |\alpha_j^{(1)}\rangle$ reaches the bound 1. Thus, combining these two results, $(1/2) I_F(|\psi\rangle, \hat{X}_{\boldsymbol{\mu}}) = 1$ for all $\boldsymbol{\mu} \in \mathcal{S}$ implies $\mathrm{Var}(\psi, \hat{X}^{(1)}) + \mathrm{Var}(\psi, \hat{X}^{(2)}) = 1$, thus $|\psi\rangle$ should be written in the form $|\psi\rangle = \left|\alpha^{(1)}\right\rangle \left|\phi^{(2 \cdots N}\right\rangle$, since different coherence states α_j have different values of $\langle \hat{x} \rangle$ or $\langle \hat{p} \rangle$. We can repeat the same process for each mode, then we finally conclude that $|\psi\rangle = \left|\alpha^{(1)}\right\rangle \cdots \left|\alpha^{(N)}\right\rangle$ is a multi-mode coherent state.

Now we prove that $\mathcal{P}(\hat{\rho}) \leq 1$ when $\hat{\rho}$ is classical. Note that a classical state can be expressed as a convex sum of multi-mode coherent states, i.e. $\hat{\rho} = \sum_i p_i \left|\boldsymbol{\alpha}_i\right\rangle \left\langle \boldsymbol{\alpha}_i\right|$ for positive p_i satisfying $\sum_i p_i = 1$. Then by the

convexity of the quantum Fisher information, we get

$$I_F(\hat{\rho}, \hat{X}_{\boldsymbol{\mu}}) \leq \sum_i p_i I_F(|\boldsymbol{\alpha}_i\rangle \langle \boldsymbol{\alpha}_i|, \hat{X}_{\boldsymbol{\mu}}) \leq 2,$$

where $I_F(|\boldsymbol{\alpha}_i\rangle \langle \boldsymbol{\alpha}_i|, \hat{X}_{\boldsymbol{\mu}}) = 2$ for any coherent state $|\boldsymbol{\alpha}\rangle$. Then by either taking optimization over $\boldsymbol{\mu}$ or averaging over $\mathcal{S} = \{\boldsymbol{\mu} | \sum_{n=1}^{N} |\mu_n|^2 = 1\}$, we have $\mathcal{P}_{\rm opt} \leq 1$ and $\mathcal{P}_{\rm mean} \leq 1$, respectively.

Next, we demonstrate that the metrological power $\mathcal{P}$ is invariant under optical linear unitaries. Note that $I_F(\hat{U}_L \hat{\rho} \hat{U}_L^\dagger, \hat{X}_{\boldsymbol{\mu}}) = I_F(\hat{\rho}, \hat{U}_L^\dagger \hat{X}_{\boldsymbol{\mu}} \hat{U}_L) = I_F(\hat{\rho}, \hat{X}_{\boldsymbol{\mu}'})$, where there exist an $2N \times 2N$ unitary matrix V such that $\boldsymbol{\mu}' = V\boldsymbol{\mu} \in \mathcal{S}$. Moreover the unitary matrix V does not change the structure of $\mathcal{S}$, i.e. $V\mathcal{S}V^\dagger = \mathcal{S}$ and $|\det V| = 1$, which guarantees that the optimal and mean metrological powers do not change by such unitaries.

Finally, we show that combining two-uncorrelated optical systems cannot increase the metrological powers. Suppose that the optical field A and B of N and M modes, respectively. Then a collective bosonic operator in the combined system can be expressed using a $2(N + M)$ dimensional real vector $\boldsymbol{\mu}$. Let us assume that the optimal metrological power $\mathcal{P}_{\rm opt}$ of the combined system is given by $\mathcal{P}_{\rm opt}(\hat{U}_L(\hat{\rho} \otimes \hat{\sigma})\hat{U}_L^\dagger) = \mathcal{P}_{\rm opt}(\hat{\rho} \otimes \hat{\sigma}) = (1/2) \max_{\boldsymbol{\mu} \in \mathcal{S}} I_F(\hat{\rho} \otimes \hat{\sigma}, \hat{X}_{\boldsymbol{\mu}})/2 = (1/2) I_F(\hat{\rho} \otimes \hat{\sigma}, \hat{X}_{\tilde{\boldsymbol{\mu}}})$, where maximum is achieved at $\{\tilde{\mu}_n\}$ and $\hat{U}_L$ does not change the metrological power $\mathcal{P}_{\rm opt}$. Note that the quadrature $\hat{X}_{\tilde{\boldsymbol{\mu}}}$ can be divided into two parts $\hat{X}_{\tilde{\boldsymbol{\mu}}} = \sqrt{\lambda} \hat{X}_{\boldsymbol{\mu}_A} \otimes \mathbb{1}_B + \sqrt{1-\lambda} \mathbb{1}_A \otimes \hat{X}_{\boldsymbol{\mu}_B}$, where

$$\boldsymbol{\mu}_A = \lambda^{-1/2} (\mathrm{Re}\tilde{\mu}_1, -\mathrm{Im}\tilde{\mu}_1, \mathrm{Re}\tilde{\mu}_2, -\mathrm{Im}\tilde{\mu}_2, \cdots, \mathrm{Re}\tilde{\mu}_N, -\mathrm{Im}\tilde{\mu}_N)^T$$

and

$$\boldsymbol{\mu}_B = \frac{(\mathrm{Re}\tilde{\mu}_{N+1}, -\mathrm{Im}\tilde{\mu}_{N+1}, \mathrm{Re}\tilde{\mu}_{N+2}, -\mathrm{Im}\tilde{\mu}_{N+2}, \cdots, \mathrm{Re}\tilde{\mu}_{N+M}, -\mathrm{Im}\tilde{\mu}_{N+M})^T}{\sqrt{1-\lambda}}$$

with $\lambda = \sum_{n=1}^{N} |\tilde{\mu}_i|^2$. Note that $|\boldsymbol{\mu}_A|^2 = 1 = |\boldsymbol{\mu}_B|^2$. Then we have

$$\begin{aligned}
\mathcal{P}_{\mathrm{opt}}(\hat{\rho}\otimes\hat{\sigma}) &= \frac{1}{2} I_F(\hat{\rho}\otimes\hat{\sigma}, \hat{X}_{\tilde{\boldsymbol{\mu}}}) \\
&= \frac{1}{2} I_F(\hat{\rho}\otimes\hat{\sigma}, \sqrt{\lambda}\hat{X}_{\boldsymbol{\mu}_A}\otimes\mathbb{1}_B + \sqrt{1-\lambda}\mathbb{1}_A\otimes\hat{X}_{\boldsymbol{\mu}_B}) \\
&= \frac{1}{2}\left[\lambda I_F(\hat{\rho}, \hat{X}_{\boldsymbol{\mu}_A}) + (1-\lambda) I_F(\hat{\sigma}, \hat{X}_{\boldsymbol{\mu}_B})\right] \\
&\leq \max\{\mathcal{P}_{\mathrm{opt}}(\hat{\rho}), \mathcal{P}_{\mathrm{opt}}(\hat{\sigma})\},
\end{aligned} \tag{4.10}$$

where we used the fact that $\frac{1}{2} I_F(\hat{\rho}, \hat{X}_{\boldsymbol{\mu_A}}) \leq \mathcal{P}_{\mathrm{opt}}(\rho)$ and $\frac{1}{2} I_F(\hat{\sigma}, \hat{X}_{\boldsymbol{\mu_B}}) \leq \mathcal{P}_{\mathrm{opt}}(\sigma)$ and $0 \leq \lambda \leq 1$ for the last inequality.

For the mean metrological power, we note that

$$\mathcal{P}_{\mathrm{mean}}(\hat{\rho}) = \frac{\mathrm{Tr}(\mathbf{F})}{4N} = \frac{1}{4N}\sum_{k=1}^{2N} I_F(\hat{\rho}, \hat{X}^{(k)}).$$

Then we have the same property for the mean metrological power,

$$\begin{aligned}
\mathcal{P}_{\mathrm{mean}}(\hat{\rho}\otimes\hat{\sigma}) &= \frac{1}{4(N+M)} \sum_{i=1}^{2(N+M)} I_F(\hat{\rho}\otimes\hat{\sigma}, \hat{X}^{(n)}) \\
&= \frac{N\mathcal{P}_{\mathrm{mean}}(\hat{\rho}) + M\mathcal{P}_{\mathrm{mean}}(\hat{\sigma})}{N+M} \\
&\leq \max\{\mathcal{P}_{\mathrm{mean}}(\hat{\rho}), \mathcal{P}_{\mathrm{mean}}(\hat{\sigma})\}.
\end{aligned}$$

□

4.3.5.2 Proof of Theorem 7

First, we prove the following statement:

Proposition 4. *For a quantum classical state* $\sum_i p_i \hat{\rho}_A^{(i)} \otimes |i\rangle_B \langle i|$ *with orthogonal basis* $\{|i\rangle_B\}$*, the quantum Fisher information with respect to the given local observable* $\hat{L}_A$ *is given by*

$$I_F\left(\sum_i p_i \hat{\rho}_A^{(i)} \otimes |i\rangle_B \langle i|, \hat{L}_A \otimes \mathbb{1}_B\right) = \sum_i p_i I_F(\hat{\rho}_A^{(i)}, \hat{L}_A). \tag{4.11}$$

Proof: Note that eigenvalues of $\sum_i p_i \hat{\rho}_A^{(i)} \otimes |i\rangle_B \langle i|$ are given by $p_i \lambda_\mu^{(i)}$, where $\lambda_\mu^{(i)}$ are eigenvalues of $\hat{\rho}_A^{(i)}$ with corresponding eigenstates $\left|\phi_\mu^{(i)}\right\rangle$. By direct calculation, we have

$$\begin{aligned}
&I_F\left(\sum_i p_i \hat{\rho}_A^{(i)} \otimes |i\rangle_B \langle i|, \hat{L}_A \otimes \mathbb{1}_B\right) \\
&= 2\sum_{i,j}\sum_{\mu,\nu} \frac{\left(p_i\lambda_\mu^{(i)} - p_j\lambda_\nu^{(j)}\right)^2}{p_i\lambda_\mu^{(i)} + p_j\lambda_\nu^{(j)}} |\langle\phi_\mu^{(i)}|_A \langle i|_B \left(\hat{L}_A \otimes \mathbb{1}_B\right) |\phi_\nu^{(j)}\rangle_A |j\rangle_B|^2 \\
&= 2\sum_{i,j}\sum_{\mu,\nu} \frac{\left(p_i\lambda_\mu^{(i)} - p_j\lambda_\nu^{(j)}\right)^2}{p_i\lambda_\mu^{(i)} + p_j\lambda_\nu^{(j)}} |\langle\phi_\mu^{(i)}|\hat{L}_A|\phi_\nu^{(j)}\rangle_A|^2 |\langle i|\,|j\rangle_B|^2 \\
&= 2\sum_i p_i \sum_{\mu,\nu} \frac{\left(\lambda_\mu^{(i)} - \lambda_\nu^{(i)}\right)^2}{\lambda_\mu^{(i)} + \lambda_\nu^{(j)}} \left|\langle\phi_\mu^{(i)}|\hat{L}_A|\phi_\nu^{(j)}\rangle_A\right|^2 \\
&= \sum_i p_i I_F(\hat{\rho}_A^{(i)}, \hat{L}_A).
\end{aligned} \tag{4.12}$$

□

Now we prove Theorem. 7:

Proof: We prove the condition (Q1): If $\hat{\rho}$ is classical, the state can be represented as a convex sum of coherent states $|\boldsymbol{\alpha}\rangle$, which leads to $\mathcal{Q}(\hat{\rho}) = 0$. Conversely, if $\mathcal{Q}(\hat{\rho}) = \min_{\{p_i,\psi_i\}} \sum_i p_i \mathcal{C}(|\psi_i\rangle) = 0$, there exists a pure state composition of $\hat{\rho} = \sum_i p_i^* |\psi_i^*\rangle \langle\psi_i^*|$ that $\mathcal{C}(|\psi_i^*\rangle) = 0$ for every i. Note that $\mathcal{C}(|\psi_i^*\rangle) = 0$ *if and only if* $|\psi_i^*\rangle$ is a coherent state by Proposition. 3, and using this decomposition, $\hat{\rho}$ can be expressed as a convex sum of coherent states, i.e. $\hat{\rho}$ is classical. Thus we $\mathcal{Q}(\hat{\rho}) = 0$ *if and only if* $\hat{\rho}$ is classical. Also, convexity (Q3) is guaranteed by the convex roof construction.

In order to prove the strong monotonicity (Q2b) of the mean metrological power, we first show that $\sum_i q_i \mathcal{C}(\hat{K}_i |\psi\rangle / \sqrt{q_i}) \leq \mathcal{C}(|\psi\rangle)$ for a set of Kraus operators $\{\hat{K}_i\}$ constructing a linear optical map and $q_i = \mathrm{Tr}\langle\psi|\hat{K}_i^\dagger \hat{K}_i |\psi\rangle$. For simplicity, we let $|\phi_i\rangle = \hat{K}_i |\psi\rangle / \sqrt{q_i}$, then there exists a classical state $\hat{\sigma}_{EE'}$ and a linear optical unitary $\hat{U}_L$, such that

$$\mathrm{Tr}_E \hat{U}_L \left(|\psi\rangle \langle\psi| \otimes \hat{\sigma}_{EE'}\right) \hat{U}_L^\dagger = \sum_i q_i |\phi_i\rangle \langle\phi_i| \otimes |i\rangle_{E'} \langle i|.$$

Note that $\mathcal{C}(|\phi_i\rangle) = (4N)^{-1}\sum_{k=1}^{2N} I_F(|\phi_i\rangle\langle\phi_i|, \hat{X}^{(k)}) - 1$, we get

$$
\begin{aligned}
&\sum_i q_i \mathcal{C}(|\phi_i\rangle) \\
&\quad = \frac{1}{4N}\sum_i q_i \sum_{k=1}^{2N} I_F\left(|\phi_i\rangle\langle\phi_i|, \hat{X}^{(k)}\right) - 1 \\
&\quad = \frac{1}{4N}\sum_{k=1}^{2N} I_F\left(\sum_i q_i |\phi_i\rangle\langle\phi_i| \otimes |i\rangle_{E'}\langle i|, \hat{X}^{(k)} \otimes \mathbb{1}_{E'}\right) - 1 \\
&\quad = \frac{1}{4N}\sum_{k=1}^{2N} I_F\left(\mathrm{Tr}_E \hat{U}_L\left(|\psi\rangle\langle\psi| \otimes \hat{\sigma}_{EE'}\right)\hat{U}_L^\dagger, \hat{X}^{(k)} \otimes \mathbb{1}_{E'}\right) - 1 \\
&\quad \leq \frac{1}{4N}\sum_{k=1}^{2N} I_F\left(\hat{U}_L\left(|\psi\rangle\langle\psi| \otimes \hat{\sigma}_{EE'}\right)\hat{U}_L^\dagger, \hat{X}^{(k)} \otimes \mathbb{1}_{EE'}\right) - 1 \\
&\quad \leq \sum_j \frac{p_j}{4N}\sum_{k=1}^{2N} I_F\left(\hat{U}_L\left(|\psi\rangle\langle\psi| \otimes |\boldsymbol{\alpha}_j\rangle_{EE'}\langle\boldsymbol{\alpha}_j|\right)\hat{U}_L^\dagger, \hat{X}^{(k)} \otimes \mathbb{1}_{EE'}\right) - 1,
\end{aligned}
$$

where $\hat{\sigma}_{EE'} = \sum_j p_j |\boldsymbol{\alpha}_j\rangle\langle\boldsymbol{\alpha}_j|$ is classical, and the first and second inequalities come from contractivity and convexity of the quantum Fisher information, respectively. We prove that

$$
\sum_{k=1}^{2N} I_F\left(\hat{U}_L\left(|\psi\rangle\langle\psi| \otimes |\boldsymbol{\alpha}_j\rangle_{EE'}\langle\boldsymbol{\alpha}_j|\right)\hat{U}_L^\dagger, \hat{X}^{(k)} \otimes \mathbb{1}_{EE'}\right) \leq \sum_{k=1}^{2N} I_F\left(|\psi\rangle\langle\psi|, \hat{X}^{(k)}\right).
$$

Suppose $\hat{\sigma}_{EE'}$ is a M-mode classical state. Then we have

$$\begin{aligned}
&\sum_{k=1}^{2N} I_F\left(\hat{U}_L\left(|\psi\rangle\langle\psi|\otimes|\boldsymbol{\alpha}_j\rangle_{EE'}\langle\boldsymbol{\alpha}_j|\right)\hat{U}_L^\dagger, \hat{X}^{(k)}\otimes\mathbb{1}_{EE'}\right)\\
&\quad= \sum_{k=1}^{2(N+M)} I_F\left(\hat{U}_L\left(|\psi\rangle\langle\psi|\otimes|\boldsymbol{\alpha}_j\rangle_{EE'}\langle\boldsymbol{\alpha}_j|\right)\hat{U}_L^\dagger, \hat{X}^{(k)}\right)\\
&\qquad - \sum_{l=1}^{2M} I_F\left(\hat{U}_L\left(|\psi\rangle\langle\psi|\otimes|\boldsymbol{\alpha}_j\rangle_{EE'}\langle\boldsymbol{\alpha}_j|\right)\hat{U}_L^\dagger, \mathbb{1}\otimes\hat{X}_{EE'}^{(l)}\right)\\
&\quad\le \sum_{k=1}^{2(N+M)} I_F\left(|\psi\rangle\langle\psi|\otimes|\boldsymbol{\alpha}_j\rangle_{EE'}\langle\boldsymbol{\alpha}_j|, \hat{X}^{(k)}\right) - 4M\\
&\quad= \sum_{l=1}^{2N} I_F\left(|\psi\rangle\langle\psi|, \hat{X}^{(l)}\right) + \sum_{l=1}^{2M} I_F\left(|\boldsymbol{\alpha}_j\rangle_{EE'}\langle\boldsymbol{\alpha}_j|, \hat{X}^{(l)}\right) - 4M\\
&\quad\le \sum_{k=1}^{2N} I_F\left(|\psi\rangle\langle\psi|, \hat{X}^{(k)}\right).
\end{aligned}$$

Finally, we get

$$\begin{aligned}
&\sum_i q_i\mathcal{C}(|\phi_i\rangle)\\
&\quad\le \sum_j \frac{p_j}{4N}\sum_{k=1}^{2N} I_F\left(\hat{U}_L\left(|\psi\rangle\langle\psi|\otimes|\boldsymbol{\alpha}_j\rangle_{EE'}\langle\boldsymbol{\alpha}_j|\right)\hat{U}_L^\dagger, \hat{X}^{(k)}\otimes\mathbb{1}_{EE'}\right) - 1\\
&\quad\le (4N)^{-1}\sum_i q_i\sum_{k=1}^{2N} I_F\left(|\psi\rangle\langle\psi|, \hat{X}^{(k)}\right) - 1\\
&\quad= \mathcal{C}(|\psi\rangle).
\end{aligned}$$

Now we prove the strong monotonicity of $\mathcal{Q}$. Suppose

$$\mathcal{Q}(\hat{\rho}) = \min_{\{p_\mu,\psi_\mu\}}\sum_\mu p_\mu\mathcal{C}(|\psi_\mu\rangle) = \sum_\mu p_\mu^*\mathcal{C}(|\psi_\mu^*\rangle),$$

where the minimum is achieved at $\hat{\rho} = \sum_\mu p_\mu^* \left|\psi_\mu^*\right\rangle \left\langle\psi_\mu^*\right|$. Then we have

$$\begin{aligned}\sum_i q_i \mathcal{Q}(\hat{K}_i \hat{\rho} \hat{K}_i^\dagger / q_i) &\leq \sum_i \sum_\mu p_\mu^* q_i^\mu \mathcal{C}\left(\hat{K}_i \left|\psi_\mu^*\right\rangle / \sqrt{q_i^\mu}\right) \\ &\leq \sum_\mu p_\mu^* \mathcal{C}(\left|\psi_\mu^*\right\rangle) \\ &= \mathcal{Q}(\hat{\rho}),\end{aligned} \tag{4.13}$$

where $\hat{K}_i \hat{\rho} \hat{K}_i^\dagger / q_i = \sum_\mu (p_\mu^* q_i^\mu / q_i) \left(\frac{\hat{K}_i \left|\psi_\mu^*\right\rangle}{\sqrt{q_i^\mu}}\right) \left(\frac{\left\langle\psi_\mu^*\right| \hat{K}_i^\dagger}{\sqrt{q_i^\mu}}\right)$ with $q_i^\mu = \left\langle\psi_\mu^*\right| \hat{K}_i^\dagger \hat{K}_i \left|\psi_\mu^*\right\rangle$. Finally, weak monotonicity can be derived by the strong monotonicity condition and convexity of $\mathcal{Q}$:

$$\mathcal{Q}\left(\sum_i \hat{K}_i \hat{\rho} \hat{K}_i^\dagger\right) \leq \sum_i p_i \mathcal{Q}\left(\hat{K}_i \hat{\rho} \hat{K}_i^\dagger / p_i\right) \leq \mathcal{Q}\left(\hat{\rho}\right), \tag{4.14}$$

where $p_i = \mathrm{Tr} \hat{\rho} \hat{K}_i^\dagger \hat{K}_i$. □

4.3.5.3 Proof of Theorem 8

Proof: Convexity is guaranteed by convexity of the quantum Fisher information. We prove that $\mathcal{M}(\hat{\rho}) = 0$ when $\hat{\rho}$ is classical. A classical quantum state has a positive-P representation, which allows us to represent $\hat{\rho} = \pi^{-1} \int d^2\alpha P(\alpha) \left|\alpha\right\rangle \left\langle\alpha\right|$ as a convex sum of coherent states. Then by convexity of $\mathcal{M}$ and using the fact that $\mathcal{M}(\left|\alpha\right\rangle \left\langle\alpha\right|) = 0$ for any coherent states, we have $\mathcal{M}(\hat{\rho}) = 0$. Weak monotonicity could be proved as follows:

We note that the optimal metrological power is contractive under partial

trace:

$$\begin{aligned}\mathcal{P}_{\rm opt}({\rm Tr}_B\hat{\rho}_{AB}) &= \frac{1}{2}\max_{\mu_A\in\mathcal{S}_{\mathcal{A}}} I_F({\rm Tr}_B\hat{\rho}_{AB},\hat{X}_{\mu_A})\\ &\leq \frac{1}{2}I_F(\hat{\rho}_{AB},\hat{X}_{\tilde{\mu}_A}\otimes\mathbb{1}_B)\\ &\leq \frac{1}{2}\max_{\mu_{AB}\in\mathcal{S}_{\mathcal{AB}}} I_F(\hat{\rho}_{AB},\hat{X}_{\mu_{AB}})\\ &= \mathcal{P}_{\rm opt}(\hat{\rho}_{AB}),\end{aligned}$$

where $\tilde{\mu}_A$ gives the maximum metrolgical power for ${\rm Tr}_B\hat{\rho}_{AB}$. Note that a linear optical map on $\hat{\rho}$ can be realized by $\Phi_L(\hat{\rho}) = {\rm Tr}_E\hat{U}_L\left(\hat{\rho}\otimes\hat{\sigma}_E\right)\hat{U}_L^\dagger$, where $\hat{\sigma}_E$ is classical and $\hat{U}_L$ is given by combinations of beam splitter operations, phase rotations, and displacement operations. Then by Proposition 3, we have $\mathcal{P}_{\rm opt}(\Phi_L(\hat{\rho})) = \mathcal{P}_{\rm opt}({\rm Tr}_E\hat{U}_L(\hat{\rho}\otimes\hat{\sigma}_E)\hat{U}_L^\dagger) \leq \mathcal{P}_{\rm opt}(\hat{U}_L(\hat{\rho}\otimes\hat{\sigma}_E)\hat{U}_L^\dagger) \leq \max\{\mathcal{P}_{\rm opt}(\hat{\rho}),\mathcal{P}(\hat{\sigma}_E)\} \leq \max\{\mathcal{P}_{\rm opt}(\hat{\rho}),1\}$, since $\mathcal{P}_{\rm opt}(\hat{\sigma}_E) \leq 1$. Then we get

$$\begin{aligned}\mathcal{M}(\Phi_L(\hat{\rho})) &= \max\{\mathcal{P}_{\rm opt}(\Phi_L(\hat{\rho}))-1,0\}\\ &\leq \max\left\{\mathcal{P}_{\rm opt}(\hat{\rho})-1,0\right\} = \mathcal{M}(\hat{\rho}).\end{aligned}$$

We now show the final condition $\mathcal{M}(\hat{\rho}^{\otimes M}) = \mathcal{M}(\hat{\rho})$. By Proposition 3, we have $\mathcal{P}_{\rm opt}(\hat{\rho}^{\otimes M}) \leq \mathcal{P}_{\rm opt}(\hat{\rho})$. Then we can always choose $\hat{X}_{\boldsymbol{\mu}} = \hat{X}_{\tilde{\boldsymbol{\mu}}_1}\otimes\mathbb{1}_{2\cdots M}$ to achieve $\mathcal{P}_{\rm opt}(\hat{\rho}^{\otimes M}) = \mathcal{P}_{\rm opt}(\hat{\rho})$, where $\tilde{\boldsymbol{\mu}}_1$ gives the maximum metrological power for $\hat{\rho}$. Thus we have $\mathcal{M}(\hat{\rho}^{\otimes M}) = \mathcal{M}(\hat{\rho})$. By the same way, we can also show that $\mathcal{M}(\hat{\rho}_A\otimes\hat{\sigma}_B) = \max\left\{\mathcal{M}(\hat{\rho}_A),\mathcal{M}(\hat{\sigma}_B)\right\}$.

□

4.3.5.4 Derivation of Eq. (4.9)

Using the Taylor expansion of $B_\Omega = \int d^N\boldsymbol{x}\sqrt{p(\boldsymbol{x})p(\boldsymbol{x}-\boldsymbol{\chi}\theta)}$ with respect to θ up to its second order, we get

$$\begin{aligned} B_\Omega &= \int d^N\boldsymbol{x}\left[p(\boldsymbol{x}) - \frac{\theta}{2}(\boldsymbol{\chi}^T\boldsymbol{\nabla}_{\boldsymbol{x}}p(\boldsymbol{x})) + \frac{\theta^2}{8}\boldsymbol{\chi}^T\boldsymbol{H}(p(\boldsymbol{x}))\boldsymbol{\chi}\right] + O(\theta^3) \\ &= 1 - \frac{\theta^2}{8}\boldsymbol{\chi}^T\left[\int d^N\boldsymbol{x}\boldsymbol{H}(p(\boldsymbol{x}))\right]\boldsymbol{\chi} + O(\theta^3), \end{aligned}$$

where the linear term of θ vanishes since $\int d^N\boldsymbol{x}\boldsymbol{\nabla}_{\boldsymbol{x}}p(\boldsymbol{x}) = 0$ and $\boldsymbol{H}(p(\boldsymbol{x}))$ is a $N \times N$ matrix with element $H_{mn} = p(\boldsymbol{x})^{-1}\frac{\partial p(\boldsymbol{x})}{\partial x_m^{\phi_m}}\frac{\partial p(\boldsymbol{x})}{\partial x_n^{\phi_n}}$.

Then, $\arccos^2(1-x) = 2x + O(x^2)$ leads to

$$\frac{\arccos^2 B_\Omega}{\theta^2} = \frac{1}{4}\boldsymbol{\chi}^T\left[\int d^N\boldsymbol{x}\boldsymbol{H}(p(\boldsymbol{x}))\right]\boldsymbol{\chi} + O(\theta^2).$$

Thus, taking the limit of $\theta \to 0$ and $\chi_n = \mathrm{Re}[\mu_n]\sin\phi_n + \mathrm{Im}[\mu_n]\cos\phi_n$, we have

$$I_F(\hat{\rho}, \hat{X}_{\boldsymbol{\mu}}) \geq \lim_{\theta\to 0}\frac{4\arccos^2 B_\Omega}{\theta^2} = \boldsymbol{\mu}^T\boldsymbol{G}\boldsymbol{\mu},$$

where $\boldsymbol{G}$ is a $2N \times 2N$ real matrix with

$$\begin{aligned} G_{kl} = \int d^N\boldsymbol{x}p(\boldsymbol{x})^{-1}&\frac{\partial p(\boldsymbol{x})}{\partial x_n^{\phi_n}}\frac{\partial p(\boldsymbol{x})}{\partial x_m^{\phi_m}} \\ &\times \begin{cases} \sin\phi_n & (k = 2n-1) \\ -\cos\phi_n & (k = 2n) \end{cases} \times \begin{cases} \sin\phi_m & (l = 2n-1) \\ -\cos\phi_m & (l = 2n) \end{cases}. \end{aligned}$$

Finally, optimizing over $\boldsymbol{\mu} \in \mathcal{S}$ leads to Eq. (4.9).

4.4 Remarks

In conclusion, we have introduced the metrological power as a non-classical resource in multi-mode optical fields. From this point of view, the nonclassicality of an optical quantum state can be understood as a resource for enhanced metrological power over the classical limit. The degree of nonclassicality quantified by optimal and mean metrological powers does not increase under linear optical maps, which can be implemented in laboratories by linear optical elements, in addition to classical states of light. It therefore belongs to the class of resource theoretical, nonclassicality measures suggested in Ref. [122]. This approach has demonstrable usefulness both conceptually and computationally, with concrete examples demonstrated for both single-mode and multi-mode cases. The most efficient quantum states to perform metrological task for quadrature operators (or displacement operations) are squeezed states, Fock states, and optical cat states, all of which are known to have macroscopic coherence according to the results in the previous chapters. Suggested measures could possibly be applied to not only multi-mode bosonic systems, but also arbitrary many-body quantum systems including spin, atomic, or optomechanical systems as well as hybrid systems attached to the optical field. This may lead to a unified description of quantum macroscopicity for both the discrete and continuous types of the system.

Chapter 5

Nonlocality test using hybrid entanglement of light

The contents of this chapter are largely based on [H. Kwon and H. Jeong, "Violation of the Bell–Clauser-Horne-Shimony-Holt inequality using imperfect photodetectors with optical hybrid states," Phys. Rev. A **88**, 052127 (2013)] Ref. [127] and [H. Kwon and H. Jeong, "Generation of hybrid entanglement between a single-photon polarization qubit and a coherent state," Phys. Rev. A **91**, 012340 (2015)] Ref. [128].

5.1 Introduction

Einstein, Podolsky and Rosen (EPR)'s argument provoked debates upon incompatibility between quantum mechanics and local realism [129]. Around thirty years after EPR's work was published, Bell in his celebrated paper suggested an inequality that enables one to test quantum mechanics against local realism [56]. Since then, various versions of Bell's inequality have been suggested including Clauser, Horne, Shimony, and Holt (CHSH)'s one known as the Bell-CHSH inequality [130]. The Bell-CHSH inequality has been theoretically studied within the frameworks of N-dimensional systems [131–133] and continuous variables in phase space [134–139].

Meanwhile, various experimental efforts have been made to observe

violation of Bell's inequality, yet no experiment has been found to be completely loophole-free. In general, experiments using atoms [140, 141] have suffered from the locality loophole [142, 143], while optical experiments [144–147] have not been free from the detection (or fair-sampling) loophole [148]. In order to close the detection loophole for the Bell-CHSH inequality test, 82.8% of detector efficiency is required when using maximally entangled bipartite system. It was shown that Bell type inequality with non-maximally entangled states could lower the threshold efficiency to 66.7% [149]. The experimental observation of Bell inequality violation using partially entangled photon without the fair-sampling assumption was reported lately [150].

In order to lower the detector efficiency threshold for a loophole-free Bell test, schemes based on high dimensional states [151–155] and multiphoton states [156, 157] have been suggested. A study on an asymmetric Bell type inequality, assuming perfect detection on one side, shows that 43% of detection efficiency is required [158], while a scheme using qudit systems requires 61.8% of threshold efficiency [155]. In principle, macroscopic entanglement enables one to perform a Bell inequality test free from the detection inefficiency [157]. Continuous variable systems with homodyne detection have also been investigated to close the detection loophole [159–162]. Atom-fields entanglement to combine the advantages of both the atomic and optical systems have been studied in the context of loophole-free Bell inequality tests [158, 161, 163–168] and several related experiments have been reported [169–171].

In this Chapter, we study optical hybrid entanglement between a polar-

ized single photon and a coherent-state field for Bell inequality tests using inefficient detectors. Especially, we are interested in an optical hybrid state with entanglement between a polarized single photon and a coherent state,

$$|\Psi\rangle = \frac{1}{\sqrt{2}} \left(|H\rangle_A |\alpha\rangle_B + |V\rangle_A |-\alpha\rangle_B \right) \tag{5.1}$$

where $|H\rangle$ and $|V\rangle$ refer to horizontal and vertical polarization state of a photon each, and $|\pm\alpha\rangle$ are coherent states of amplitudes $\pm\alpha$. Such hybrid entangled states have been proven to be particularly useful for deterministic quantum teleportation and resource-efficient quantum computing using linear optics [172]. In the viewpoint of quantum macroscopicity in Chapter 3 and nonclassicality in Chapter 4, the optical hybrid state $|\Psi\rangle$ contains the high amount of nonclassical resources as much as the optical cat state $|\alpha\rangle + |-\alpha\rangle$ when the coherent state amplitude α is sufficiently large. For example, it is straightforward to show that the nonclassicality measure $\mathcal{M}$ in Chapter 4 for this state has its maximum value $\mathcal{M}(|\Psi\rangle) = 2\alpha^2$ that scales with the average photon number of the state when $\alpha \gg 1$. In the first part of this chapter, we demonstrate that the optical hybrid entanglement can be utilized to close the detection loophole in the Bell-CHSH inequality tests.

In the second part of this chapter, we propose a nondeterministic scheme to generate an optical hybrid state between a polarized single photon and a coherent-state field. Very recently, approximate implementations of hybrid entanglement between a qubit of the vacuum and single photon and a qubit of coherent states were demonstrated using the photon addition and subtraction techniques [14, 15]. The state explored in Ref. [14] was in the form of

$|0\rangle\,|\alpha\rangle+|1\rangle\,|-\alpha\rangle$ while a similar state of $(|0\rangle+|1\rangle)\,|\alpha\rangle+(|0\rangle-|1\rangle)\,|-\alpha\rangle$ was approximately demonstrated in Ref. [15], where $|0\rangle$ is the vacuum, $|1\rangle$ is the single photon, and $|\pm\alpha\rangle$ are coherent states of amplitudes $\pm\alpha$. However, the state required to perform the aforementioned applications in Refs. [127,172] was in fact in the form of $|H\rangle\,|\alpha\rangle + |V\rangle\,|-\alpha\rangle$; i.e., the first mode should be in a *definite single-photon state* in the horizontal (H) or vertical (V) polarization. This type of hybrid entanglement, despite its usefulness, cannot be generated using the photon addition or subtraction as performed in Refs. [14, 15] because the first mode should be in a single photon state with definitely one photon. In principle, a cross-Kerr nonlinear interaction can be used to generate the required form of hybrid entanglement [173, 174], but it is a highly demanding task to achieve a clean nonlinear interaction using current technology [175–181]. In this dissertation, we demonstrate that by starting with a polarization-entangled state $|H\rangle\,|V\rangle + |V\rangle\,|H\rangle$ and the optical cat state $|\alpha\rangle + |-\alpha\rangle$, we can possibly obtain a desired optical hybrid state with a high fidelity by using displacement operators, beam splitters, and on-off detectors.

5.2 Nonlocality test using optical hybrid states

In this section, we employ two different kinds of measurements for the coherent-state field, photon on/off measurement and photon number parity measurement, to investigate the Bell-CHSH inequality. We find that the Bell-CHSH inequality is violated for low coherent amplitudes ($|\alpha| < 1.0$) with detection efficiency higher than 67%. When realistic detection effi-

ciency is assumed (*i.e.,* smaller than 98.68%), the scheme based on on/off measurements gives larger Bell violation than the one based on photon number parity measurements, while nearly perfect detector efficiency provides higher Bell values close to Cirel'son's bound $2\sqrt{2}$ for the parity measurement scheme. However, threshold values for detection efficiencies over which Bell violations occur are similar for both the measurement schemes.

5.2.1 Bell-CHSH inequality using on/off and parity measurements

In order to perform Bell inequality tests (see Fig. 10), an entangled state should be shared by two locally separate parties. With regard to the state in Eq. (5.30), the single photon part with the polarization degree of freedom and the coherent state part with amplitudes $\pm\alpha$ are subscripted by *A* and *B*, respectively. Each party may locally perform unitary operations and dichotomic measurements. In order to construct a Bell-CHSH inequality, each measurement outcome is determined as either $+1$ or -1. We may choose $\hat{\Pi}_A = |H\rangle\langle H| - |V\rangle\langle V|$ for polarization measurements for the single-photon part and

$$\hat{\Pi}_B = \begin{cases} |0\rangle\langle 0| - \sum_{n=1}^{\infty} |n\rangle\langle n| & (\text{on/off}) \\ \sum_{n=0}^{\infty} \left(|2n\rangle\langle 2n| - |2n+1\rangle\langle 2n+1|\right) & (\text{parity}) \end{cases} \tag{5.2}$$

for on/off and photon number parity measurements each. Outcomes ± 1 denote no-click/click events for on/off measurements and even/odd number

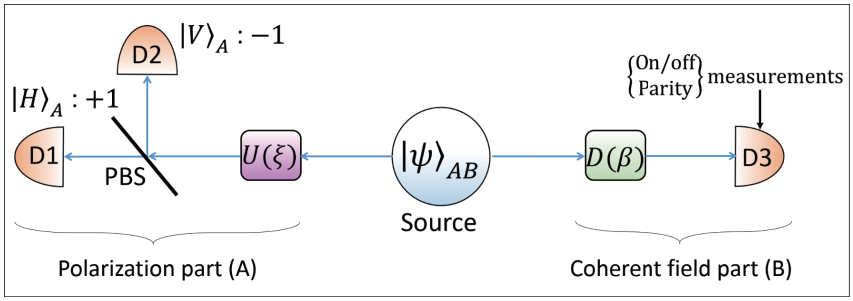

Figure 10: Bell inequality test using an optical hybrid state with on/off and parity measurements.

results for photon number parity measurements. An arbitrary unitary operation on a single photon qubit with the qubit basis of $|H\rangle$ and $|V\rangle$ can be represented by

$$\hat{U}(\xi) = \begin{pmatrix} \cos|\xi| & \frac{\xi}{|\xi|}\sin|\xi| \\ -\frac{\xi^*}{|\xi|}\sin|\xi| & \cos|\xi| \end{pmatrix}$$

with complex variable ξ. The displacement operation, $\hat{D}(\beta) = e^{\beta\hat{a}^\dagger - \beta^*\hat{a}}$, is used a unitary operation on the coherent state part (*i.e.*, mode B), where β is a complex variable. A previous result shows that the displacement operator approximately acts as a qubit rotation for a coherent-state qubit with basis $|\pm\alpha\rangle$ [139]. The expectation value of the joint measurement is obtained as

$$E(\xi,\beta) = \left\langle \hat{O}_A \otimes \hat{O}_B \right\rangle, \tag{5.3}$$

where $\hat{O}_A(\xi) = \hat{U}(\xi)\hat{\Pi}_A\hat{U}^\dagger(\xi)$ and $\hat{O}_B(\beta) = \hat{D}(\beta)\hat{\Pi}_B\hat{D}^\dagger(\beta)$. The Bell-CHSH inequality is then defined as $|B(\xi_1,\xi_2,\beta_1,\beta_2)| \leq 2$ with the

Bell function

$$B\left(\xi_1,\xi_2,\beta_1,\beta_2\right)=E\left(\xi_1,\beta_1\right)+E\left(\xi_1,\beta_2\right)+E\left(\xi_2,\beta_2\right)-E\left(\xi_2,\beta_1\right). \tag{5.4}$$

We define $\xi=-(\theta/2)e^{-i\phi}$ and $\beta=|\beta|e^{i\Phi}$ with $0\leq\theta<\pi$, $0\leq\phi$ and $\Phi<2\pi$ for simplicity. Without loss of generality, we take α to be real because the phase of α may absorbed by Φ. We obtain the expectation values as

$$\begin{aligned}E^{\mathrm{On/off}}\left(\theta,\phi,|\beta|,\Phi\right)=&\,2\cos\theta e^{-\left(|\alpha|^2+|\beta|^2\right)}\sinh\left(2|\alpha||\beta|\cos\Phi\right)\\&+2\sin\theta e^{-\left(|\alpha|^2+|\beta|^2\right)}\cos\left(2|\alpha||\beta|\sin\Phi-\phi\right)\\&-\sin\theta e^{-2|\alpha|^2}\cos\phi,\end{aligned} \tag{5.5}$$

$$\begin{aligned}E^{\mathrm{Parity}}\left(\theta,\phi,|\beta|,\Phi\right)=&\,\cos\theta e^{-2\left(|\alpha|^2+|\beta|^2\right)}\sinh\left(4|\alpha||\beta|\cos\Phi\right)\\&+\sin\theta e^{-2|\beta|^2}\cos\left(4|\alpha||\beta|\sin\Phi-\phi\right)\end{aligned} \tag{5.6}$$

by applying on/off and photon number parity measurements, respectively, on the coherent-state part.

5.2.2 Photodetector efficiency and the detection loophole

A physical model of an imperfect photodetector with detection efficiency p is described by a beam splitter of transmission coefficient $\sqrt{p}$ before a perfect photodetector. In terms of positive operator valued measurement (POVM) with the photon number basis, a photodetector with efficiency p

may be written as [182],

$$\hat{E}_p^{(n)} = \sum_{m=0}^{\infty} \binom{n+m}{n} p^n (1-p)^m \left|n+m\right\rangle \left\langle n+m\right| . \tag{5.7}$$

Then the effective on/off measurement of detection efficiency η_B becomes

$$\begin{aligned} \hat{\Pi}_{B,\text{eff}}^{\text{On/off}} &= \hat{E}_{\eta_B}^{(0)} - \sum_{n=1}^{\infty} \hat{E}_{\eta_B}^{(n)} \\ &= \sum_{m=0}^{\infty} \Big[2(1-\eta_B)^m \left|m\right\rangle \left\langle m\right| \\ &\quad - \sum_{n=0}^{\infty} \binom{n+m}{n} \eta_B^n (1-\eta_B)^m \left|n+m\right\rangle \left\langle n+m\right| \Big] . \end{aligned} \tag{5.8}$$

Similarly, the effective photon number parity measurement is given by

$$\begin{aligned} &\hat{\Pi}_{B,\text{eff}}^{\text{parity}} = \hat{E}_{\eta_B}^{(\text{even})} - \hat{E}_{\eta_B}^{(\text{odd})} \\ &= \sum_{m=0}^{\infty} \sum_{n=0}^{\infty} \Bigg[\binom{2n+m}{2n} \eta_B^{2n} (1-\eta_B)^m \left|2n+m\right\rangle \left\langle 2n+m\right| \\ &- \tbinom{2n+1+m}{2n+1} \eta_B^{2n+1} (1-\eta_B)^m \left|2n+1+m\right\rangle \left\langle 2n+1+m\right| \Bigg] . \end{aligned} \tag{5.9}$$

In order to avoid the detection loophole, we assign $+1$ for a "no-detection" outcome on the polarization part. Provided the polarization measurement detection efficiency is η_A, the expectation value for the combined measurement is given by

$$E_{\text{eff}} = \eta_A \left\langle \hat{O}_A \otimes \hat{O}_{B,\text{eff}} \right\rangle + (1-\eta_A) \operatorname{Tr}_B \left[\hat{O}_{B,\text{eff}} \hat{\rho}_B \right] , \tag{5.10}$$

where $\hat{\rho}_B$ is a reduced density matrix obtained by tracing over polarization

part A, *i.e.*

$$\hat{\rho}_B = \mathrm{Tr}_A(\rho) = \frac{1}{2}\left(|\alpha\rangle\langle\alpha| + |-\alpha\rangle\langle-\alpha|\right). \tag{5.11}$$

Each term in Eq. (5.9) could be directly calculated as

$$\begin{aligned}\left\langle \hat{O}_A \otimes \hat{O}_{B,\mathrm{eff}}^{\mathrm{On/off}} \right\rangle = {} & 2\cos\theta e^{-\eta_B\left(|\alpha|^2+|\beta|^2\right)} \sinh\left(2\eta_B|\alpha||\beta|\cos\Phi\right) \\ & +2\sin\theta e^{-(2-\eta_B)|\alpha|^2-\eta_B|\beta|^2} \cos\left(2\eta_B|\alpha||\beta|\sin\Phi-\phi\right) \\ & -\sin\theta e^{-2|\alpha|^2}\cos\phi,\end{aligned} \tag{5.12}$$

$$\mathrm{Tr}_B\left[\hat{O}_{B,\mathrm{eff}}^{\mathrm{On/off}}\hat{\rho}_B\right] = 2e^{-\eta_B\left(|\alpha|^2+|\beta|^2\right)}\cosh\left(2\eta_B|\alpha||\beta|\cos\Phi\right) - 1 \tag{5.13}$$

for photon on/off measurements and

$$\begin{aligned}\left\langle \hat{O}_A\hat{O}_{B,\mathrm{eff}}^{\mathrm{Parity}} \right\rangle = {} & \cos\theta e^{-2\eta_B\left(|\alpha|^2+|\beta|^2\right)} \sinh\left(4\eta_B|\alpha||\beta|\cos\Phi\right) \\ & +\sin\theta e^{-2(1-\eta_B)|\alpha|^2-2\eta_B|\beta|^2} \cos\left(4\eta_B|\alpha||\beta|\sin\Phi-\phi\right),\end{aligned} \tag{5.14}$$

$$\mathrm{Tr}_B\left[\hat{O}_{B,\mathrm{eff}}^{\mathrm{Parity}}\hat{\rho}_B\right] = e^{-2\eta_B\left(|\alpha|^2+|\beta|^2\right)}\cosh\left(4\eta_B|\alpha||\beta|\cos\Phi\right) \tag{5.15}$$

for photon number parity measurements.

In order to observe violation of the Bell-CHSH inequality, it is important to find optimizing conditions for local unitary variables under which the Bell functions have largest values. The optimizing conditions presented throughout this Chapter are numerically found [183], and wherever possible, we try to find corresponding analytical expressions.

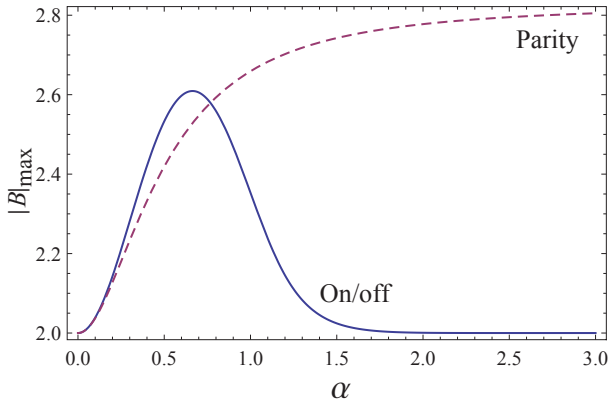

Figure 11: Maximized Bell value $|B|_{\max}$ for varying α with perfect detector efficiency. The solid curve refers to photon on/off measurements while the dashed curve to photon number parity measurements.

5.2.3 Perfect photodetector efficiency

We first suppose perfect efficiencies for all detectors used for Bell inequality tests. In the case of photon on/off measurements, optimizing conditions can be obtained as [166]

$$\xi_1 = -\frac{\pi}{4},\ \xi_2 = 0,\ \beta_1 = -\beta_2 = -|\beta| \tag{5.16}$$

with $|\beta|$ satisfying

$$|\beta|\left(1+\sinh\left(2|\alpha||\beta|\right)\right) = |\alpha|\cosh\left(2|\alpha||\beta|\right). \tag{5.17}$$

We plot the Bell function in Fig. 11 and note that as the coherent amplitude $|\alpha|$ increases the maximized Bell value increases up to $|B|_{\max}^{\mathrm{On/off}} \approx 2.61$ for $|\alpha| \approx 0.664$. However, Fig. 11 also shows that further increase of $|\alpha|$ results in lower maximized Bell values. This can be attributed to the fact

that the probability of "no-click" on a photodetector becomes lower when $|\alpha|$ becomes larger [139].

We also find the optimizing conditions for photon number parity measurements as

$$\xi_1 = -\frac{\pi}{4},\ \xi_2 = i\frac{\pi}{4},\ \beta_1 = -\beta_2 = -i|\beta| \tag{5.18}$$

with $|\beta|$ satisfying $\tan\left[4|\alpha||\beta|\right] = (|\alpha| - |\beta|)/(|\alpha| + |\beta|)$ nearest to zero. One may expect that Bell value would increase as $|\alpha|$ increases because probabilities to have even and odd photon number in a coherent state become equal as $|\alpha| \to \infty$. In practice, we note that Bell value of parity measurements rapidly approaches to Cirel'son's bound $2\sqrt{2}$ when $|\alpha| \gg 1$.

5.2.4 Imperfect detection for coherent-state fields

Now we consider the situation of perfect polarization measurements ($\eta_A = 1$) and imperfect coherent field measurements ($\eta_B \neq 1$). Optimizing conditions for photon on/off measurements can be obtained by $\xi_1 = -\pi/4$, $\xi_2 = 0$ and $\beta_1 = -\beta_2 = -|\beta|$ to be real with $|\beta|$ satisfying

$$|\beta|e^{-2(1-\eta_B)|\alpha|^2} + |\beta|\sinh\left(2\eta_B|\alpha||\beta|\right) - |\alpha|\cosh\left(2\eta_B|\alpha||\beta|\right) = 0. \tag{5.19}$$

In this case, the Bell value becomes

$$\begin{aligned} &B^{\mathrm{On/off}}\left(\xi_1, \xi_2, \beta_1, \beta_2\right) \\ &= 4e^{-\eta_B\left(|\alpha|^2+|\beta|^2\right)}\left[e^{-(1-\eta_B)|\alpha|^2} + \sinh\left(2\eta_B|\alpha||\beta|\right)\right] - 2e^{-2|\alpha|^2}. \end{aligned} \tag{5.20}$$

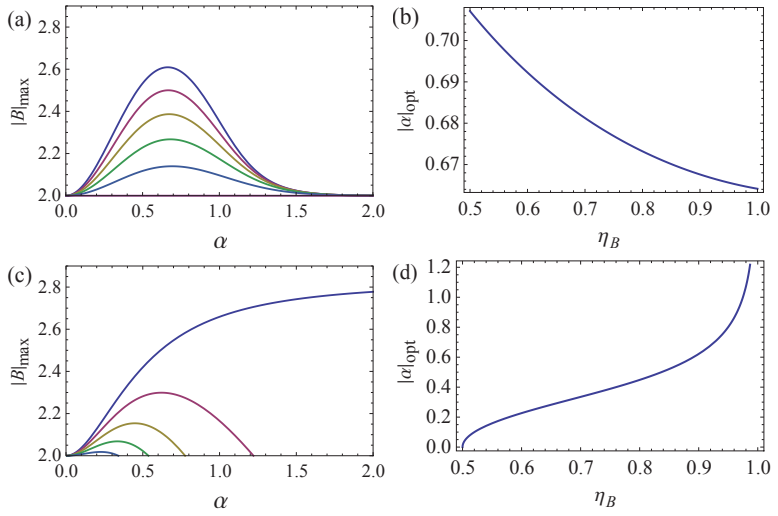

Figure 12: (a) Maximized Bell value for on/off measurements $|B|_{\max}^{\rm on/off}$ and (b) optimizing $|\alpha|_{\rm opt}$ for each coherent measurement detection efficiency. (c) Maximized Bell value for parity measurements $|B|_{\max}^{\rm parity}$ and (d) optimizing $|\alpha|_{\rm opt}$. In both the cases, the detection efficiency η_B for the coherent-state part decreases by 0.1 from the perfect value ($\eta_B = 1$) to $\eta_B = 0.5$.

Figure 12 shows that the maximum Bell value is obtained for $0.66 < |\alpha| < 0.71$ and the optimizing coherent amplitude $|\alpha_{\rm opt}|$ monotonically decreases as the detector efficiency increases. Violation of the Bell-CHSH inequality occurs until the detection efficiency reaches 0.5. This result is consistent with the equivalent Bell inequality test using entanglement between an atom and a coherent state in a cavity [166].

We find that optimizing conditions for photon number parity measurements are $\xi_1 = -\pi/4$, $\xi_2 = i\pi/4$ and $\beta_1 = -\beta_2 = -i|\beta|$ to be pure imaginary. Here, $|\beta|$ is the solution of

$$\tan\left(4\eta_B|\alpha||\beta|\right) = \frac{|\alpha| - |\beta|}{|\alpha| + |\beta|} \tag{5.21}$$

nearest to zero, and the Bell function is

$$B^{\mathrm{Parity}}(\xi_1, \xi_2, \beta_1, \beta_2) = 2e^{-2(1-\eta_B)|\alpha|^2 - 2\eta_B|\beta|^2} \left(\cos\left(4\eta_B|\alpha||\beta|\right) + \sin\left(4\eta_B|\alpha||\beta|\right)\right). \tag{5.22}$$

The optimizing coherent amplitude, $|\alpha_{\mathrm{opt}}|$, increases when the detection efficiency becomes larger. This is opposite to the case on/off measurement scheme, due to the fact when the efficiency of the photon number parity measurement is low, $|\alpha|$ should be small to reduce the possibility of parity flips. In most of imperfect detector efficiency conditions, the on/off measurement scheme gives higher violation of the Bell-CHSH inequality than the parity measurement scheme. However, the values of the detection efficiency required to violate the Bell-CHSH inequality are the same (50%) for both the schemes.

5.2.5 Imperfect detectors for both measurements

We now consider the most realistic case in which both the polarization measurement and the coherent field measurement are imperfect ($\eta_A < 1$ and $\eta_B < 1$). In this case, a nontrivial calculation is needed to obtain the optimizing conditions. It is still sufficient to take real ξ and β for optimizing conditions of photon on/off measurements, but with $|\beta_1| \neq |\beta_2|$. On the other hand, the optimizing parameters for photon number parity measurements tend to have different conditions by detection efficiency of photodetector. When the detection efficiency is high, we find $|\xi_1| = |\xi_2| = \pi/4$ and β_1, β_2 to be pure imaginary for the optimization. If the detector efficiency is

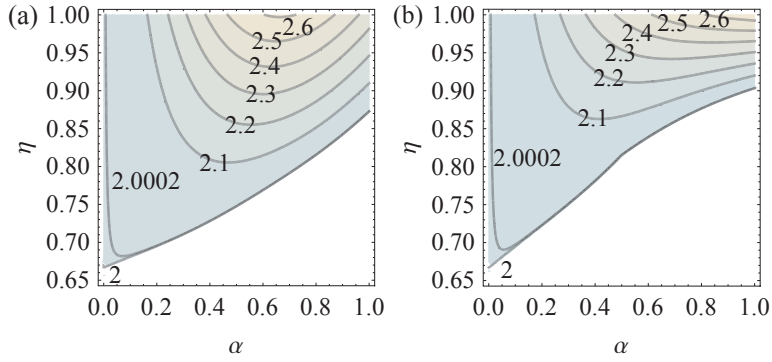

Figure 13: Maximized Bell-CHSH functions in terms of detection efficiency η for both modes and coherent amplitude α for (a) on/off and (b) parity measurement schemes. The detection efficiency threshold to violate the Bell-CHSH inequality is about 67% when the coherent amplitude is low.

low, the optimizing conditions could be chosen to be the same with those of the on/off measurement scheme (see Appendix).

We first assume the same detection efficiency $\eta_A = \eta_B = \eta$ on the polarization and the coherent field measurements. Figure 13 shows that the degree of Bell violation and the optimizing coherent amplitudes for both the measurement schemes decrease when the detector efficiency η decreases.

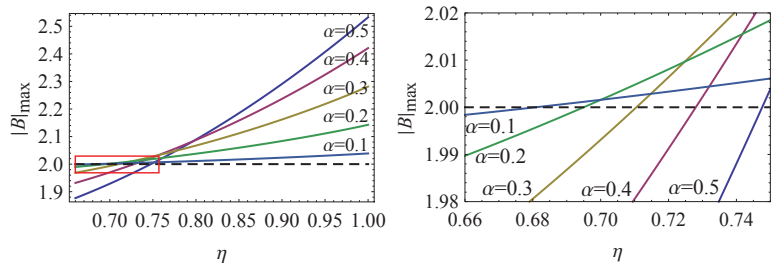

Figure 14: Maximum Bell value via detector efficiency with varying coherent amplitude from 0.1 to 0.5 for the on/off measurement scheme. The right-hand-side figure represents the boxed region of the left-hand-side one.

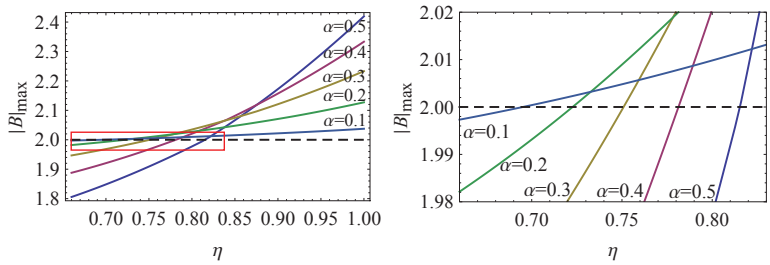

Figure 15: Maximum Bell values against detection efficiency with varying coherent amplitudes from 0.1 to 0.5 for the parity measurement scheme. The right-hand-side figure represents the boxed region of the left-hand-side one.

For example, with $\eta = 0.8$, on/off measurements gives the maximum Bell violation of $|B|_{\max}^{\text{on/off}} \approx 2.091$ at $|\alpha| \approx 0.458$, while parity measurements gives $|B|_{\max}^{\text{parity}} \approx 2.035$ at $|\alpha| \approx 0.293$. If detector efficiency becomes $\eta = 0.7$, the maximum Bell value and the optimizing coherent amplitude decrease to $|B|_{\max}^{\text{on/off}} \approx 2.0022$ ($|\alpha| \approx 0.155$) and $|B|_{\max}^{\text{parity}} \approx 2.0006$ ($|\alpha| \approx 0.078$) for each the measurement scheme. Figure 14 and 15 reveal that there is a trade-off between the degree of Bell violation and the detector efficiency threshold by using different coherent amplitudes $|\alpha|$. Employing a low coherent amplitude demands low detection efficiency in order to see Bell inequality violation but the degree of the violation would be small. Also we note from Fig. 16(a) that with symmetric detector efficiency η lower than 98.68%, on/off measurements provides higher Bell violation than parity measurements.

We numerically find that the Bell-CHSH inequality violation occurs until the detection efficiency reaches to 67% for both the measurement schemes as presented in Fig. 13. This value of the detection efficiency is lower than 82.8% obtained by employing maximally entangled states and similar with

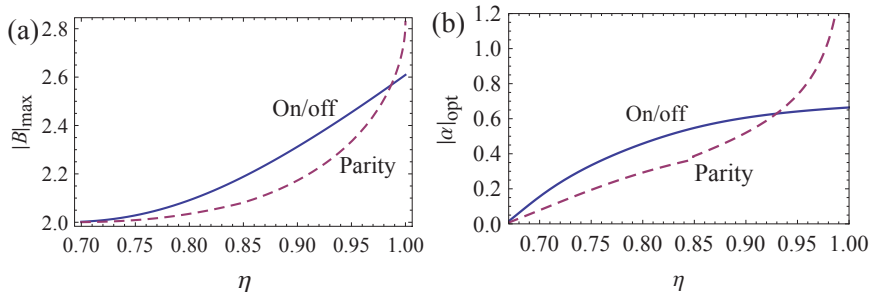

Figure 16: (a) Comparison of Bell violation $|B|_{\max}$ (b) and optimizing coherent amplitude $|\alpha|_{\text{opt}}$ between on/off(solid line) and parity(dashed line) measurements assuming symmetric detector efficiency η. On/off measurements give higher Bell value than parity measurements for $\eta < 0.9868$.

the threshold efficiency for the Bell's inequality test using non-maximally entangled states [149]. We note that the maximum Bell violation occurs at $|\alpha| < 0.664$ for on/off measurements of any symmetric detector efficiency higher than the threshold efficiency 67%. Similarly, the optimizing coherent amplitude for parity measurements is within the range $|\alpha| < 1.0$ when the detector efficiency is between the threshold (67%) and 97.7% (see Fig. 16(b)).

In real experiments, actual values of the detection efficiency for the two separate local measurements may be different. This realistic situation could be studied by taking the effective joint measurement defined by Eq. (5.10) with local detection efficiencies η_A and η_B. We plot the numerically optimized Bell function together with threshold regions for each measurement scheme in Fig. 17. The optimizing conditions have been found through non-trivial calculations as detailed in Appendix. As presented in Fig. 18, the on/off measurement scheme provides higher violation of the Bell-CHSH in-

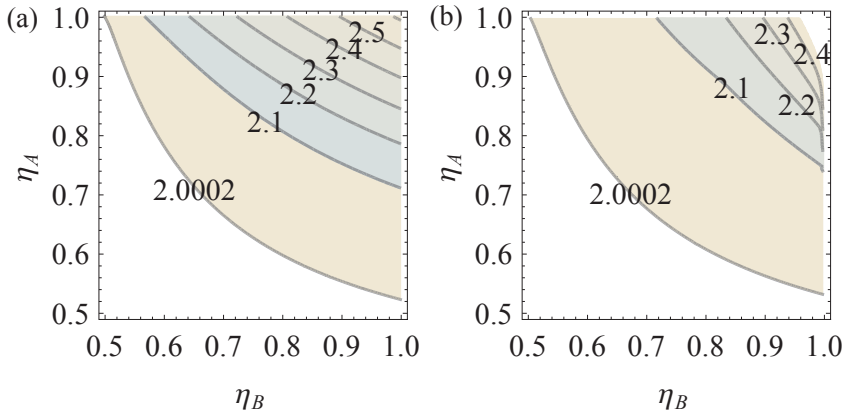

Figure 17: Maximized Bell-CHSH value as a function of detection efficiencies for (a) on/off and (b) parity measurement schemes. Axis labels η_A and η_B refer to polarization (single photon) and coherent field measurement efficiencies, respectively. The optimizing coherent amplitudes were taken for each detection efficiency.

equality than the parity measurement scheme for most values of the detector efficiency. Only when the coherent field detection efficiency η_B is close to 1, parity measurements give higher Bell violation. Figure 17 shows that the conditions for the Bell-CHSH inequality to be violated are similar for two different measurement schemes. This can be attributed to the facts that the probability distributions for two different measurement schemes (*i.e.* "click" vs "no-click" for the on/off scheme and "odd" vs "even" or the parity one) are similar for low coherent amplitudes and low detection efficiency leads to the same optimizing conditions for both the measurement schemes.

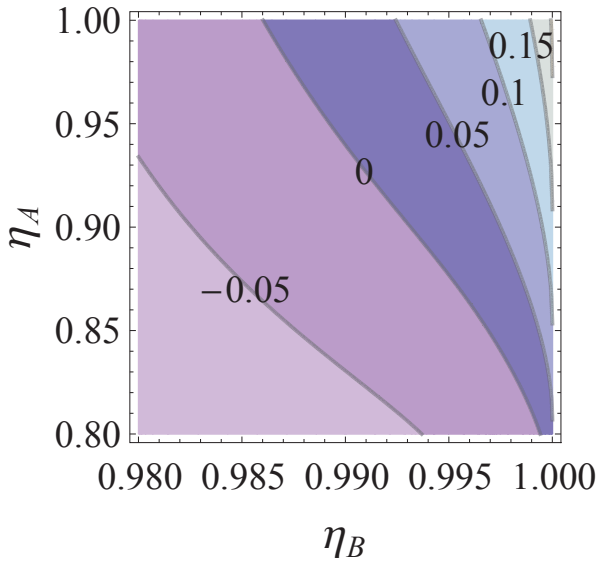

Figure 18: Subtracted value, $|B|_{\max}^{\text{Parity}} - |B|_{\max}^{\text{On/off}}$, values for different detection efficiencies η_A and η_B. Each $|B|_{\max}$ is obtained by taking its optimizing coherent amplitude.

5.2.6 Appendix: Optimization of the Bell value for on/off and parity measurements

We have numerically found maximum Bell values and corresponding optimizing conditions [183]. After numerical trials, we find that it is sufficient to take real values of the unitary parameters, ξ and β, in order to obtain those maximum Bell values for on/off measurements. Under this condition, Eqs. (5.12) and (5.13) can be represented in terms of θ and $|\beta|$ as

$$\begin{cases} \left\langle \hat{O}_A \otimes \hat{O}_{B,\mathrm{eff}}^{\mathrm{On/off}} \right\rangle = \mp 2\cos\theta e^{-\eta_B\left(|\alpha|^2+|\beta|^2\right)} \sinh\left(2\eta_B|\alpha||\beta|\right) \\ \qquad\qquad\qquad\qquad - \sin\theta e^{-2|\alpha|^2} + 2\sin\theta e^{-(2-\eta_B)|\alpha|^2-\eta_B|\beta|^2}, \\ \mathrm{Tr}_B\left[\hat{O}_{B,\mathrm{eff}}^{\mathrm{On/off}}\hat{\rho}_B\right] = 2e^{-\eta_B\left(|\alpha|^2+|\beta|^2\right)}\cosh\left(2\eta_B|\alpha||\beta|\right) - 1, \end{cases} \tag{5.23}$$

where $\mp$ corresponds to negative/positive β. The Bell function B can be constructed using Eqs. (5.4) and (5.10). In oder to find optimizing values, we take derivatives of B to be zero with respect to each parameter as

$$\left\{ \frac{\partial B}{\partial \theta_1}, \frac{\partial B}{\partial \theta_2}, \frac{\partial B}{\partial \beta_1}, \frac{\partial B}{\partial \beta_2} \right\} = 0, \tag{5.24}$$

which leads to a set of equations

$$\begin{cases} \tan\theta_1 = \frac{e^{-2(1-\eta_B)|\alpha|^2}\left(e^{-\eta_B|\alpha|^2} - e^{-\eta_B|\beta_1|^2} - e^{-\eta_B|\beta_2|^2}\right)}{e^{-\eta_B|\beta_1|^2}\sinh(2\eta_B|\alpha||\beta_1|) - e^{-\eta_B|\beta_2|^2}\sinh(2\eta_B|\alpha||\beta_2|)}, \\ \tan\theta_2 = -\frac{e^{-2(1-\eta_B)|\alpha|^2}\left(e^{-\eta_B|\beta_1|^2} - e^{-\eta_B|\beta_2|^2}\right)}{e^{-\eta_B|\beta_1|^2}\sinh(2\eta_B|\alpha||\beta_1|) + e^{-\eta_B|\beta_2|^2}\sinh(2\eta_B|\alpha||\beta_2|)}, \\ \left(|\beta_1|\sinh(2\eta_B|\alpha||\beta_1|) - |\alpha|\cosh(2\eta_B|\alpha||\beta_1|)\right)(\cos\theta_1 - \cos\theta_2) \\ \qquad\qquad -e^{-2(1-\eta_B)|\alpha|^2}|\beta_1|\left(\sin\theta_1 - \sin\theta_2\right) = 0, \\ \Big[\left(-|\beta_2|\sinh(2\eta_B|\alpha||\beta_2|) + |\alpha|\cosh(2\eta_B|\alpha||\beta_2|)\right)(\cos\theta_1 + \cos\theta_2) \\ \qquad -e^{-2(1-\eta_B)|\alpha|^2}|\beta_2|\left(\sin\theta_1 + \sin\theta_2\right)\Big] \\ + \frac{2(1-\eta_A)}{\eta_A}\left(-|\beta_2|\cosh(2\eta_B|\alpha||\beta_2|) + |\alpha|\sinh(2\eta_B|\alpha||\beta_2|)\right) = 0. \end{cases} \tag{5.25}$$

The scheme based on parity measurements undergoes two different op-

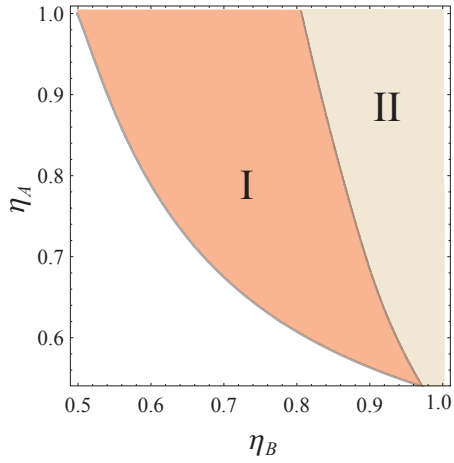

Figure 19: Optimizing conditions for parity measurements with detection efficiencies η_A and η_B. Shaded areas I and II are regions where the Bell-CHSH inequality is violated. Region I has optimizing conditions with real ξ and β, while region II has optimizing conditions with $|\xi| = \pi/4$ and pure imaginary β.

timizing conditions subject to detection efficiencies η_A and η_B. Region I in Fig. 19 corresponds to optimizing conditions for low efficiency detectors, where real values of ξ and β are taken. We apply this condition to Eqs. (5.14) and (5.15) and obtain the expectation value as

$$\begin{aligned} E_{\rm eff}^{\rm Parity,low} = \eta_A \Big[& \mp 2\cos\theta e^{-2\eta_B\left(|\alpha|^2+|\beta|^2\right)} \sinh\left(4\eta_B|\alpha||\beta|\right) \\ & + \sin\theta e^{-2(1-\eta_B)|\alpha|^2-2\eta_B|\beta|^2} \Big] \\ & + (1-\eta_A) e^{-2\eta_B\left(|\alpha|^2+|\beta|^2\right)} \cosh\left(4\eta_B|\alpha||\beta|\right), \end{aligned} \tag{5.26}$$

where $\theta = -2\xi$ and $\mp$ corresponds to negative/positive β. Using Eq. (5.24), we obtain a set of equations,

$$
\begin{cases}
\tan\theta_1 = -\frac{e^{-2(1-2\eta_B)|\alpha|^2}\left(e^{-2\eta_B|\beta_1|^2}+e^{-2\eta_B|\beta_2|^2}\right)}{e^{-2\eta_B|\beta_1|^2}\sinh(4\eta_B|\alpha||\beta_1|)-e^{-2\eta_B|\beta_2|^2}\sinh(4\eta_B|\alpha||\beta_2|)}, \\
\tan\theta_1 = -\frac{e^{-2(1-2\eta_B)|\alpha|^2}\left(e^{-2\eta_B|\beta_1|^2}-e^{-2\eta_B|\beta_2|^2}\right)}{e^{-2\eta_B|\beta_1|^2}\sinh(4\eta_B|\alpha||\beta_1|)+e^{-2\eta_B|\beta_2|^2}\sinh(4\eta_B|\alpha||\beta_2|)}, \\
\left(|\beta_1|\sinh(4\eta_B|\alpha||\beta_1|) - |\alpha|\cosh(4\eta_B|\alpha||\beta_1|)\right)(\cos\theta_1-\cos\theta_2) \\
\qquad -e^{-2(1-2\eta_B)|\alpha|^2}|\beta_1|\,(\sin\theta_1-\sin\theta_2)=0, \\
\Big[\left(-|\beta_2|\sinh(4\eta_B|\alpha||\beta_2|) + |\alpha|\cosh(4\eta_B|\alpha||\beta_2|)\right)(\cos\theta_1+\cos\theta_2) \\
\qquad -e^{-2(1-2\eta_B)|\alpha|^2}|\beta_2|\,(\sin\theta_1+\sin\theta_2)\Big] \\
+\frac{2(1-\eta_A)}{\eta_A}\left(-|\beta_2|\cosh(4\eta_B|\alpha||\beta_2|) + |\alpha|\sinh(4\eta_B|\alpha||\beta_2|)\right)=0,
\end{cases}
\tag{5.27}
$$

and find the optimizing conditions.

Optimization for the high detection efficiencies (region II in Fig. 19) can be obtained by taking $|\xi_1| = |\xi_2| = \pi/4$ and β as pure imaginary number. The expectation value then becomes

$$
\begin{aligned}
E_{\text{eff}}^{\text{Parity,high}} = \eta_A\, e^{-2(1-\eta_B)|\alpha|^2-2\eta_B|\beta|^2}\cos\left(4\eta_B|\alpha||\beta| \pm \phi\right) \\
+(1-\eta_A)e^{-2\eta_B\left(|\alpha|^2+|\beta|^2\right)}\cosh\left(4\eta_B|\alpha||\beta|\right),
\end{aligned}
\tag{5.28}
$$

where ϕ is a phase factor of ξ and $\pm$ corresponds with negative/positive $-i\beta$. In this case, we take similar steps with Eq. (5.24) but using a set of parameters of $\{\phi_1, \phi_2, |\beta_1|, |\beta_2|\}$, and find optimizing conditions by solving a set of equations:

$$
\begin{cases}
e^{-2\eta_B|\beta_1|^2}\sin\left(4\eta_B|\alpha||\beta_1|+\phi_1\right) \\
\qquad\qquad = e^{-2\eta_B|\beta_2|^2}\sin\left(4\eta_B|\alpha||\beta_2|-\phi_1\right), \\
\\
e^{-2\eta_B|\beta_1|^2}\sin\left(4\eta_B|\alpha||\beta_1|+\phi_2\right) \\
\qquad\qquad = -e^{-2\eta_B|\beta_2|^2}\sin\left(4\eta_B|\alpha||\beta_2|-\phi_2\right), \\
\\
|\beta_1|\left(\cos(4\eta_B|\alpha||\beta_1|+\phi_1)-\cos(4\eta_B|\alpha||\beta_1|+\phi_2)\right) \\
\quad +|\alpha|\left(\sin(4\eta_B|\alpha||\beta_1|+\phi_1)-\sin(4\eta_B|\alpha||\beta_1|+\phi_2)\right)=0, \\
\\
|\beta_2|\left(\cos(4\eta_B|\alpha||\beta_2|-\phi_1)+\cos(4\eta_B|\alpha||\beta_2|-\phi_2)\right) \\
\quad +|\alpha|\left(\sin(4\eta_B|\alpha||\beta_2|-\phi_1)+\sin(4\eta_B|\alpha||\beta_2|-\phi_2)\right) \\
\qquad\qquad + \frac{2(1-\eta_A)}{\eta_A}|\beta_2|e^{2(1-2\eta_B)|\alpha|^2}=0.
\end{cases}
\tag{5.29}
$$

5.3 Generation of optical hybrid states

Entangled light fields have been extensively explored as tools for testing quantum mechanics and resources for quantum information processing. An intriguing challenge in this subject is to entangle different types of states of light such as microscopic and macroscopic states or wavelike and particle-like states [11–15, 184–188]. Some of those states have been found useful for quantum information applications [127, 166, 172, 189]. Recently, hybrid entanglement between a single photon in the polarization basis and a coherent state was found to be particularly useful for loophole-free Bell inequality tests [127], deterministic quantum teleportation, and resource-efficient quantum computation [172]. It was also shown that this type of hybrid entanglement can be purified using linear optical elements and the parity check gates [190]. While single photons are regarded as nonclassical states as light quanta, coherent states are considered to be classical states as their P functions are well defined [89] and they are robust against decoherence as "pointer states" [90]. In this regard, the hybrid entanglement is closely related to Schrödinger's *Gedankenexperiment*, where the fate of a classical object, the cat, is entangled with the state of a single atom [6].

In this section, we suggest a nondeterministic scheme to generate the desired form of hybrid entanglement between a single-photon polarization qubit and a coherent-state field. Our scheme requires a superposition of coherent states (SCS), $|\alpha\rangle + |-\alpha\rangle$ [10, 191–194], and a polarization entangled photon pair, $|H\rangle|V\rangle + |V\rangle|H\rangle$, as resources, in addition to beam splitters, the displacement operation and four photodetectors. We find that even

when inefficient detectors are used, an arbitrarily high fidelity can be obtained by adjusting a beam-splitter ratio, and the displacement amplitude. This proposal is experimentally feasible using a squeezed single photon (or a squeezed vacuum state) as a good approximation of an ideal SCS [195]. Remarkably, reasonably high fidelities may still be obtained using on-off detectors with low efficiencies and available resource states under current technology.

5.3.1 Generation Scheme

We aim to generate the optical hybrid state with amplitude α_f

$$|\Psi_\varphi(\alpha_f)\rangle_{AB} = \frac{1}{\sqrt{2}}\left(|H\rangle_A |\alpha_f\rangle_B + e^{i\varphi}|V\rangle_A |-\alpha_f\rangle_B\right), \tag{5.30}$$

where $|\pm\alpha_f\rangle_B$ are coherent states in the field mode B and φ is a relative phase factor. As discussed in the previous sections, this type of state shows obvious properties as macroscopic entanglement when α is sufficiently large. A classification of hybrid entanglement was attempted [196], according to which the state in Eq. (5.30) is categorized as a discrete-variable-like hybrid entanglement. This type of entanglement was also characterized by a matrix Wigner function in the context of trapped ions [197].

In order to generate the hybrid entanglement, as shown in Fig. 20, we first need to prepare a polarization entangled photon pair and a SCS as

$$|\chi\rangle_{12} \otimes |\mathrm{SCS}_\varphi(\alpha_i)\rangle_3, \tag{5.31}$$

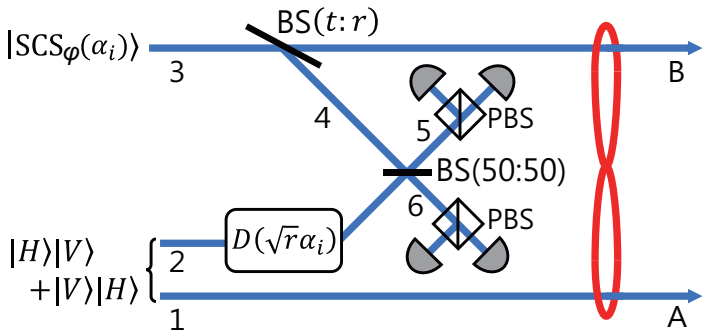

Figure 20: Generation scheme for hybrid entanglement. The beam-splitter reflectivity r and the amplitude α_i of the SCS determine the amplitude $\sqrt{r}\alpha_i$ of the displacement operation.

where $|\chi\rangle_{12} = (|H\rangle_1 |V\rangle_2 + |V\rangle_1 |H\rangle_2)/\sqrt{2}$ and $|\mathrm{SCS}_\varphi(\alpha_i)\rangle_3 = N_\varphi(|\alpha_i\rangle_3 + e^{i\varphi}|-\alpha_i\rangle_3)$ with $N_\varphi = (2 + 2e^{-2|\alpha_i|^2}\cos\varphi)^{-1/2}$. We suppose that α_i and α_f are real without losing generality throughout this section. A beam splitter of transmissivity t (reflectivity $r = 1 - t$) splits a coherent state $|\alpha\rangle$ into $|\sqrt{r}\alpha\rangle |\sqrt{t}\alpha\rangle$. The unbalanced beam splitter in Fig. 20 thus transforms $|\mathrm{SCS}_\varphi(\alpha_i)\rangle_3$ into $|\sqrt{r}\alpha_i\rangle_4 |\sqrt{t}\alpha_i\rangle_B + e^{i\varphi}|-\sqrt{r}\alpha_i\rangle_4 |-\sqrt{t}\alpha_i\rangle_B$. At the same time, the displacement operation is performed on mode 2 as

$$\hat{D}_2(\sqrt{r}\alpha_i)\,(|H\rangle_A |V\rangle_2 + |V\rangle_A |H\rangle_2)\,,$$

where $\hat{D}(\alpha) = e^{\alpha\hat{a}^\dagger - \alpha^*\hat{a}}$, and $\hat{a}^\dagger$ and $\hat{a}$ are the creation and annihilation operators. The state after the beam splitter and the displacement operation can be expressed as

$$
\begin{aligned}
&[\hat{D}_4(\sqrt{r}\alpha_i)\hat{D}_B(\sqrt{t}\alpha_i) + e^{i\varphi}\hat{D}_4(-\sqrt{r}\alpha_i)\hat{D}_B(-\sqrt{t}\alpha_i)] \\
&\otimes \hat{D}_2(\sqrt{r}\alpha_i)(\hat{a}^\dagger_{1H}\hat{a}^\dagger_{2V} + \hat{a}^\dagger_{1V}\hat{a}^\dagger_{2H})\,|0\rangle_1\,|0\rangle_2\,|0\rangle_4\,|0\rangle_B\,,
\end{aligned}
\tag{5.32}
$$

in terms of operators acting on the vacuum states.

A 50:50 beam splitter as shown in Fig. 20 is then used to mix the reflected part of $|\mathrm{SCS}_\varphi(\alpha_i)\rangle_3$ (mode 4) and the displaced part of $|\chi\rangle_{12}$ (mode 2) in order to erase 'which path' information. The unitary matrix corresponding to the beam splitter can be represented as

$$
\begin{pmatrix} \hat{a}_6 \\ \hat{a}_5 \end{pmatrix} = \begin{pmatrix} \cos\xi & -ie^{i\phi}\sin\xi \\ -ie^{-i\phi}\sin\xi & \cos\xi \end{pmatrix} \begin{pmatrix} \hat{a}_4 \\ \hat{a}_2 \end{pmatrix}, \tag{5.33}
$$

where we choose $\xi = \pi/4$ and $\phi = \pi/2$ to model the 50:50 beam splitter. The operators of modes 2 and 4 are then transformed as $\hat{a}_2 \to (\hat{a}_5 + \hat{a}_6)/\sqrt{2}$ and $\hat{a}_4 \to (-\hat{a}_5 + \hat{a}_6)/\sqrt{2}$, respectively, and it is also straightforward to show $\hat{D}_4(\alpha)\hat{D}_2(\beta) \to \hat{D}_5[(-\alpha+\beta)/\sqrt{2}]\hat{D}_6[(\alpha+\beta)\sqrt{2}]$ After passing through a 50:50 beam splitter, the operators for modes 2 and 4 evolve as

$$
\hat{D}_4(\alpha)\hat{D}_2(\beta)\hat{a}^\dagger_{2\lambda} \to \hat{D}_5\left(\frac{-\alpha+\beta}{\sqrt{2}}\right)\hat{D}_6\left(\frac{\alpha+\beta}{\sqrt{2}}\right)\frac{\hat{a}^\dagger_{5\lambda} + \hat{a}^\dagger_{6\lambda}}{\sqrt{2}}, \tag{5.34}
$$

where λ indicates the polarization direction, H or V. By taking $\alpha = \pm\sqrt{r}\alpha_i$ and $\beta = \sqrt{r}\alpha_i$, only one of the displacement operators survives with amplitude $\sqrt{2r}\alpha_i$ in modes 5 and 6, while operators in the other modes, $\hat{a}_A$ and $\hat{a}_B$, remain the same. Using Eqs. (5.32) and (5.34), we find the state right

before reaching the polarizing beam splitters (PBSs) in Fig. 20 as

$$\begin{aligned}|\psi_\varphi\rangle =& \frac{N_\varphi}{2}\Big[|H\rangle_A \hat{D}_6(\sqrt{2r}\alpha_i)\left(|V\rangle_5|0\rangle_6+|0\rangle_5|V\rangle_6\right)\left|\sqrt{t}\alpha_i\right\rangle_B \\ &+ e^{i\varphi}|H\rangle_A \hat{D}_5(\sqrt{2r}\alpha_i)\left(|V\rangle_5|0\rangle_6+|0\rangle_5|V\rangle_6\right)\left|-\sqrt{t}\alpha_i\right\rangle_B \\ &+ |V\rangle_A \hat{D}_6(\sqrt{2r}\alpha_i)\left(|H\rangle_5|0\rangle_6+|0\rangle_5|H\rangle_6\right)\left|\sqrt{t}\alpha_i\right\rangle_B \\ &+ e^{i\varphi}|V\rangle_A \hat{D}_5(\sqrt{2r}\alpha_i)\left(|H\rangle_5|0\rangle_6+|0\rangle_5|H\rangle_6\right)\left|-\sqrt{t}\alpha_i\right\rangle_B\Big].\end{aligned} \tag{5.35}$$

The final step is to measure two single photons, one for mode 5 and the other for mode 6, in different polarizations. The first measurement operator can be expressed as

$$\hat{\Pi} = \mathbb{1}_A \otimes |0\rangle\langle 0|_{5H} \otimes |1\rangle\langle 1|_{5V} \otimes |1\rangle\langle 1|_{6H} \otimes |0\rangle\langle 0|_{6V} \otimes \mathbb{1}_B. \tag{5.36}$$

The second and third terms of Eq. (5.35) are excluded by the conditioning measurement Π. It produces to the ideal hybrid state as

$$\hat{\rho} = \frac{\mathrm{Tr}_{56}\left[\hat{\Pi}|\psi_\varphi\rangle\langle\psi_\varphi|\right]}{\langle\psi_\varphi|\Pi|\psi_\varphi\rangle} = \left|\hat{\Psi}_\varphi(\alpha_f)\right\rangle\langle\Psi_\varphi(\alpha_f)|_{AB} \tag{5.37}$$

where $\alpha_f = \sqrt{t}\alpha_i$. The success probability to obtain the hybrid state is

$$\begin{aligned}P^\varphi &= \langle\psi_\varphi|\hat{\Pi}|\psi_\varphi\rangle \\ &= N_\varphi^2(1-t)\alpha_i^2 e^{-2(1-t)\alpha_i^2} = N_\varphi^2(\frac{1}{t}-1)\alpha_f^2 e^{-2(\frac{1}{t}-1)\alpha_f^2}.\end{aligned} \tag{5.38}$$

The success probability for a given value of α_i can be maximized by taking $t = 1 - 1/(2\alpha_i^2)$ with the hybrid state size $\alpha_f = \sqrt{\alpha_i^2 - 1/2}$. In this

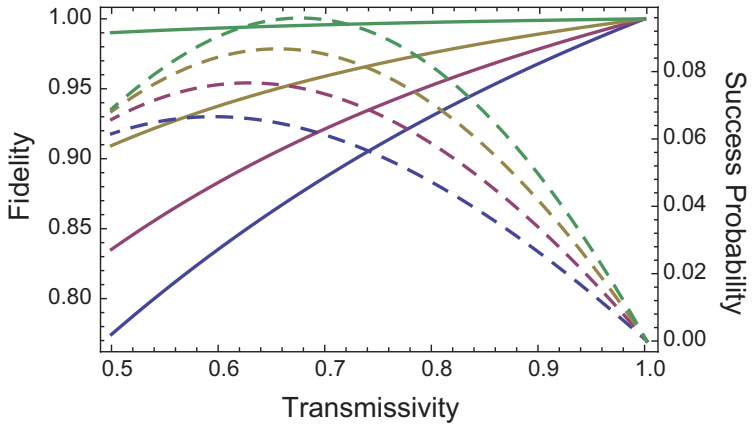

Figure 21: Fidelity (solid curves) and total success probability (dashed curves) of the hybrid entangled state $|\Psi_\pi(\alpha_f)\rangle_{AB}$ for the beam-splitter transmissivity t. The amplitude of the target hybrid state is assumed to be $\alpha_f = 1$, and four cases are plotted with detection efficiencies $\eta = 0.7$, 0.8, 0.9, and 0.99 (starting from the bottom).

case, P^φ approaches $1/(8e) \approx 4.60\%$ when the initial amplitude α_i is large enough.

The other measurement event of $\hat{\Pi}' = \mathbb{1}_A \otimes |1\rangle\langle 1|_{5H} \otimes |0\rangle\langle 0|_{5V} \otimes |0\rangle\langle 0|_{6H} \otimes |1\rangle\langle 1|_{6V} \otimes \mathbb{1}_B$ results in the bit-flipped hybrid states $|V\rangle_A |\alpha_f\rangle_B + e^{i\varphi} |H\rangle_A |-\alpha_f\rangle_B$. It can be converted to the target state by performing a simple bit-flip operation on mode A or a π-phase shift on mode B. The total success probability is therefore $P^\varphi_{\rm tot} = 2P^\varphi$. We can also change the relative phase of $|\chi\rangle_{12}$ in order to change the relative phase φ of the generated hybrid state.

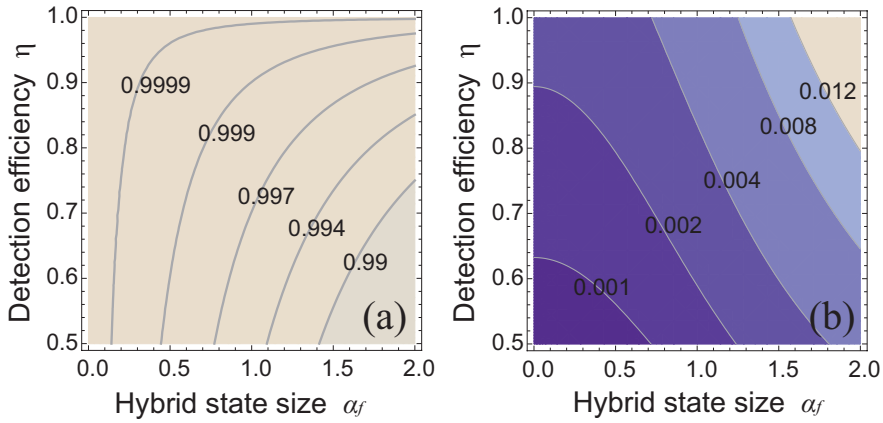

Figure 22: (a) Fidelity and (b) total success probability for state $|\Psi_\pi(\alpha_f)\rangle_{AB}$ in terms of its amplitude (α_f) and detection efficiency (η). The transmissivity of the beam splitter is assumed to be $t = 0.99$.

5.3.2 Detection inefficiency and vacuum mixtures

We need to consider effects of imperfect photodetectors that may lower the fidelity between the generated hybrid state and the ideal one. An imperfect photodetector with quantum efficiency η can be expressed as a positive operator-valued measurement

$$\hat{E}_\eta^{(n)} = \sum_{m=0}^{\infty} \binom{n+m}{m} \eta^n (1-\eta)^m \, |n+m\rangle \langle n+m| \tag{5.39}$$

in the photon number basis. The total measurement operator for our scheme described in Fig. 1 then becomes

$$\hat{\Pi}_\eta = \mathbb{1}_A \otimes \hat{E}_{\eta,5H}^{(0)} \otimes \hat{E}_{\eta,5V}^{(1)} \otimes \hat{E}_{\eta,6H}^{(1)} \otimes \hat{E}_{\eta,6V}^{(0)} \otimes \mathbb{1}_B, \tag{5.40}$$

and the heralded state is given by

$$\hat{\rho}_\eta = \frac{\mathrm{Tr}_{56}\left[\hat{\Pi}_\eta \left|\psi_\varphi\right\rangle \left\langle\psi_\varphi\right|\right]}{\left\langle\psi_\varphi\right|\hat{\Pi}_\eta \left|\psi_\varphi\right\rangle}. \tag{5.41}$$

In the case of imperfect detection, the fidelity and the success probability can be calculated as

$$\mathcal{F}_\eta^\varphi = {}_{AB}\left\langle\Psi_\varphi\right|\rho_\eta \left|\Psi_\varphi\right\rangle_{AB} = \frac{1}{2}\left(1 + e^{-2(1-\eta)(\frac{1}{t}-1)\alpha_f^2}\right) \tag{5.42}$$

and

$$P_{\eta,\mathrm{tot}}^\varphi = 2\langle\psi_\varphi|\hat{\Pi}_\eta \left|\psi_\varphi\right\rangle = 2N_\varphi^2\eta^2(\frac{1}{t}-1)\alpha_f^2 e^{-2\eta(\frac{1}{t}-1)\alpha_f^2}, \tag{5.43}$$

respectively. The fidelity and the success probability of the heralded state depend on η, α_f and t. We emphasize that as shown in Eq. (5.42), even if the detection efficiency η is limited, the hybrid state can be generated with an arbitrarily high fidelity by taking $t \to 1$. The cost to obtain a high fidelity is to tolerate a low success probability which becomes zero as the fidelity reaches unity. Figures 21 and 22 show the fidelity and the success probability by changing various parameters.

In a real experiment, the polarization entangled photon pair $\left|\chi\right\rangle_{12}$ used for our scheme may be mixed with the vacuum state $\left|0\right\rangle_{12}$ for modes 1 and 2. The effective form of such a mixed state is

$$\hat{\rho}_\chi = z\big(\left|\chi\right\rangle\left\langle\chi\right|\big)_{12} + (1-z)\big(\left|0\right\rangle\left\langle 0\right|\big)_{12}, \tag{5.44}$$

where $0 < z \leq 1$. Remarkably, the vacuum component can be filtered by the conditioning measurement Π. When states $|0\rangle_{12} \otimes |\mathrm{SCS}_{\varphi}(\alpha_i)\rangle_3$ are initially prepared, the states for modes 5 and 6 will become $\left|\sqrt{2r}\alpha_i\right\rangle_5 |0\rangle_6$ or $|0\rangle_5 \left|\sqrt{2r}\alpha_i\right\rangle_6$ before the heralding measurement [see Eq. (5.35)], and one of the modes will not contain any photons. Therefore, there is no chance to get the successful measurement event (i.e., single-photon measurement on both modes 5 and 6). Meanwhile, the success probability decreases by factor z as the procedure starting with the vacuum state always fails.

5.3.3 Use of approximate resource states

The SCSs required as resources for our scheme have been experimentally demonstrated while their fidelities and sizes are more or less limited [10, 191–194]. As an example, it has been shown that a photon-subtracted squeezed state (or equivalently, a squeezed single photon [198]) well approximates an ideal SCS, $|\mathrm{SCS}_{\pi}(\alpha)\rangle \propto |\alpha\rangle - |-\alpha\rangle$, for relatively small values of α [195, 199], and its experimental demonstrations have been reported [191–194]. A squeezed single-photon state in the Fock basis is

$$\hat{S}(s)\,|1\rangle = \sum_{n=0}^{\infty} \frac{(\tanh s)^n}{(\cosh s)^{3/2}} \frac{\sqrt{(2n+1)!}}{2^n n!}\,|2n+1\rangle\,, \tag{5.45}$$

where $\hat{S}(s) = e^{-(s/2)(\hat{a}^2 - \hat{a}^{\dagger 2})}$ and s is the squeezing parameter. Its fidelity to an ideal state $|\mathrm{SCS}_{\pi}(\alpha)\rangle$ is

$$\mathcal{F}(\alpha, s) = |\langle \mathrm{SCS}_{\pi}(\alpha)|\hat{S}(s)\,|1\rangle\,|^2 = \frac{2\alpha^2 e^{\alpha^2(\tanh s - 1)}}{(\cosh s)^3(1 - e^{-2\alpha^2})}. \tag{5.46}$$

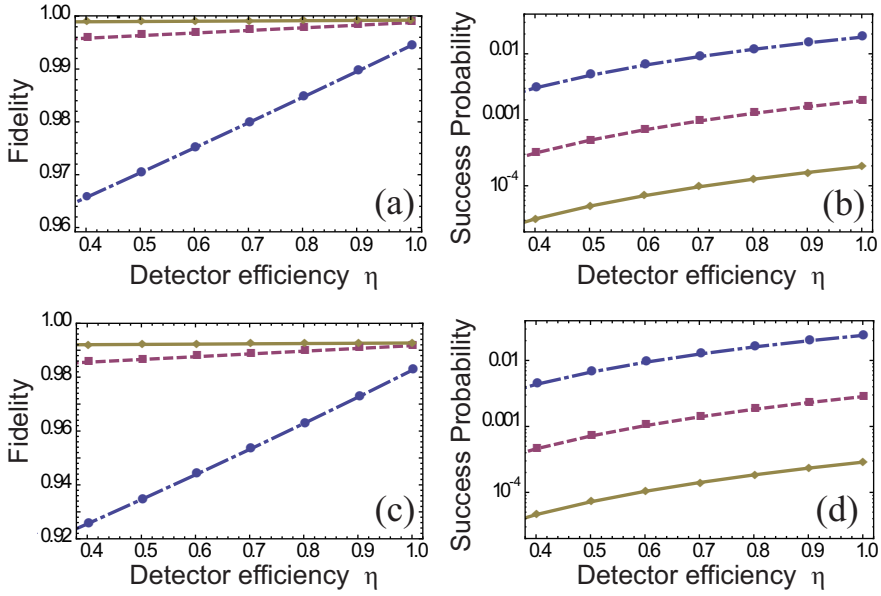

Figure 23: (a), (c) Fidelity and (b), (d) total success probability for state $|\Psi_\pi(\alpha_f)\rangle_{AB}$ using photon-subtracted squeezed states as approximate SCSs. The squeezing parameters used to obtain the photon-subtracted squeezed states are $s = 0.161$ (upper figures) and $s = 0.313$ (lower figures). The transmissivity is $t = 0.9$ (dot-dashed lines), $t = 0.99$ (dashed lines), and $t = 0.999$ (solid lines), respectively. The vacuum portion of the polarization entangled pair is assumed to be $1 - z = 0.5$.

For example, squeezing parameters $s = 0.161$ and 0.313 approximate $|\mathrm{SCS}_\pi(\alpha_i)\rangle$ with amplitudes $\alpha_i = 0.7$ and 1 with fidelities $\mathcal{F} = 0.9998$ and 0.997, respectively [195]. We choose these two values for our investigation.

We note that for a small squeezing parameter s, it is sufficient to reduce the state (5.45) in the number basis with an appropriate cutoff number, n_{cut}, for our numerical calculations. For example, the amplitude ratio of $n = 7$ to $n = 0$ of state (5.45) is less than 0.0005 for $s = 0.313$ (and even smaller for $s = 0.161$), thus we take the cut-off number $n_{\mathrm{cut}} = 7$, where the actual

photon number cutoff is $2n_{\rm cut}+1=15$ from Eq. (5.45). We can also model the beam-splitter of transmissivity t ($r=1-t$) in the photon number basis, which transforms incoming modes i and j into outgoing modes i' and j' as

$$|n\rangle_i\,|m\rangle_j \to \sum_p^n \sum_q^m B_{pq}^{nm}\,|p+m-q\rangle_{i'}\,|n-p+q\rangle_{j'}\,, \tag{5.47}$$

where $B_{pq}^{nm}=\binom{n}{p}\binom{m}{q}\sqrt{\frac{(n-p+q)!(m-q+p)!}{n!m!}}\sqrt{t}^{p+q}\sqrt{r}^{n+m-p-q}(-1)^{n-p}$. Numerical calculations using $n_{\rm cut}$ and the beam splitter model in the photon number basis are applied in order to calculate the fidelity and the success probability with approximate resource states. Figure 23 shows that the squeezing parameter of $s=0.161$ ($s=0.313$) and the vacuum portion of $z=0.5$ result in the fidelity of the heralded hybrid entanglement with fidelity $\mathcal{F}>0.996$ ($\mathcal{F}>0.986$) and amplitude $\alpha_f\approx 0.7$ ($\alpha_f\approx 1.0$) by taking transmissivity $t\geq 0.99$ and assuming realistic detector efficiency $\eta\geq 0.4$. We emphasize that the two chosen amplitudes here, $\alpha_f\approx 0.7$ and $\alpha_f\approx 1.0$, for hybrid entanglement were suggested as the best values for a loophole-free Bell test [127] and for the hybrid-qubit quantum computation [172], respectively. The success probability of the conditioning measurement with $t=0.99$ varies from $P_{\rm tot}\approx 10^{-4}$ to $P_{\rm tot}\approx 10^{-3}$ by increasing the detection efficiency η from 0.4 to 1.

In order to investigate a degree of entanglement for the heralded hybrid states, we evaluate negativity of the partial transpose [200–202], $E(\hat{\rho})=||\hat{\rho}^{T_A}||-1=-2\sum_i\lambda_i^-$, where $\hat{\rho}^{T_A}$ is the partial transpose of $\hat{\rho}$ and λ_i^- are its negative eigenvalues. The degree $E(\hat{\rho})$ ranges from 0 to 1, while an ideal hybrid state of $\alpha\gg 1$ results in $E(\hat{\rho})\approx 1$. The degrees of entanglement

are $E(\hat{\rho}) = 0.922$ ($E(\hat{\rho}) = 0.982$) for squeezing parameters $s = 0.161$ ($s = 0.313$) by taking $t = 0.99$, $z = 0.5$, and $\eta = 0.7$. The entanglement degrees can be compared with those of the ideal hybrid states with $\alpha_f = 0.7$ and $\alpha_f = 1.0$, i.e., $E(\hat{\rho}) = 0.927$ and $E(\hat{\rho}) = 0.991$, respectively.

5.3.4 Imperfect on-off detectors and SPDC sources

An on-off photodetector (e.g., avalanche photodiode) typically used in a laboratory does not distinguish between a single photon and two or more photons. Furthermore, a realistic polarized photon pair generated by spontaneous parametric down conversion (SPDC) contains undesired vacuum and higher order terms in addition to state $|\chi\rangle$.

On-off photodetection changes the conditioning measurement of Eq. (5.40) to

$$\hat{\Pi}_{\eta}^{\mathrm{on-off}} = \mathbb{1}_A \otimes \hat{E}_{\eta,5H}^{(0)} \otimes \hat{E}_{\eta,5V}^{(\mathrm{click})} \otimes \hat{E}_{\eta,6H}^{(\mathrm{click})} \otimes \hat{E}_{\eta,6V}^{(0)} \otimes \mathbb{1}_B, \qquad (5.48)$$

where $\hat{E}^{(\mathrm{click})} = \mathbb{1} - \hat{E}^{(0)} = \sum_{m=0}^{\infty}[1-(1-\eta)^m]\,|m\rangle\langle m|$. The polarization entangled state created by SPDC can be represented by $|\mathrm{SPDC}_\chi\rangle = \exp(\xi\hat{K}_+ + \xi^*\hat{K}_-)\,|0\rangle_{12}$, where $\hat{K}_+ = \hat{a}_{1H}^\dagger\hat{a}_{2V}^\dagger + \hat{a}_{1V}^\dagger\hat{a}_{2H}^\dagger$ and $\hat{K}_- = \hat{K}_+^\dagger$ with the squeezing parameter ξ. The state can be simplified as

$$|\mathrm{SPDC}_\chi\rangle = \sqrt{1-\lambda^2}\sum_{n=0}^{\infty}\lambda^n\,|\Phi_n\rangle_{12}\,, \qquad (5.49)$$

where $\lambda = \tanh|\xi|$ is the interaction strength and

$$|\Phi_n\rangle_{12} = (n+1)^{-1/2} \sum_{m=0}^{n} |m\rangle_{1H} |n-m\rangle_{1V} |n-m\rangle_{2H} |m\rangle_{2V}$$

. In this case, the probability ratio for $|\Phi_n\rangle$ has an order of $\mathcal{O}(\lambda^{2n})$. Note that $|\Phi_0\rangle$ is the vacuum state and $|\Phi_1\rangle = |\chi\rangle$. The total success probability of the final heralding measurement using the SPDC source then becomes

$$P_{\text{tot}} = (1-\lambda^2)\left[P_{\text{vac}} + \lambda^2 P_{|\chi\rangle} + \lambda^4 P_{|\Phi_2\rangle} + \mathcal{O}(\lambda^6)\right], \tag{5.50}$$

where P_{vac}, $P_{|\chi\rangle}$, and $P_{|\Phi_2\rangle}$ are success probabilities when the input state was the vacuum, $|\chi\rangle$, and $|\Phi_2\rangle$, respectively. Generally, λ in the SPDC source has a small value so that higher order terms can be neglected. We shall ignore $\mathcal{O}(\lambda^6)$ in the following calculations.

The input state of $|\chi\rangle$ is the only desired state for generating the hybrid entanglement and apparently successful heralding measurements of all the other input states will degrade the fidelity of the generated state. The fidelity $\mathcal{F}_{\text{eff}}$ of the finally generated state under these more realistic conditions is

$$\begin{aligned} \mathcal{F}_{\text{eff}} &= \frac{(1-\lambda^2)\lambda^2 P_{|\chi\rangle}}{P_{\text{tot}}}\mathcal{F} \\ &\approx \frac{P_{|\chi\rangle}}{\lambda^{-2}P_{\text{vac}} + P_{|\chi\rangle} + \lambda^2 P_{|\Phi_2\rangle}}\mathcal{F}. \end{aligned} \tag{5.51}$$

We calculate P_{vac}, $P_{|\chi\rangle}$ and $P_{|\Phi_2\rangle}$ using the numerical method in the number basis as explained in the previous section. We plot the final fidelities $\mathcal{F}_{\text{eff}}$ for several choices of on-off detection efficiencies η and the beam-splitter

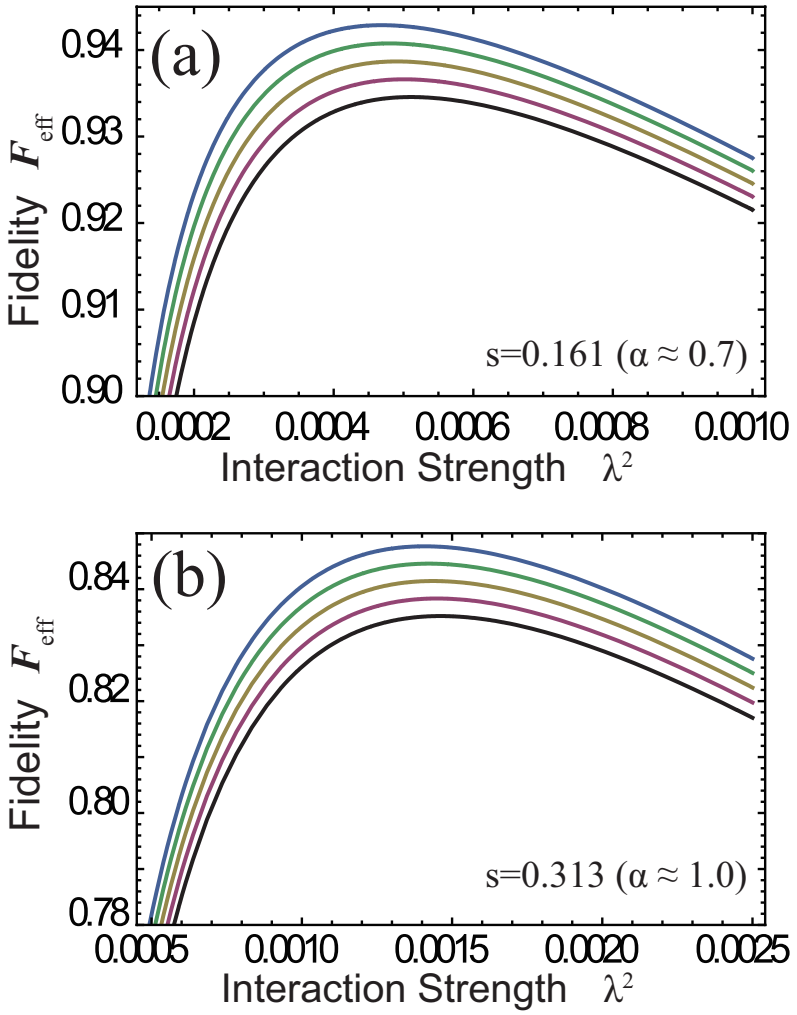

Figure 24: Expected fidelity of the generated hybrid entanglement when a squeezed single-photon state and a SPDC source with interaction strength λ are applied to the scheme using inefficient on-off detectors. The squeezing parameters are (a) $s = 0.161$ and (b) $s = 0.313$ while the beam-splitter transmissivity is $t = 0.99$ for both cases. The efficiencies of the on-off detectors are $\eta = 0.9, 0.7, 0.5, 0.3$, and 0.1 starting from the top.

transmissivity $t = 0.99$ in Fig. 5.3.4. Remarkably, the fidelities are insensitive to inefficiency η of the on-off detectors even though it reduces the success probabilities of the scheme. The fidelities are reasonably high for large regions of experimentally relevant values of the interaction strength λ.

For example, we can obtain the hybrid state of $\alpha_f = 0.7$ and $\mathcal{F}_{\rm eff} \approx 0.939$ using the SPDC source of $\lambda = 2.2 \times 10^{-2}$ and a squeezed single-photon state of $s = 0.161$ with on-off detectors of 50% efficiency, while the success probability is reduced to $P_{\rm tot} = 5.1 \times 10^{-7}$. As another example, the hybrid state of $\alpha_f = 1$ and $\mathcal{F}_{\rm eff} \approx 0.842$ can be generated using the SPDC source of $\lambda = 3.8 \times 10^{-2}$ and a squeezed single-photon state of $s = 0.313$ with the on-off detectors of 50% efficiency while the success probability is $P_{\rm tot} = 2.4 \times 10^{-6}$. Figure 5.3.4 shows that the fidelities are still reasonably high even when the detection efficiency is as low as 10%. We also note that dark counts during the heralding detection process may be another factor to degrade the final fidelity, and photodetectors with ultralow dark count rates compared to quantum efficiency [203–207] may be used for high fidelities. On the other hand, we expect that the effects of dark counts may be limited at a reasonable level using current technology as done for this type of experiment [14, 15].

5.4 Remarks

We have studied Bell inequality test with hybrid entanglement between polarization of a single photon and a coherent state field. We have investigated two different kinds of measurements, on/off and photon number parity measurement, on the coherent field to find Bell violations with optimizing conditions with of perfect and realistic detectors. With perfect detectors, on/off measurements give the maximum Bell violation of ≈ 2.61 at $\alpha \approx 0.664$, while parity measurements give the violation approaching Cirel'son's bound $(2\sqrt{2})$ for large values of the coherent amplitude ($\alpha \gg 1$).

In order to see the Bell-CHSH inequality violation without the detection loophole, the detector efficiency $\eta > 67\%$ is required for both on/off and parity measurement schemes. It is important to note that small coherent amplitudes for hybrid entanglement are needed to obtain the low required efficiency while there is a trade-off between the threshold efficiency and the degree of Bell violation in terms of the coherent amplitudes. Nevertheless, a coherent amplitude of $|\alpha| < 1.0$ is sufficient to obtain the maximum Bell violation for the most cases of the detection efficiency. Comparing two different measurement schemes, we have found that on/off measurements provide higher violation of Bell inequality than parity measurements under realistic conditions ($\eta < 98.68\%$), although the violation does not reach Cirel'son's bound. However, the threshold values of detection efficiency to violate Bell inequality are similar between both the measurement schemes.

Our results may be used to experimentally explore loophole-free Bell inequality tests. Required detection efficiency for a loophole-free Bell test

is within reach of current technology [208–210]. The generation of hybrid entanglement is a challenging task since it requires a clean cross-Kerr nonlinearity, while efforts are being made to obtain high fidelity cross-Kerr interactions [177–179]. It is also possible, in principle, to approximately generate arbitrary multimode entangled states using single-photon sources, coherent states, and single-photon detectors [211]. In this context, a possible attempt for the generation of hybrid entanglement is to explore combinations of experimentally available photon addition and subtraction techniques [212–215] as investigated for the generation of some exotic quantum states [216–218].

It is interesting to note that coherent states are considered most classical among all pure states while single photons are typical microscopic quantum systems. In this sense, Bell inequality tests using the optical hybrid states may reveal a significant feature of nonlocality between quantum and classical systems. It will be an interesting future work to explore quantum nonlocality with optical hybrid entanglement using "classical" measurements [219, 220].

We have also suggested a scheme to generate hybrid entanglement between a single photon qubit and a coherent state qubit. Unlike previous proposals [14, 15, 188], our scheme enables one to generate the exact form of hybrid entanglement, without approximation, required for resource-efficient optical hybrid quantum computation [172] and loophole-free Bell inequality tests [127]. The required resources are an SCS, an entangled photon pair, the displacement operation, four photodetectors, and beam splitters. Even when photodetectors with limited efficiencies are used, hybrid entanglement with

an arbitrarily high fidelity can be generated at the price of a lower success probability. We have also analyzed fidelities of the generated states when a SPDC source, an approximate SCS, and on-off detectors with low efficiencies are used for the scheme. Even under these realistic assumptions, hybrid entanglement with high fidelities may be obtained. According to our analysis, experimental implementation of our scheme seems feasible using current technology despite some expected experimental imperfections.

Chapter 6

Many-body coherence in quantum thermodynamics

The contents of this chapter are largely based on [H. Kwon, H. Jeong, D. Jennings, B. Yadin, and M. S. Kim, "Clock/work trade-off relation for coherence in quantum thermodynamics", arXiv: 1711.03395 (2017)] [221].

6.1 Introduction

Thermodynamics describes the physical nature of a macroscopic system composed of a large number of particles. Based on its intimate relation with information theory, expanding the domain of thermodynamics into the quantum regime has raised interests. One of the questions in quantum thermodynamics is the impact of quantum coherences on the laws of thermodynamics. The cost of creating quantum coherences [222–226] and quantum correlations [227–233] and extractable work from those quantum effects have been studied.

The discovery of connections between entanglement and the second law of thermodynamics has inspired recent attempts to describe thermodynamics using quantum resource theories [234–246]. A resource theory provides a tool to identify allowed transitions by a constrained operation, which is often called a *free operation*. The theory of entanglement [24, 25]

and the theories of quantum coherence [22,23], thermodynamics (athermality) [237, 239], and reference frame (asymmetry) [67–70, 247] have been studied in the framework of the resource theory to quantify the amount of resource contained in a given state. The free operation, the so-called thermal operation (TO), in quantum thermodynamics can be characterized as a unitary interaction between a system and a bath preserving the total system-bath Hamiltonian, and the second law of thermodynamics has been studied by introducing the free energies for quantum states [237, 238]. Lostaglio *et. al* [235, 236] and Ćwikliński *et. al* [234] studied implications of the second law of thermodynamics beyond the free energies to show that the quantum coherences do not increase under TO's, and that information-theoretic analysis based on symmetry principles must be employed. However, quantum thermodynamics under TO's in many-body systems have not been well studied especially for high dimensional quantum systems with coherence.

In this Chapter, we illustrate ways to understand quantum coherences in many-body systems by the scope of quantum resource theory. We describe how thermodynamic coherence splits into two kinds – "internal" coherence that admits an energetic value in terms of thermodynamic work, and "external" coherence that does not have energetic value, but instead corresponds to the functioning of the system as a quantum clock. For the latter form of coherence we provide dynamical constraints that relate to quantum metrology and macroscopicity, while for the former, we show that quantum states exist that have finite internal coherence yet with zero deterministic work value. Finally, under minimal thermodynamic assumptions, we establish a clock/work trade-off relation between these two types of coherences.

This can be viewed as a form of time-energy conjugate relation within quantum thermodynamics that bounds the total maximum of clock and work resources for a given system.

6.2 Resource theory of quantum thermodynamics

6.2.1 Thermal operation and quantum free energy

First we construct the resource theory of quantum thermodynamics by characterizing free states and free operations. Suppose the a given system with Hamiltonian $\hat{H}_S$ and a bath with its Hamiltonian $\hat{H}_B$. In the aspect of classical thermodynamics, the bath is in a equilibrium at temperature T that can be described as a Gibbs state

$$\hat{\gamma}_B = Z_B^{-1} e^{-\beta \hat{H}_B},$$

by which the entropy is maximized for a fixed energy. Then we can impose the energy preserving condition to a thermal process acting on the total system-bath state. We additionally assume that the total system-bath state is closed system from other environments that every process in this joint system can be described by a unitary operation. This operation is called a TO on the system state $\hat{\rho}_S$ that can be mathematically written as [234–238]

$$\Lambda_\beta(\hat{\rho}_S) = \mathrm{Tr}_{B'}\left[\hat{U}(\hat{\rho}_S \otimes \hat{\gamma}_B)\hat{U}^\dagger\right], \quad \text{(Free operation)} \tag{6.1}$$

where $\hat{\gamma}_B = Z_B^{-1} e^{-\beta \hat{H}_B}$ is a Gibbs state at temperature T with the partition function $Z_B = \mathrm{Tr}[e^{-\beta \hat{H}_B}]$, $\hat{U}$ is any unitary operator satisfying

$$[\hat{U}, \hat{H}_S + \hat{H}_B] = 0,$$

and $\mathrm{Tr}_{B'}$ refers to tracing out any subsystem of total system-bath. The inverse temperature parameter is given by $\beta = (k_B T)^{-1}$ with k_B being the Boltzmann factor. Note that the resource-free state for a TO is the Gibbs state of the system

$$\hat{\gamma} = Z_S^{-1} e^{-\beta \hat{H}_S} \quad (\text{Free state})$$

with $Z_S = \mathrm{Tr}[e^{-\beta \hat{H}_S}]$, which is in equilibrium with the thermal bath.

In order to identify the amount of resource which does not increase under TO's, the quantum free energy function

$$F(\hat{\rho}) = k_B T S(\hat{\rho}||\hat{\gamma}) - k_B T \log Z_S = \langle \hat{H} \rangle_{\hat{\rho}} - k_B T S(\hat{\rho}) \tag{6.2}$$

plays a central role in the regime of macroscopic systems [237, 238]. In the language of resource theory, the quantum free energy becomes a *monotone* under a TO, or the quantum thermodynamic process. Here, $\langle \hat{H} \rangle_{\hat{\rho}} = \mathrm{Tr} \hat{\rho} \hat{H}$, $S(\hat{\rho}) = -\mathrm{Tr} \hat{\rho} \log \hat{\rho}$ is the von Neumann entropy, and $S(\hat{\rho}||\hat{\sigma}) = \mathrm{Tr} \hat{\rho} (\log \hat{\rho} - \log \hat{\sigma})$ is the quantum relative entropy. A more general form of the free energy $F_\alpha(\hat{\rho}) = k_B T S_\alpha(\hat{\rho}||\hat{\gamma}) - k_B T \log Z_B$ based on the Renyi divergence

$S_\alpha(\hat{\rho}||\hat{\gamma})$ where

$$S_\alpha(\hat{\rho}||\hat{\sigma}) = \begin{cases} \frac{1}{\alpha-1}\log \mathrm{Tr}[\hat{\rho}^\alpha \hat{\sigma}^{1-\alpha}], & \alpha \in [0,1) \\ \frac{1}{\alpha-1}\log \mathrm{Tr}\left[\left(\hat{\sigma}^{\frac{1-\alpha}{2\alpha}}\hat{\rho}\hat{\sigma}^{\frac{1-\alpha}{2\alpha}}\right)^\alpha\right], & \alpha > 1, \end{cases}$$

were shown to be a complete set of monotones for classical states in the presence of TOs with catalysts [238].

6.2.2 Many-body correlations in quantum free energies

In a many-body system, the free energy can be contained in the local parties and their correlations. Furthermore, these correlations can be exchanged into free energies in local parties. To this end, we define the correlation in the free energy as the difference between the total free energy and the sum of free energies in the local parties:

$$C_\alpha(\hat{\rho}_{1:2:\cdots:N}) := (k_B T)^{-1}\left[F_\alpha(\hat{\rho}) - \sum_{i=1}^{N} F_\alpha(\hat{\rho}_i)\right], \tag{6.3}$$

where $\hat{\rho}_i$ is a local state of i-th party given by tracing out all the remaining parties. In the limiting case of $\alpha \to 1$, the free energy correlation becomes the total correlation in terms of von Neumann entropy, $\lim_{\alpha\to 1} C_\alpha(\hat{\rho}_{1:2:\cdots:N}) = S(\hat{\rho}) - \sum_{i=1}^{N} S(\hat{\rho}_i) := I(\hat{\rho}_{1:2:\cdots:N})$. Also, we note that the free-energy correlations $C_\alpha(\hat{\rho}_{1:2:\cdots:N})$ vanish for all α if the state is in a product form $\hat{\rho}_1 \otimes \hat{\rho}_2 \otimes \cdots \otimes \hat{\rho}_N$.

In order to study the free energy transfer from correlations, we compare

a product state $|\psi\rangle = |0\rangle_1 |1\rangle_2$ and an entangled state $|\phi\rangle = (|0\rangle_1 |1\rangle_2 + |1\rangle_1 |0\rangle_2)/\sqrt{2}$ for a bipartite two-level system with Hamiltonian $\hat{H}_{1(2)} = \omega_0 |1\rangle\langle 1|$ for each party. The sums of the local free energies are given by $\sum_{i=1}^{2} F(\psi_i) = \omega_0$ and $\sum_{i=1}^{2} F(\phi_i) = \omega_0 - 2k_B T$, respectively. Although the sum of the local free energies for $|\psi\rangle$ is larger than that of $|\phi\rangle$, the difference matches to the free energy correlation difference between $I(\psi_{1:2}) = 0$ and $I(\phi_{1:2}) = 2k_B T$. This relation also holds for every α-free energy. Note that the states ψ and ϕ are interconvertible under TOs, since they are in the same energy eigenspace. Thus it is clear that by the process $|\psi\rangle \overset{\text{TO}}{\longleftrightarrow} |\phi\rangle$, some amount of local free energy is converted into entanglement, raising correlation between the two parties, and vise versa.

Now we derive the free energy conditions when the system and bath are interacting under a TO. When the system-bath interaction is given by an unitary evolution $\hat{U}$ satisfying the energy conservation $[\hat{H}_S + \hat{H}_B, \hat{U}] = 0$, we obtain the following conserved quantity:

$$\Delta F_\alpha(\hat{\rho}_S) + \Delta F_\alpha(\hat{\rho}_B) + k_B T \Delta C_\alpha(\hat{\rho}_{S:B}) = 0. \tag{6.4}$$

Note that Eq. (6.4) holds generally of systems and baths: the system and bath can be initially coupled and the bath is not needed in thermal equilibrium. By the above relation, we can understand that the free energy of the system is leaked out by TO's either through the free energy correlation between the system and bath. In particular, when the system and the bath are initially uncorrelated, we retrieve the second law of thermodynamics [237, 238], given by $\Delta F_\alpha(\hat{\rho}_S) \leq 0$ for every α.

6.3 The role of coherence in quantum thermodynamics

6.3.1 Internal and external coherences in many-body systems

In this section, we will focus on a N-partite system with non-interacting subsystems. In this case, a Hamiltonian could be written as

$$\hat{H}_{\mathrm{tot}} = \sum_{i=1}^{N} \hat{H}_i$$

and we additionally assume that each i-th local Hamiltonian $\hat{H}_i$ has an non-degenerate energy spectrum of $\{E_i\}$ with local energy-eigenstates $|E_i\rangle$. Then a quantum state of this system could be represented as

$$\hat{\rho} = \sum_{\boldsymbol{E},\boldsymbol{E}'} \rho_{\boldsymbol{E}\boldsymbol{E}'} \left|\boldsymbol{E}\right\rangle \left\langle \boldsymbol{E}'\right|,$$

where $\boldsymbol{E} = (E_1, E_2, \cdots, E_N)$ is a string of local energies and $|\boldsymbol{E}\rangle = |E_1 E_2 \cdots E_N\rangle$ is a corresponding energy eigenstate. We also define the total energy of the string $\mathcal{E}_{\boldsymbol{E}} := \sum_{i=1}^{N} E_i$.

In order to describe classical thermodynamic properties of this system, the energy distribution of local energies and the correlation between them are both needed. This information is given by diagonal terms of density matrix $P(\boldsymbol{E}) = \mathrm{Tr}\left[\hat{\Pi}_{\boldsymbol{E}}\hat{\rho}\right] = \rho_{\boldsymbol{E}\boldsymbol{E}}$, where $\hat{\Pi}_{\boldsymbol{E}} = \left|\boldsymbol{E}\right\rangle \left\langle \boldsymbol{E}\right|$. On the other hand, a quantum system could contain more terms beyond classical energy distribution, given by coherence contained in off-diagonal elements $\left|\boldsymbol{E}\right\rangle \left\langle \boldsymbol{E}'\right|$

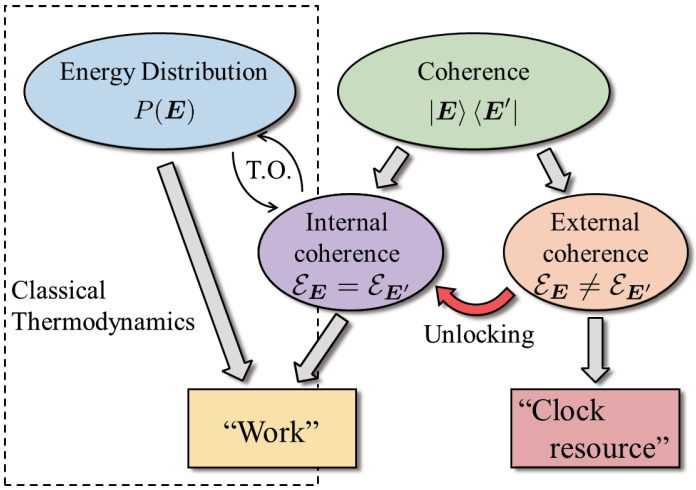

Figure 25: Schematic relationship between thermodynamic resources for many-body quantum systems.

for $\boldsymbol{E} \neq \boldsymbol{E}'$ (not necessarily $\mathcal{E}_{\boldsymbol{E}} \neq \mathcal{E}_{\boldsymbol{E}'}$) in a density matrix. This coherence can be further categorized into two types, coherence in the same energy level $\mathcal{E}_{\boldsymbol{E}} = \mathcal{E}_{\boldsymbol{E}'}$ and between different energy levels $\mathcal{E}_{\boldsymbol{E}} \neq \mathcal{E}_{\boldsymbol{E}'}$. In this section, we define them as *internal coherence* and *external coherence*, and study how each can be utilized in work extraction process and high-resolution time measurement, respectively.

As illustrated in Fig. 25, internal coherence may be used to extract work, however it has been shown that external coherences obey a super-selection rule (called "work-locking") that forbids work extraction, and is unavoidable if one wishes to explicitly account for all sources of coherence in thermodynamics [235]. We study this phenomenon by defining the process of extracting work *purely from the coherence*, without affecting the classical energy statistics. We find the conditions under which work can be

deterministically extracted in this way from a pure state.

Secondly, external coherences can be interpreted as 'clock resources' that can be used for quantum-mechanical tasks that require timing. This metrological advantage can be quantified by the quantum Fisher information [107] and the skew information [79] which give a new restriction of the state transformation by a TO. Based on the discussions in previous Chapters 3 and 4 on macroscopic coherence, a quantum state with a high clock resource can be interpreted as macroscopic quantum states. The result of this Chapter also provides the intuition that entangled states with a large energy gap, such as GHZ states that contains macroscopic coherences, cannot be generated from a product state using a TO. Finally, we derive a fundamental trade-off inequality between the quantum Fisher Information and the extractable work from coherence demonstrating how a system's potential for producing work is limited by its ability to act as a clock and vice-versa.

6.3.2 Work extraction using quantum correlation and coherence

The system-bath correlation in Eq. (6.4) may not be useful in thermodynamic processes since we do not have full access to the bath, in general. On the other hand, we can expect that the free energy correlations between the subsystems might be useful in thermodynamic tasks. It have been studied that thermodynamic work can be extracted from correlations [228–230, 232, 233]. In particular, we demonstrate that extra work can be extracted from many-body quantum coherences without changing the classical energy dis-

tribution $P(\boldsymbol{E})$ of the system.

We consider the following type of work extraction process

$$\hat{\rho} \otimes |0\rangle \langle 0|_W \xrightarrow{\text{TO}} \hat{\sigma} \otimes |W\rangle \langle W|_W,$$

by which the energy level of a work qubit is raised $|0\rangle_W$ to $|W\rangle_W$ with a work Hamiltonian $\hat{H}_W = W |W\rangle \langle W|_W$. In the case of energy block-diagonal states, which only contains internal coherences, the maximum amount of extractable work is given by [238]

$$W_{\hat{\rho}\to\hat{\sigma}} = k_B T \inf_{\alpha} \left[F_\alpha(\hat{\rho}) - F_\alpha(\hat{\sigma}) \right].$$

In order to construct work extraction preserving the energy statistics, we investigate extractable work by TO from a energy block-diagonal state $\hat{\rho}$ to its fully-dephased state $\hat{\rho}_{\text{diag}} = \sum_{\boldsymbol{E}} \hat{\Pi}_{\boldsymbol{E}} \hat{\rho} \hat{\Pi}_{\boldsymbol{E}} = \sum_{\boldsymbol{E}} P(\boldsymbol{E}) \hat{\Pi}_{\boldsymbol{E}}$, which has the same classical energy distribution $P(\boldsymbol{E})$ with $\hat{\rho}$. We assume that $\hat{H}_{\text{tot}} = \sum_{i=1}^{N} \hat{H}_i$ with non-degenerate local Hamiltonians $\hat{H}_i$, then local free energies of $\hat{\rho}$ and $\hat{\rho}_{\text{diag}}$ are the same, since $\hat{\rho}_i = \hat{\rho}_{\text{diag},i}$ for every local party. Thus, the extractable work comes from the difference of the free energy correlations:

$$\begin{aligned} W_{\text{coh}} &= \inf_{\alpha} \left[F_\alpha(\hat{\rho}) - F_\alpha(\hat{\rho}_{\text{diag}}) \right] \\ &= k_B T \inf_{\alpha} \left[C_\alpha(\hat{\rho}) - C_\alpha(\hat{\rho}_{\text{diag}}) \right]. \end{aligned}$$

It is important to notice that $\Delta C_\alpha(\hat{\rho}) := C_\alpha(\hat{\rho}) - C_\alpha(\hat{\rho}_{\text{diag}})$ is the quantum contribution to the free energy correlations since $C_\alpha(\hat{\rho}_{\text{diag}})$ describes

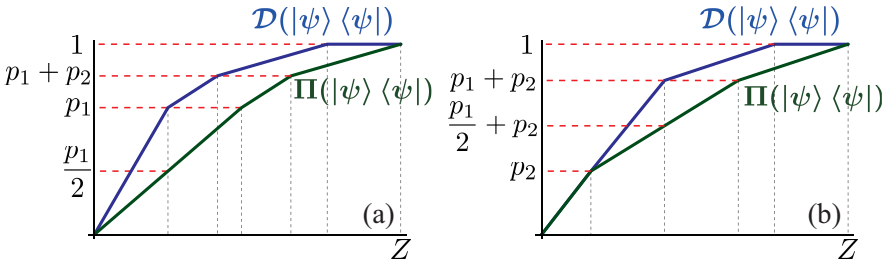

Figure 26: Thermomajorization graph for the energy-block diagonal state $\mathcal{D}(|\psi\rangle\langle\psi|)$ and its projection to an incoherent state $\Pi(|\psi\rangle\langle\psi|)$ for a two-qubit state $|\psi\rangle$ studied in the text with coefficients p_1 and p_2. Z represents the partition function of the system. (a) When $p_1 e^{\beta\omega_0}$ is the maximum among $p_i e^{\beta E_i}$, $W_{\rm coh}$ is positive, but (b) if another energy (e.g. $p_2 e^{2\beta\omega_0}$ in the plot) obtains the maximum, $W_{\rm coh} = 0$.

the classical correlations given by the energy statistics $P(\boldsymbol{E})$. We also note that $\Delta C_\alpha(\hat{\rho}) \geq 0$ for every α, thus there is always additional correlation contained in equi-level quantum coherence.

For example, consider extracting work from coherence in the pure two-qubit state

$$|\psi\rangle = \sqrt{p_0}\,|00\rangle + \sqrt{p_1}\left(\frac{|01\rangle + |10\rangle}{\sqrt{2}}\right) + \sqrt{p_2}\,|11\rangle\,,$$

where each qubit has local Hamiltonain $H_i = \omega_0\,|1\rangle\langle 1|$. As shown in Fig. 26 using the concept of thermomajorization [241], we have $W_{\rm coh} > 0$ only for sufficiently large p_1.

Furthermore, we find the necessary and sufficient condition for pure states to extract a non-zero amount of work deterministically from internal coherences even if the state is not in energy block-diagonal:

Observation 1. *For an N-partite pure many-body quantum state with energy distribution $P(\boldsymbol{E})$, a deterministic extraction of non-zero work is possible without changing energy distributions if and only if the state contains internal coherence for $\mathcal{E}^*$ such that $\mathcal{E}^* = \underset{\mathcal{E}}{\operatorname{argmax}}\ p_{\mathcal{E}} e^{\beta\mathcal{E}}$, where $p_{\mathcal{E}} = \sum_{\mathcal{E}_{\boldsymbol{E}}=\mathcal{E}} P(\boldsymbol{E})$.*

Proof: After energy block diagonalizing, the state can be written as $\mathcal{D}(|\Psi\rangle\langle\Psi|) = \sum_{\mathcal{E}} p_{\mathcal{E}} |\psi_{\mathcal{E}}\rangle\langle\psi_{\mathcal{E}}|$, where $|\psi_{\mathcal{E}}\rangle$ are pure eigenstates of energy $\mathcal{E}$. Suppose $\mathcal{E}^*$ gives the maximum value of $\log p_{\mathcal{E}} e^{\beta\mathcal{E}}$. Then we have

$$\begin{aligned} W_{\mathrm{coh}} &= \inf_{\alpha} \left[F_\alpha(\mathcal{D}(\hat{\rho})) - F_\alpha(\Pi(\hat{\rho}))\right] \\ &= \inf_{\alpha} \left(\frac{1}{\alpha-1}\right) \log \left[\frac{\sum_{\mathcal{E}} p_{\mathcal{E}}^{\alpha} e^{-\beta(1-\alpha)\mathcal{E}}}{\sum_{\mathcal{E}} e^{(1-\alpha)S_\alpha(\hat{\rho}_{\mathcal{E}-\mathrm{diag}})} p_{\mathcal{E}}^{\alpha} e^{-\beta(1-\alpha)\mathcal{E}}}\right], \end{aligned} \tag{6.5}$$

where $\hat{\rho}_{\mathcal{E}-\mathrm{diag}} = \Pi(|\psi_{\mathcal{E}}\rangle\langle\psi_{\mathcal{E}}|)$ is a fully dephased state in the energy eigenspace $\mathcal{E}$. Then we notice that $S_\alpha(\hat{\rho}_{\mathcal{E}-\mathrm{diag}})) > 0$ for any $\alpha \in [0,\infty)$, unless $\hat{\rho}_{\mathcal{E}-\mathrm{diag}}$ is incoherent (i.e. no internal coherence for $\mathcal{E}$). This leads to $F_\alpha(\mathcal{D}(\hat{\rho})) - F_\alpha(\Pi(\hat{\rho})) > 0$ for any finite value of α. In the limit $\alpha \to \infty$, $F_\infty(\mathcal{D}(\hat{\rho})) - F_\infty(\Pi(\hat{\rho})) = \log p_{\mathcal{E}^*} e^{\beta\mathcal{E}^*} - \max_{\mathcal{E},\lambda_{\mathcal{E}}} p_{\mathcal{E}}\lambda_{\mathcal{E}} e^{\beta\mathcal{E}} > 0$, unless $\hat{\rho}_{\mathcal{E}^*-\mathrm{diag}}$ is incoherent. Here, $\lambda_{\mathcal{E}}$ are eigenvalues of $\hat{\rho}_{\mathcal{E}-\mathrm{diag}}$. Thus if a pure state does not contain internal coherence for $\mathcal{E}^*$, $W_{\mathrm{coh}} \leq F_\infty(\mathcal{D}(\hat{\rho})) - F_\infty(\Pi(\hat{\rho})) = 0$. Conversely, if the state contains internal coherence for $\mathcal{E}^*$, $F_\alpha(\mathcal{D}(\hat{\rho})) - F_\alpha(\Pi(\hat{\rho})) > 0$ for all $\alpha \in [0,\infty)$, thus positive work can be extracted. □

By applying this result to the pure two-qubit state discussed above, we have the necessary condition $p_1 > (1 + e^{\beta\omega_0} + e^{-\beta\omega_0})^{-1}$ and the sufficient

condition $p_1 > e^{\beta\omega_0}/(1+e^{\beta\omega_0})$ to extract positive amount of work from coherence, i.e. $W_{\rm coh} > 0$ that is independent of p_0 and p_2.

We also consider the reverse process of generating quantum correlation from work. For energy block diagonal state, the work cost to transform $\hat{\rho}$ with internal coherence from $\hat{\rho}_{\rm diag}$ is given by $W_{\rm cost} = k_B T \sup_\alpha \Delta C_\alpha(\hat{\rho})$. The relation $W_{\rm coh} \leq W_{\rm cost}$ shows that we cannot have the cyclic process, in general. Coherence-work interconversion is only possible in the following case:

Observation 2. *Given a many-body system with N subsystems, an equally superposed state $|\Psi\rangle = \sum_{\mathcal{E}_{\boldsymbol{E}}=\mathcal{E}_0} \frac{1}{\sqrt{d(\mathcal{E}_0)}} |\boldsymbol{E}\rangle$ within an energy eigenspace with energy $\mathcal{E}_0$ and degeneracy $d(\mathcal{E}_0)$ can be interconverted with the decohered state $\hat{\rho}^{\Psi}_{\rm diag} = \sum_{\mathcal{E}_{\boldsymbol{E}}=\mathcal{E}_0} d(\mathcal{E}_0)^{-1} |\boldsymbol{E}\rangle\langle\boldsymbol{E}|$ in a single-shot TO, with $k_B T \Delta I = k_B T \log d(\mathcal{E}_0)$ amount of work extracted/consumed.*

Here, ΔI is the total correlation difference between $|\Psi\rangle$ and $\hat{\rho}^{\Psi}_{\rm diag}$ which coincides with ΔC_α for every α. For a two level N-particle system, Dicke states $|N,k\rangle = \binom{N}{k}^{-1/2} \sum_P P(|1\rangle^k |0\rangle^{N-k})$ with permutations P between local parties, are good examples. In this case, the total amount of quantum correlations extracted (generated) into (from) work under a TO, i.e. $W = k_B T \log \binom{N}{k}$. When $N \gg 1$ and the excitation rate is given by $r = k/N$, work per particle is given by $k_B T H(r)$, where $H(r) = -r\log r - (1-r)\log(1-r)$ is a binary entropy. In other words, a Dicke state with excitation rate r contains $H(r)$ amount of correlation per particle which gives extra thermodynamic resource beyond classical energy distribution which can be interconverted into work.

We emphasize that this type of work extraction process directly converts the coherence and correlations into work without any measurement or information storage as in Maxwell's demon [248, 249] or the Szilard engine [229] in quantum regime. In other words, we do not need to consider how does a system change during measurements, and the family of the free energies is only needed quantity to evaluate the deterministic work extraction process. Also our result could be compared to other previous studies [226, 233] that only quantum contribution of the free energy correlation can be used in our work extraction process, without changing any classical property $P(\boldsymbol{E})$ of the system. We point out that this kind of work extraction in a single-shot regime is due to internal coherences. The above compact result does not generalize for external coherences, such as those we discuss in the next section.

6.3.3 Coherence as a clock resource

Now we show a different aspect of quantum coherence as a "time reference" when a quantum state contains external coherences. Suppose we have a superposition of different energy eigenstates $|\psi_0\rangle = \sum_{\boldsymbol{E}} \sqrt{P(\boldsymbol{E})}\,|\boldsymbol{E}\rangle$. After the unitary evolution for time t, the state would evolve into $|\psi_t\rangle = \sum_{\boldsymbol{E}} \sqrt{P(\boldsymbol{E})} e^{-i\mathcal{E}_{\boldsymbol{E}} t/\hbar}\,|\boldsymbol{E}\rangle$. In order to estimate the evolution time t, we may perform a set of measurement $\{\hat{M}_k\}$ on the final state . In this case, the resolution of a quantum clock is given by $(\Delta t)^2 = \langle(\hat{t} - t)^2\rangle$, where $\hat{t}$ is the time estimator from the measurement set $\{\hat{M}_k\}$. It is known that the bound of this clock resultion is given by the quantum Cramér -Rao bound [107]

$(\Delta t)^2 \geq (4I_F(\hat{\rho}, \hat{H}_S))^{-1}$, where $I_F(\hat{\rho}, \hat{H}_S) = 2\sum_{i,j} \frac{(\lambda_i - \lambda_j)^2}{\lambda_i + \lambda_j} |\langle i|\hat{H}_S|j\rangle|^2$ is the quantum Fisher information when λ_i and $|i\rangle$ are the eigenvalues and eigenstates of $\hat{\rho}$, respectively. This bound is saturated when we use the optimal measurement set of $\{\hat{M}_k\}$ to estimate the time. For this optimal setting, the larger the quantum Fisher information, the higher the resolution of clock possible.

We note that external coherences can act as a *clock resource*, with various frequency components with the frequency difference $\Delta\omega = (\mathcal{E}_{\boldsymbol{E}} - \mathcal{E}_{\boldsymbol{E}'})/\hbar$. The quantum state containing coherence between more distant energy states(i.e., high frequency ω) leads to more enhanced quantum clock [250, 251], or equivalently a large value of the quantum Fisher information. On the other hand, internal coherences cannot be used as this type of clock since they are stationary under the time evolution. Another family of relevant measures of the clock resolution is the skew information $I_\alpha(\hat{\rho}, \hat{H}_S) = \mathrm{Tr}(\hat{\rho}\hat{H}_S) - \mathrm{Tr}(\hat{\rho}^\alpha \hat{H}_S \hat{\rho}^{1-\alpha}\hat{H}_S)$ for $0 \leq \alpha \leq 1$, which coincides with the quantum Fisher information for pure states, $I_\alpha(|\psi\rangle\langle\psi|, \hat{H}_S) = I_F(|\psi\rangle\langle\psi|, \hat{H}_S)/4 = \mathrm{Var}(\psi, \hat{H}_S) = \langle\psi|\hat{H}_S^2|\psi\rangle - \langle\psi|\hat{H}_S|\psi\rangle^2$ [70,79,107]. Recently, a similar approach on the "time reference" in quantum thermodynamics have been suggested by using a different type of clock resource [240].

We can show that even though a quantum state might very poor at providing work in the form of ordered energy, it can still function as a good time reference. An important result from the time covariance of a TO is that, in the absence of additional coherent resources, work cannot be extracted from coherence between different energy levels due to the "work

locking" phenomenon [235]. Different protocols such as using collective operation for n copies of the state [226, 237] or using ancillary coherence resources [222, 223, 235, 237] are required to extract work from this type of coherence. A canonical example of this is a "coherent Gibbs state", which is a pure state having the same energy distribution as the Gibbs state, $|\gamma\rangle = \sum_E \sqrt{\frac{e^{-\beta E}}{Z_S}} |E\rangle$ for non-degenerate energy levels E. The extractable work from the state is zero since the energy block-diagonalized state of $|\gamma\rangle$ is the Gibbs state. However, the state can still manifest a quantum advantage for the task of the precise time measurement with $I_F(|\gamma\rangle, \hat{H}_S) = 4\frac{\partial^2}{\partial\beta^2} \log Z_S$.

Furthermore, the quantum Fisher and skew information are based on monotone metrics [252, 253], and monotonically decrease under covariant operations with respect to the time translation [69]. Then it can be seen that the resolution quantum clock gives an additional constraint on the second law of quantum thermodynamics in following sense:

Observation 3. *Under a TO given by Λ_β, the quantum Fisher (skew) information $I_{F(\alpha)}$ of a quantum system always decreases, i.e.*

$$\Delta I_{F(\alpha)} = I_{F(\alpha)}(\Lambda_\beta(\hat{\rho}_S), \hat{H}_S) - I_{F(\alpha)}(\hat{\rho}_S, \hat{H}_S) \leq 0. \tag{6.6}$$

We highlight that this condition is independent from the ones discussed previously given by the monotonicity of a family of asymmetry measures $A_\alpha(\hat{\rho}_S) = S_\alpha(\hat{\rho}_S||\mathcal{D}(\hat{\rho}_S))$ [235] and modes of asymmetry $\sum_{\mathcal{E}_{\boldsymbol{E}}-\mathcal{E}_{\boldsymbol{E}'}=\omega} |\rho_{\boldsymbol{E}\boldsymbol{E}'}|$ [69, 236].

We present an example showing that our asymmetry quantifiers give constraints on quantum thermodynamics independent from those due to the

free energies F_α or the coherence measures A_α. Let us consider the transformation by a thermal process of the initial state

$$\hat{\rho} = \begin{pmatrix} 0.5 & 0 & 0.1 & 0.1 \\ 0 & 0.2 & 0 & 0 \\ 0.1 & 0 & 0.25 & 0.1 \\ 0.1 & 0 & 0.1 & 0.05 \end{pmatrix}$$

to the final state

$$\hat{\sigma} = \begin{pmatrix} 0.5 & 0.099 & 0.099 & 0.099 \\ 0.099 & 0.25 & 0 & 0 \\ 0.099 & 0 & 0.2 & 0 \\ 0.099 & 0 & 0 & 0.05 \end{pmatrix}$$

with the Hamiltonian $\hat{H} = \sum_{n=0}^{3} n\omega \left|n\right\rangle \left\langle n\right|$. It can be checked that the free energies F_α and coherence measures A_α of the initial state $\hat{\rho}$ are larger than those of the final state $\hat{\sigma}$. Furthermore, each mode of coherence is decreased from 0.1 to 0.099. However, the skew information values for $\alpha = 1/2$ are given by $I_{1/2}(\hat{\rho}, \hat{H}) = 0.153$ and $I_{1/2}(\hat{\sigma}, \hat{H}) = 0.163$; the quantum Fisher information values are $I_F(\hat{\rho}, \hat{H}) = 0.843$ and $I_F(\hat{\sigma}, \hat{H}) = 0.959$ (all in units of ω^2). Thus a thermal process cannot transform $\hat{\rho}$ into $\hat{\sigma}$, but such a transformation is not disallowed by the restrictions given by F_α or A_α. This is due to that the coherence monotones given by the quantum Fisher information and skew information capture not only the degree of coherence between different energy eigenstates, but also take account of how much

energy level spacing exists in each coherence term.

We also illustrate the physical meaning of this condition in a many-body system. We note that for a product state $\hat{\rho}^{\otimes N}$ with the same Hamiltonian $\hat{H}_0 = \hat{H}_i$ for each party, the quantum Fisher (skew) information are additive: $I_{F(\alpha)}(\hat{\rho}^{\otimes N}, \hat{H}_{\rm tot}) = N I_{F(\alpha)}(\hat{\rho}, \hat{H}_0) \leq N||\hat{H}_0||^2$, where $||\cdot||$ is the operator norm. On the other hand, the N-partite GHZ state $\hat{\sigma}_{N-{\rm GHZ}} = 2^{-1/2}(|0\rangle^{\otimes N} + |1\rangle^{\otimes N})$ gives quadratic scaling of the quantum Fisher (skew) information on the system size, $I_{F(\alpha)}(\hat{\sigma}_{N-{\rm GHZ}}, \hat{H}_{\rm tot}) = O(N^2)$. Thus the restriction given by Eq. (6.6) well matches the physical intuition that TO's cannot transformation from a product state to a GHZ state. More generally, it is known that $I_F(\hat{\rho}) \leq kN$ for k-producible states [109], thus genuine multi-partite entanglement is necessary to achieve a large "clock resource" of $O(N^2)$ in N-partite systems.

Let us now look at how these external coherences in a many-body quantum state behave in the thermodynamic limit, by considering many copies of them $\hat{\rho}^{\otimes n}$, and compare our approach with the previous arguments [234–236]. In the case of the asymptotic state transformation, the asymmetry measure given by A_α has a negligible effect on identifying the transformation rate when many copies of the state is considered as $\lim_{n\to\infty} A_\alpha(\hat{\rho}^{\otimes n})/n = 0$, for any α [235]. On the other hand, due to the additive nature of the quantum Fisher (skew) information, we note that their regularizations do not vanish $\lim_{n\to\infty} I_{F(\alpha)}(\hat{\rho}^{\otimes n}, \hat{H}_n)/n = I_{F(\alpha)}(\hat{\rho}, \hat{H}_0) \neq 0$, unless the state is energy bock-diagonal. This implies that this kind of resources remains as a significant resource even in the thermodynamic limit.

Moreover, we consider the asymptotic state transformation rate by a

TO from the state $\hat{\rho}$ to $\hat{\sigma}$, defined by

$$R_{\rm TO}(\hat{\rho} \to \hat{\sigma}) = \sup\{R : \lim_{n\to\infty} \inf_{\Lambda_\beta} ||\Lambda_\beta(\hat{\rho}^{\otimes n}) - \hat{\sigma}^{\otimes Rn}||_1 = 0\},$$

which indicates how many copies of the target state can be generated from the resource states; $\hat{\rho}^{\otimes n} \to \hat{\sigma}^{\otimes Rn}$ when $n \gg 1$. For a special case of gapless(i.e., every successive pair of numbers in the spectrum is identical) pure states $|\psi\rangle$ and $|\phi\rangle$, the optimal rate of the asymptotic transition by a *covariant* operation under the time translation is given by $R_{\rm cov}(|\psi\rangle \to |\phi\rangle) = {\rm Var}(\psi, \hat{H}_S)/{\rm Var}(\phi, \hat{H}_S)$ [67]. Since every TO is a covariant under the time translation [235], the state transformation rate without a coherent catalysis is bounded by $R_{\rm TO}(|\psi\rangle \to |\phi\rangle) \leq R_{\rm cov}(|\psi\rangle \to |\phi\rangle) = \frac{{\rm Var}(\psi,\hat{H}_S)}{{\rm Var}(\phi,\hat{H}_S)}$. This implies that the asymmetry based on the quantum Fisher (skew) information provides an additional restriction beyond the free energy for the state transformation rate in the asymptotic limit. Our result could be compared with a previous study by Brandão *et al.* [237] that the optimal rate by a TO is given by $R^*_{\rm TO}(\hat{\rho} \to \hat{\sigma}) = S(\hat{\rho}||\hat{\gamma})/S(\hat{\sigma}||\hat{\gamma})$, when the catalyst of the maximally coherent state $|\chi\rangle = |H|^{-1/2} \sum_{h\in H} |h\rangle$ with $H = \{0, \ldots, 2n^{2/3}\}$ is allowed to be used. Here, we point out that although the catalyst $|\chi\rangle$ has dimension sub-linear in n, it has a super-linear amount of coherent resources $I_F(\chi, \hat{H}_S) = (4/3)n^{2/3}(n^{2/3} + 1) \propto n^{4/3}$.

6.4 Trade-off relation between work and clock resources

Having examined the two types of thermodynamic coherence independently, it is natural to ask if there is a relation between them. In this section, we demonstrate that there is always a tradeoff between work and clock coherence resources. We first observe that extractable work from coherence is constrained by the number of degeneracies in the same energy eigenspaces. More precisely, we can show following:

Proposition 5 (Work bound)**.** *For a given energy distribution $p_{\mathcal{E}}$, the extractable work from coherence is upper bounded as follows:*

$$W_{\mathrm{coh}} \leq k_B T \sum_{\mathcal{E}} p_{\mathcal{E}} \log g_{\mathcal{E}}, \tag{6.7}$$

where $g_{\mathcal{E}}$ is the dimension of the eigenspace of energy level $\mathcal{E}$.

Proof: Note that

$$\begin{aligned} W_{\mathrm{coh}} &= \inf_{\alpha} \left[F_\alpha(\mathcal{D}(\hat{\rho})) - F_\alpha(\Pi(\hat{\rho})) \right] \\ &\leq F(\mathcal{D}(\hat{\rho})) - F(\Pi(\hat{\rho})) \\ &= k_B T \left[S(\Pi(\hat{\rho})) - S(\mathcal{D}(\hat{\rho})) \right]. \end{aligned} \tag{6.8}$$

Since both $\Pi(\hat{\rho})$ and $\mathcal{D}(\hat{\rho})$ are energy-block diagonal, we can express $\Pi(\hat{\rho}) = \sum_{\mathcal{E},\lambda} p^{\Pi}_{\mathcal{E},\lambda} \left|\mathcal{E},\lambda\right\rangle \left\langle \mathcal{E},\lambda\right|$ and $\mathcal{D}(\hat{\rho}) = \sum_{\mathcal{E},\lambda} p^{\mathcal{D}}_{\mathcal{E},\lambda} \left|\mathcal{E},\lambda\right\rangle \left\langle \mathcal{E},\lambda\right|$ for $\lambda = 1, 2, \cdots, g_{\mathcal{E}}$

with $\sum_{\lambda=1}^{g_\mathcal{E}} p^{\Pi}_{\mathcal{E},\lambda} = \sum_\lambda p^{\mathcal{D}}_{\mathcal{E},\lambda} = p_\mathcal{E}$. Then we have

$$\begin{aligned} S(\Pi(\hat{\rho})) - S(\mathcal{D}(\hat{\rho})) &= \sum_{\mathcal{E}} p_\mathcal{E} \sum_{\lambda=1}^{g_\mathcal{E}} \left[\frac{p^{\mathcal{D}}_{\mathcal{E},\lambda}}{p_\mathcal{E}} \log \frac{p^{\mathcal{D}}_{\mathcal{E},\lambda}}{p_\mathcal{E}} - \frac{p^{\Pi}_{\mathcal{E},\lambda}}{p_\mathcal{E}} \log \frac{p^{\Pi}_{\mathcal{E},\lambda}}{p_\mathcal{E}} \right] \\ &\leq \sum_{\mathcal{E}} p_\mathcal{E} \log g_\mathcal{E}, \end{aligned} \tag{6.9}$$

since $S(\hat{\rho}) - S(\hat{\sigma}) \leq \log d$ for d-dimensional states $\hat{\rho}$ and $\hat{\sigma}$. □

6.4.1 Clock/work trade-off relation: Two-level local Hamiltonian systems

We show that extractable work from coherence is bounded by the quantum Fisher information in an N-particle two-level system:

Theorem 9 (Trade-off between work–clock resources for a two-level system)**.** *For an N-particle two-level system with the energy level difference ω_0, extractable work from coherence $W_{\rm coh}$ and clock-resource given by the quantum Fisher information I_F satisfy following inequality:*

$$W_{\rm coh} \leq k_B T N (\log 2) H_b \left(\frac{1}{2} \left[1 - \sqrt{\frac{I_F(\hat{\rho}, \hat{H})}{N^2 \omega_0^2}} \right] \right), \tag{6.10}$$

where $\hat{H}$ is the total Hamiltonian of the system and $H_b(r) = -r \log_2 r - (1-r)\log_2(1-r)$ is the binary entropy.

Proof: In an N-particle two-level system with energy difference ω_0, the degeneracy of the energy level $\mathcal{E}$ is given by $g_\mathcal{E} = \binom{N}{n}$, where $\mathcal{E} = \omega_0 n$. By

using the fact that

$$\binom{N}{n} \leq 2^{NH_b\left(\frac{n}{N}\right)}$$

for every N and n, we obtain

$$W_{\mathrm{coh}} \leq k_B T \sum_{\mathcal{E}} p_{\mathcal{E}} \log \binom{N}{n} \leq N k_B T (\log 2) \sum_{\mathcal{E}} p_{\mathcal{E}} H_b(n/N), \quad (6.11)$$

where Proposition 5 has been applied to obtain the first inequality. Furthermore, we can express the binary entropy as

$$H_b(x) = 1 - \frac{1}{2\log 2} \sum_{j=1}^{\infty} \frac{(1-2x)^{2j}}{j(2j-1)}.$$

For a given probability distribution p_x and $j \geq 1$ we have

$$\sum_x p_x (1-2x)^{2j} \geq \left[\sum_x p_x (1-2x)^2\right]^j = (1-2y)^{2j},$$

where $y = \frac{1}{2}\left[1 \pm \sqrt{(1-2\bar{x})^2 + 4\mathrm{Var}_x}\right]$ with $\bar{x} = \sum_x p_x x$ and $\mathrm{Var}_x = \sum_x p_x (x-\bar{x})^2$. Then we have

$$\begin{aligned}
\sum_x p_x H_b(x) &= 1 - \frac{1}{2\log 2} \sum_{j=1}^{\infty} \sum_x p_x \frac{(1-2x)^{2j}}{j(2j-1)} \\
&\leq 1 - \frac{1}{2\log 2} \sum_{j=1}^{\infty} \frac{(1-2y)^{2j}}{j(2j-1)} \\
&= H_b(y).
\end{aligned}$$

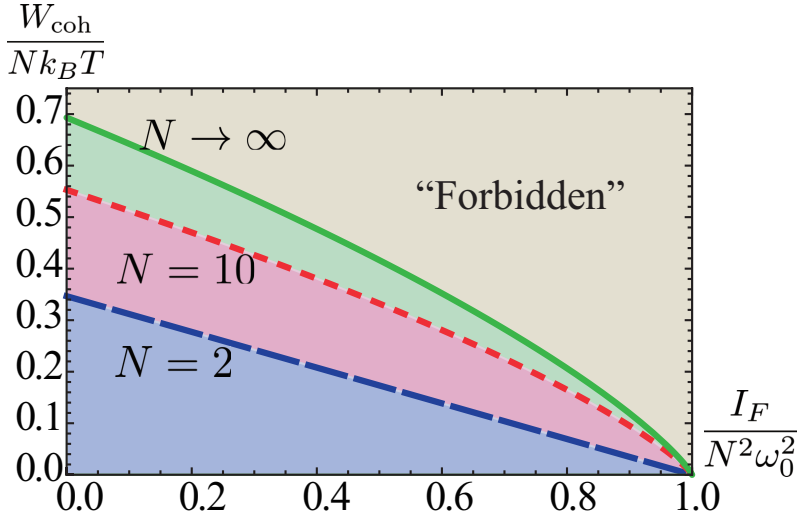

Figure 27: Trade-off between extractable work from coherence and clock resource. The solid line refers to Eq. (6.10), the dashed line refers to Eq. (6.13) for $N = 2$, and the dotted line refers the tighter bound with $N = 10$.

By substituting this result into Eq. (6.11), we obtain

$$W_{\rm coh} \leq Nk_BT(\log 2)H_b\left(\frac{1}{2}\left[1 \pm \sqrt{\left(1 - \frac{2\bar{E}}{N\omega_0}\right)^2 + \frac{4{\rm Var}_{\hat{H}}}{N^2\omega_0^2}}\right]\right), \tag{6.12}$$

where $\bar{E} = \langle \hat{H} \rangle_{\hat{\rho}}$ and ${\rm Var}_{\hat{H}} = \langle (\hat{H} - \bar{E})^2 \rangle_{\hat{\rho}}$. Note that H_b is symmetric about $x = 1/2$ and monotonically increasing for $x \leq 1/2$. We also note that $4{\rm Var}_{\hat{H}} \geq I_F(\hat{\rho}, \hat{H})$ for every quantum state $\hat{\rho}$. These observations lead to $H_b\left(\frac{1}{2}\left[1 \pm \sqrt{\left(1 - \frac{2\bar{E}}{N\omega_0}\right)^2 + \frac{4{\rm Var}_{\hat{H}}}{N^2\omega_0^2}}\right]\right) \leq H_b\left(\frac{1}{2}\left[1 - \sqrt{\frac{I_F(\hat{\rho},\hat{H})}{N^2\omega_0^2}}\right]\right)$, which completes the proof. □

This trade-off relation decribed in Fig. 27 shows that a quantum state cannot contain maximum amount of both work and clock resources at the

same time. Note that when the clock resource is the maximum $I_F = N\omega_0^2$, no work can be extracted from coherence $W_{\rm coh} = 0$. Conversely, if extractable work form coherent is the maximum, $W_{\rm coh} = Nk_BT\log 2$, the state cannot be utilized as a quantum clock as $I_F = 0$. If N is an even small number, we can tighten the bound by replacing $k_BTN(\log 2)$ with $k_BT\log\binom{N}{N/2}$. In particular, we derive a tighter trade-off condition when $N = 2$,

$$W_{\rm coh} + (k_BT\log 2)\left(\frac{I_F(\hat{\rho},\hat{H})}{4\omega_0^2}\right) \leq k_BT\log 2. \tag{6.13}$$

Proof: Suppose the state has probability p_0, p_1, and p_2 for each energy level 0, ω_0 and $2\omega_0$. By using Eq. (6.11) for $N = 2$, we have $W_{\rm coh} \leq k_BT(\log 2)p_1$, since the state has a degeneracy in the energy-eigenspace only for $\mathcal{E} = \omega_0$. In this case, energy variance $\mathrm{Var}_{\hat{H}}$ is given by

$$\mathrm{Var}_{\hat{H}} = \omega_0^2(-p_1^2 + p_1 - 4p_2^2 + 4p_2 - 4p_1p_2),$$

which leads to the maximum value of p_1,

$$p_1^{\max} = 1 - \mathrm{Var}_{\hat{H}}/\omega_0^2,$$

for a given value of $\mathrm{Var}_{\hat{H}}$. Again, we can use $4\mathrm{Var}_{\hat{H}} \geq I_F(\hat{\rho},\hat{H})$ to get

$$W_{\rm coh} \leq k_BT(\log 2)p_1^{\max} = k_BT(\log 2)\left(1 - \frac{I_F(\hat{\rho},\hat{H})}{4\omega_0^2}\right).$$

which is the desired inequality. □

We demonstrate that the GHZ-state $|\psi_{\rm GHZ}\rangle = 2^{-1/2}(|0\rangle^{\otimes N} + |1\rangle^{\otimes N})$

and Dicke states $|N,k\rangle = \binom{N}{k}^{-1/2} \sum_P P(|1\rangle^k |0\rangle^{N-k})$ with permutations P between local parties, which are the limiting cases of this trade-off relation. Extractable work from coherence for a Dicke state is given by $W_{\mathrm{coh}} = Nk_BT \log \binom{N}{k} \approx k_BT(\log 2)H_b(r)$ for a large number of $N \gg 1$ and the excitation rate $r = k/N$. Note that a Dicke state contains $NH_b(r)$ amount of correlation due to coherence, given by the amount of total correlation $\sum_{i=1}^N S(\hat{\rho}_i) - S(\hat{\rho})$ subtracted by its classical correlation without coherence $\sum_{i=1}^N S(\Pi(\hat{\rho})_i) - S(\Pi(\hat{\rho}))$, where we define $\hat{\sigma}_i$ to be density matrices for ith subsystems of $\hat{\sigma}$ and $S(\hat{\sigma})$ is the von Neumann entropy. This observation validly shows that internal coherence yields extra thermodynamic resource beyond classical energy distribution to extract work. However, any Dicke state does not contain clock resource (i.e., $I_F = 0$) since they are in energy eigenspace of $\mathcal{E} = k\omega_0$. In particular, when the half of the particles are excited ($k = N/2$), extractable work reaches the maximum $W_{\mathrm{coh}} = Nk_BT \log 2$, saturating the bounds Eq. (6.10) and (6.13). On the other hand, the GHZ-state behaves in an opposite way. Note that the GHZ-state gives the maximum clock resource of $I_F(|\psi_{\mathrm{GHZ}}\rangle, \hat{H}) = N^2\omega_0^2$, while $\mathcal{D}(|\psi_{\mathrm{GHZ}}\rangle \langle\psi_{\mathrm{GHZ}}|)$ does not contain internal coherences that no extra work can be extracted from coherence, i.e., $W_{\mathrm{coh}} = 0$. In this case, we can also see that the both bounds Eq. (6.10) and (6.13) in a different point.

6.4.2 Clock/work trade-off relation: General case

Furthermore, our two-level trade-off relation can be generalized into an arbitrary N-particle system.

Theorem 10. *For an N-particle system with $d^{(n)}$-level local energy spectrum $\{E_1^{(n)}, E_2^{(n)}, \cdots, E_{d^{(n)}}^{(n)}\}$ for nth particle (not necessarily to have equal energy-level differences and can be degenerate) work and clock resource satisfy following relation:*

$$W_{\rm coh} + k_B T \left(\frac{I_F(\hat{\rho}, \hat{H})}{2\Delta_E^2} \right) \leq k_B T \sum_{n=1}^{N} \log d^{(n)}, \tag{6.14}$$

where $\Delta_E^2 = \sum_{n=1}^{N} (\Delta_E^{(n)})^2$ with $\Delta_E^{(n)}$ to be the maximum energy difference of the $n^{\rm th}$ local party.

Proof: In this case, the degeneracy $g_{\mathcal{E}}$ of the energy $\mathcal{E}$ is given by

$$g_{\mathcal{E}} = \prod_{n=1}^{N} d^{(n)} f_{\mathcal{E}},$$

where $f_{\mathcal{E}} = \sum_{\mathcal{E}_{\boldsymbol{E}}=\mathcal{E}} P(\boldsymbol{E})$ is a probability (or frequency) to have the energy $\mathcal{E}$ in the N-particle system, since $\prod_{n=1}^{N} d^{(n)}$ is total possible numbers of $\boldsymbol{E}$. Then $f_{\mathcal{E}}$ can be considered as a probability distribution of a variable $X_N = \sum_{i=n}^{N} E_n$ from the distribution of independent random variables of E_n for nth party. In our case, E_n is strictly bounded by $E_1^{(n)} \leq E_n \leq E_{d^{(n)}}^{(n)}$ and it has the same probability $P(E_n = E_i^{(n)}) = 1/d^{(n)}$ for every $i = 1, 2, \cdots, d^{(n)}$ and zero for all other cases. Hoeffding's inequality [254], then shows that

$$P(X_N - \mu_E \geq t) \leq \exp\left[-\frac{2t^2}{\Delta_E^2} \right],$$

where $\mu_E := \mathbb{E}(X_N) = \mathbb{E}\left(\sum_{n=1}^{N} E_n\right) = \sum_{n=1}^{N}\sum_{i=1}^{d^{(n)}}\left(\frac{E_i^{(n)}}{d^{(n)}}\right)$ and $\Delta_E^2 = \sum_{n=1}^{N}(\Delta_E^{(n)})^2$. Using this, the upper bound of $f_{\mathcal{E}}$ is given by

$$f_{\mathcal{E}} = P(X_N = \mathcal{E}) \leq P(X_N \geq \mathcal{E}) \leq \exp\left[-\frac{2(\mathcal{E}-\mu_E)^2}{\Delta_E^2}\right].$$

Again using Proposition 1, we have

$$\begin{aligned}
W_{\text{coh}} &\leq k_B T \sum_{\mathcal{E}} p_{\mathcal{E}} \log g_{\mathcal{E}} \\
&= k_B T \sum_{\mathcal{E}} p_{\mathcal{E}} \log\left(\prod_{n=1}^{N} d^{(n)} f_{\mathcal{E}}\right) \\
&= k_B T \sum_{n=1}^{N} \log d^{(n)} + k_B T \sum_{\mathcal{E}} p_{\mathcal{E}} \log f_{\mathcal{E}} \\
&\leq k_B T \sum_{n=1}^{N} \log d^{(n)} - \frac{2k_B T}{\Delta_E^2} \sum_{\mathcal{E}} p_{\mathcal{E}} (\mathcal{E}-\mu_E)^2 \\
&= k_B T \sum_{n=1}^{N} \log d^{(n)} - \frac{2k_B T}{\Delta_E^2} \text{Var}_{\hat{H}} - \frac{2k_B T}{\Delta_E^2} (\bar{E}-\mu_E)^2 \\
&\leq k_B T \sum_{n=1}^{N} \log d^{(n)} - k_B T \left(\frac{I_F(\hat{\rho}, \hat{H})}{2\Delta_E^2}\right),
\end{aligned} \tag{6.15}$$

where the last inequality is from the fact $4\text{Var}_{\hat{H}} \geq I_F(\hat{\rho}, \hat{H})$. □

We point out that Theorem 10 provides less tight bound than the previous bounds for a two level system, since it is possible to have maximum amount of clock resource ($\max[I_F(\hat{\rho}, \hat{H})] = N\Delta_E^2$) with nonzero amount of work resource. Yet the bound again shows that any quantum state cannot obtain both the maximum clock and work resources from thermodynamic coherence.

For systems with the same local d-level Hamiltonians our bound reduces into

$$\bar{w}_{\rm coh} + k_B T \left(\frac{I_F(\hat{\rho}, \hat{H})}{2N^2 \Delta_0^2} \right) \leq k_B T \log d, \tag{6.16}$$

where $\bar{w}_{\rm coh} = W_{\rm coh}/N$ is extractable work per particle and $\Delta_E^2 = N\Delta_0^2$ where Δ_0 is the maximum energy difference between the local energy eigenvalues. In thermodynamic limit, an accumulation of microscopic coherences given by a produce state $\hat{\rho}^{\otimes N}$ does not effect the ability to extract work from coherence since $I_F(\hat{\rho}^{\otimes N}, \hat{H})/N^2 \to 0$ for $N \gg 1$.

In real experimental situation, it is hard to access exact energy level with prefect prevision, so we may impose finite energy gap ϵ in energy levels. Under this assumption, we view states with an ϵ-energy gap to be "essentially the same" energy and so can carry internal coherences for approximate work extraction. In order to introduce the energy gap ϵ, we divide the energy spectrum into intervals

$$\mathcal{E}_m = \begin{cases} \left[\mu_E + \left(m - \frac{1}{2}\right)\epsilon, \mu_E + \left(m + \frac{1}{2}\right)\epsilon\right) & \text{for } m > 0 \\ \left(\mu_E + \left(m - \frac{1}{2}\right)\epsilon, \mu_E + \left(m + \frac{1}{2}\right)\epsilon\right] & \text{for } m < 0 \\ \left(\mu_E + \left(m - \frac{1}{2}\right)\epsilon, \mu_E + \left(m + \frac{1}{2}\right)\epsilon\right) & \text{for } m = 0 \end{cases},$$

where each interval has an energy width ϵ.

Consequently, we define the energy distribution for mth interval $p_m^\epsilon = \sum_{\mathcal{E}\in\mathcal{E}_m} p_\mathcal{E}$ and its degeneracy $g_m^\epsilon = \sum_{\mathcal{E}\in\mathcal{E}_m} g_\mathcal{E}$, respectively. If we allow the ϵ energy gap for internal coherences, the amount of extractable work is

upper bounded by

$$\begin{aligned} W_{\rm coh}^{\epsilon} &\leq \sum_m p_m^{\epsilon} \log g_m^{\epsilon} \\ &= \sum_{n=1}^{N} \log d^{(n)} + \sum_m p_m^{\epsilon} \log f_m^{\epsilon}, \end{aligned} \tag{6.17}$$

where f_m^{ϵ} is the frequency to be in the mth energy interval. The upper bound of f_m^{ϵ} is then given by

$$\begin{aligned} f_m^{\epsilon} = P(X_N \in \mathcal{E}_m) &\leq P\left(|X_N - (\mu_E + \epsilon m)| \geq \frac{1}{2}\epsilon \right) \\ &\leq \begin{cases} \exp\left[-\frac{2(|m|-1/2)^2\epsilon^2}{\Delta_E^2} \right] & (m \neq 0) \\ 1 & (m = 0) \end{cases}. \end{aligned}$$

By following the same argument with Theorem 2, we have

$$\begin{aligned} W_{\rm coh}^{\epsilon} &\leq \sum_{n=1}^{N} \log d^{(n)} - \sum_{m \neq 0} p_m^{\epsilon} \left[\frac{2(|m| - \frac{1}{2})^2\epsilon^2}{\Delta_E^2} \right] \\ &= \sum_{n=1}^{N} \log d^{(n)} - \frac{2}{\Delta_E^2} \left[\sum_m p_m^{\epsilon} |m|^2 \epsilon^2 - \epsilon \sum_m p^{\epsilon} |m| + \frac{1}{4}\epsilon^2 \sum_{m \neq 0} p_m^{\epsilon} \right]. \end{aligned} \tag{6.18}$$

When $\mathcal{E} \in \mathcal{E}_m$, we use the fact that $\mu_E + (m - 1/2)\epsilon \leq \mathcal{E} \leq \mu_E +$

$(m+1/2)\epsilon$ to show

$$\begin{aligned}\sum_{\mathcal{E}} p_{\mathcal{E}}(\mathcal{E}-\mu_E)^2 &= \sum_m \sum_{\mathcal{E}\in\mathcal{E}_m} p_{\mathcal{E}}(\mathcal{E}-\mu_E)^2 \\ &\leq \sum_m \left(\sum_{\mathcal{E}\in\mathcal{E}_m} p_m^\epsilon\right)\left(m^2\epsilon^2+|m|\epsilon+\frac{1}{4}\epsilon^2\right) \\ &= \sum_m p_m^\epsilon m^2\epsilon^2 + \epsilon\sum_m p_m^\epsilon|m| + \frac{1}{4}\epsilon^2.\end{aligned}$$

By substituting this inequality into (6.18), then we finally get the following trade-off relation by allowing a small energy gap ϵ,

$$W_{\rm coh}^\epsilon + k_BT\left(\frac{I_F(\hat{\rho},\hat{H})}{2\Delta_E^2}\right) \leq k_BT\sum_{n=1}^N \log d^{(n)} + R(\epsilon), \tag{6.19}$$

where the correction term is given by

$$R(\epsilon) = \frac{2\epsilon}{\Delta_E^2}\sum_m p_m^\epsilon|m| - \frac{\epsilon^2}{2\Delta_E^2}p_0^\epsilon.$$

6.5 Remarks

In this chapter, we have studied that thermodynamic coherence in a many-body system can be decomposed into time- and energy-related components. The resource theory of quantum thermodynamics has been introduced to analyze the role of quantum coherence. In this point of view, thermodynamical properties of a quantum state cannot be entirely explained in terms of "energy distribution", but "coherence" as a fully quantum property must be additionally considered. Based on this observation, we have demonstrated that many-body coherence contributing to the thermodynamic free energy can be converted into work by a thermal process, without changing the classical energy statistics. We have illustrated that this work-yielding resource comes from correlations due to coherence in a multipartite system. A different aspect of coherences has been investigated in this chapter that external coherences between different energy eigenstates can be utilized as a clock resource and introduced quantitative measures of this resource given by the quantum Fisher (skew) information. This new resource leads to additional constraints for a state transformation by a TO, particularly in many-body systems. As a result, a superposition between distinct energy states, such as a GHZ-state cannot be generated using a TO. Remarkably, we have found a trade-off relation between these two different thermodynamic coherence resources. By following this trade-off relation, a quantum state cannot contain both the maximum amount of work and clock resources at the same time. Our results give new insights into how energy- and time-related properties are related to each other in the quantum thermodynamics.

Chapter 7

Conclusion

In this dissertation, we have studied macroscopic quantum properties emerged from quantum coherence between classically distinct physical states. Macroscopic quantum coherence can be quantified as a resource to perform non-classical tasks, and can be used for various applications in both practical and fundamental aspects. We summarize this dissertation by remarking the following questions for macroscopic quantum coherence raised in the introduction:

1. "How can we quantify it?"— We have reviewed some basic concepts of coherence and introduce the recent approach of coherence and asymmetry using the framework of resource theory. In this point of view, we have suggested two different approaches to quantify macroscopic coherence. One way to quantify macroscopic coherence is adding "weighted sum of coherences" by which size of the system and degree of coherence can be captured at the same time. Another possible measure has been suggested as a "disturbance based measure of macroscopic coherence" , based on the physical property that coarse-grained measurements cause intensive disturbance of the coherences between physically distinct states. We have demonstrated that both approaches can consistently quantify macroscopic coherence in different types of physical systems including spin and bosonic system, and we also have established the connection between them to construct a general

framework for macroscopic quantumness.

2. "Why it is hard to observe in our lives?"— According to "Weighted measure" and "disturbance based measure" of macroscopic quantum coherence, a quantum state with the large degree of macroscopic coherence allows us to observe macroscopic quantum phenomena under the fuzzy reference frame alignment and coarse-grained measurement, respectively. At the same time, however, these conditions would rapidly degrade the macroscopic coherence of quantum states, causing the quantum-to-classical transition even in a short timescale. We have pointed out that both kinds of quantum-to-classical transition can be simultaneously explained by the decoherence model in which the system linearly interacts with a thermal bath. This integrated approach demonstrates that it is hard to see such macroscopic coherence in the presence of thermal environment.

3. "What can we do with it?"— Meanwhile, macroscopic coherence can be used to perform nonclassical tasks, including quantum metrology and nonlocality tests. We have shown that the enhanced metrology in multimode optical fields necessarily requires nonclassical resources such as optical cat states containing macroscopic coherence. Another interesting application has been suggested that hybrid entanglement between quantum (particle-like) and classical (or wave-like) degree of freedom in optical fields could be useful to test the detection-loop-hole free Bell inequality violation.

In connection with these questions, we also have investigated how many-body coherence roles in quantum thermodynamics. We have shown that coherence in many-body systems can be decomposed into time and energy components, where the former can be utilized as a resource for a quantum

clock while the latter can extract extra work from the thermal bath. Furthermore, these two different types of resources have been shown to obey a trade-off relation that clock/work resources in quantum thermodynamics compensate each other.

To conclude, we have revealed several novel properties and applications of macroscopic quantumness originated from the quantum coherence, yet there are still many things unknown about macroscopic coherence in both theoretical and practical aspects. I hope this dissertation can help researchers to explore the essence of macroscopic quantumness from a fundamental viewpoint, with an eye towards possible applications in quantum technology.

Bibliography

[1] L. de Broglie, Nature **112**, 540 (1923).

[2] G. I. Taylor, Proc. Cambridge Philos. Soc. 15, **114** (1909)

[3] P. A. M. Dirac, *The Principles of Quantum Mechanics* (Oxford University, Oxford, 1958).

[4] C. Davisson and L. H. Germer, Phys. Rev. **30**, 705 (1927).

[5] A. Tonomura, J. Endo, T. Matsuda, T. Kawasaki, and H. Ezawa, Am. J. Phys. **57**, 117 (1989).

[6] E. Schrödinger, Naturwissenschaften **23**, 807 (1935).

[7] M. Brune, E. Hagley, J. Dreyer, X. Maître, A. Maali, C. Wunderlich, J. M. Raimond, and S. Haroche, Phys. Rev. Lett. **77**, 4887 (1996).

[8] C. Monroe, D. M. Meekhof, B. E. King, and D. J. Wineland, Science **272** 1131 (1996).

[9] T. Kovachy, P. Asenbaum, C. Overstreet, C. A. Donnelly, S. M. Dickerson, A. Sugarbaker, J. M. Hogan, and M. A. Kasevich, Nature **528**, 530 (2015).

[10] A. Ourjoumtsev, H. Jeong, R. Tualle-Brouri, and P. Grangier, Nature **448**, 784 (2007).

[11] R. Ghobadi, A. Lvovsky, C. Simon, Phys. Rev. Lett. **110**, 170406 (2013).

[12] N. Bruno, A. Martin, P. Sekatski, N. Sangouard, R.T. Thew, N. Gisin, Nat. Phys. **9**, 545 (2013).

[13] A.I. Lvovsky, R. Ghobadi, A. Chandra, A.S. Prasad, C. Simon, Nat. Phys. **9**, 541 (2013).

[14] H. Jeong, A. Zavatta, M. Kang, S.-W. Lee, L. S. Costanzo, S. Grandi, T. C. Ralph, and M. Bellini, Nat. Photonics **8**, 564 (2014).

[15] O. Morin, K. Haung, J. Liu, H. L. Jeannic, C. Fabre, and J. Laurat, Nat. Photonics **8**, 570 (2014).

[16] B. Vlastakis, G. Kirchmair, Z. Leghtas, S. E. Nigg, L. Frunzio, S. M. Girvin, M. Mirrahimi, M. H. Devoret, and R. J. Schoelkopf, Science **342**, 607 (2013).

[17] T. A. Palomaki, J. D. Teufel, R. W. Simmonds, K. W. Lehnert, Science **342**, 710 (2013).

[18] E. E. Wollman, C. U. Lei, A. J. Weinstein, J. Suh, A. Kronwald, F. Marquardt, A. A. Clerk, K. C. Schwab, Science **349**, 952 (2015).

[19] M. Arndt, O. Nairz, J. Vos-Andreae, C. Keller, G. van der Zouw, and A. Zeilinger, Nature **401**, 680 (1999); O. Nairz, M. Arndt, and A/ Zeilinger, Am. J. Phys. **71**, 319 (2003).

[20] O. Romero-Isart, M. L. Juan, R. Quidant, and J. I. Cirac, New J. Phys. **12**, 033015 (2010).

[21] S. Gerlich, S. Eibenberger, M. Tomandl, S. Nimmrichter, K. Hornberger, P. J. Fagan, J. Tu¨xen, M. Mayor, and M. Arndt, Nat. Commun. **2**, 263 (2011).

[22] T. Baumgratz, M. Cramer, and M. B. Plenio, Phys. Rev. Lett. **113**, 140401 (2014).

[23] A. Winter and D. Yang, Phys. Rev. Lett. **116**, 120404 (2016).

[24] M. B. Plenio and S. Virmani, Quantum Inf. Comput. **7**, 1 (2007).

[25] R. Horodecki, P. Horodecki, M. Horodecki, and K. Horodecki, Rev. Mod. Phys. **81**, 865 (2009).

[26] C. H. Bennett and G. Brassard, *Proc. of the IEEE International Conference on Computers, Systems and Signal Processing, Bangalore, India* (IEEE, New York, 1984), p. 175.

[27] A. K. Ekert, Phys. Rev. Lett. **67**, 661 (1991).

[28] N. Gisin, G. Ribordy, W. Tittel, and Hugo Zbinden, Rev. Mod. Phys. **74**, 145 (2002); V. Scarani, H. Bechmann-Pasquinucci, N. J. Cerf, M. Dušek, Norbert Lütkenhaus, and Momtchil Peev, Rev. Mod. Phys. **81**, 1301 (2009).

[29] R. P. Feynman, Int. J. Theor. Phys. **21**, 467 (1982).

[30] P. W. Shor, SIAM J. Comput. **26**, 1484 (1997).

[31] D. Deutsch and R. Jozsa, Proc. R. Soc. London Ser. A **439**, 553 (1992).

[32] T. D. Ladd, F. Jelezko, R. Laflamme, Y. Nakamura, C. Monroe, and J. L. O'Brien, Nature (London) **464**, 45 (2010).

[33] K. C. Tan, S. Omkar and H. Jeong, arXiv:1704.07572.

[34] C. H. Bennett and S. J. Wiesner, Phys. Rev. Lett. **69**, 2881 (1992).

[35] C. H. Bennett, G. Brassard, C. Crépeau, R. Jozsa, A. Peres, and W. K. Wootters, Phys. Rev. Lett. **70**, 1895 (1993).

[36] L. -M. Duan and C. Monroe, Rev. Mod. Phys. **82**, 1209 (2010).

[37] A. J. Leggett, Prog. Theor. Phys. Suppl. **69**, 80 (1980).

[38] W. Dür, C. Simon, and J.I. Cirac, Phys. Rev. Lett. **89** 210402 (2002).

[39] A. Shimizu and T. Miyadera, Phys. Rev. Lett. **89** 270403 (2002).

[40] G. Björk and P.G.L. Mana, J. Opt. B: Quantum Semiclassical Opt. **6** 429 (2004).

[41] A. Shimizu and T. Morimae, Phys. Rev. Lett. **95** 090401 (2005).

[42] E.G. Cavalcanti and M.D. Reid, Phys. Rev. Lett. **97** 170405 (2006).

[43] J.I. Korsbakken, K.B. Whaley, J. Dubois, and J.I. Cirac, Phys. Rev. A **75** 042106 (2007).

[44] C. -W. Lee and H. Jeong, Phys. Rev. Lett. **106**, 220401 (2011).

[45] F. Fröwis and W. Dür, New J. Phys.**14**, 093039 (2012).

[46] S. Nimmrichter and K. Hornberger, Phys. Rev. Lett. **110**, 160403 (2013).

[47] P. Sekatski, N. Sangouard, and N. Gisin, Phys. Rev. A **89**, 012116 (2014).

[48] B. Yadin and V. Vedral, Phys. Rev. A **92**, 022356 (2015).

[49] F. Fröwis, N. Sangouard, and N. Gisin, Opt. Comm. **337**, 2 (2015).

[50] H. Jeong, M. Kang, and H. Kwon, Opt. Commun. **337**, 12 (2015).

[51] C. -Y. Park, M. Kang, C.-W. Lee, J. Bang, S.-W. Lee, and H. Jeong, Phys. Rev. A **94**, 052105 (2016).

[52] B. Yadin and V. Vedral, Phys. Rev. A **93**, 022122 (2016).

[53] H. Kwon, C.-Y. Park, K.-C. Tan, and and H. Jeong, New J. Phys. **19**, 043024 (2017).

[54] F. Fröwis, P. Sekatski, W. Dür, N. Gisin, and N. Sangouard, arXiv:1706.06173.

[55] A. J. Leggett and A. Garg. Phys. Rev. Lett. **54**, 857 (1985).

[56] J. S. Bell, Rev. Mod. Phys. **38**, 447 (1966).

[57] J. Kofler and Č. Brukner, Phys. Rev. A **87**, 052115 (2013).

[58] H. Kwon, C.-Y Park, K.-C. Tan, D. Ahn, and H Jeong, arXiv:1704.06469 (2017).

[59] V. Vedral and M. B. Plenio, Phys. Rev. A **57**, 1619 (1998).

[60] C. H. Bennett, D. P. DiVincenzo, J. Smolin, and W. K. Wootters, Phys. Rev. A **54**, 3824 (1996).

[61] A. Streltsov, G. Adesso, M. B. Plenio, arXiv:1609.02439 (2016).

[62] K. C. Tan, H. Kwon, C.-Y. Park, and H. Jeong, Phys. Rev. A **94**, 022329 (2016).

[63] L. -H. Shao, Z. Xi, H. Fan, and Y. Li, Phys. Rev. A **91**, 042120 (2015).

[64] A. Streltsov, U. Singh, H. S. Dhar, M. N. Bera, and G. Adesso, Phys. Rev. Lett. **115**, 020403 (2015).

[65] S. Luo and Q. Zhang, Phys. Rev. A **69**, 032106 (2004); S. Luo, Proc. Am. Math. Soc. **132**, 885 (2004).

[66] E. Lieb, Adv. Math. **11**, 267 (1973).

[67] G. Gour and R. W. Spekkens, New J. Phys. **10**, 033023 (2008).

[68] I. Marvian and R. W. Spekkens, New J. Phys. **15**, 033001 (2013).

[69] I. Marvian and R. W. Spekkens, Phys. Rev. A **90**, 062110 (2014).

[70] I. Marvian and R. W. Spekkens, Phys. Rev. A **94**, 052324 (2016).

[71] M. Skotiniotis and G. Gour, New J. Phys. **14**, 073022 (2012).

[72] V. Giovannetti, S. Lloyd, and L. Maccone, Science **306**, 1330 (2004).

[73] V. Giovannetti, S. Lloyd, and L. Maccone, Phys. Rev. Lett. **96** 010401 (2006).

[74] I. Marvian, R. W. Spekkens, and P. Zanardi, Phys. Rev. A **93**, 052331 (2016).

[75] I. Marvian and R. W. Spekkens, Nat. Commun. **5**, 3821 (2014).

[76] M. Piani, M. Cianciaruso, T. R. Bromley, C. Napoli, N. Johnston, and G. Adesso, Phys. Rev. A **93**, 042107 (2016).

[77] K. Bu, N. Anand, U. Singh, arXiv:1703.01266.

[78] D. Poulin, Phys. Rev. A **71**, 022102 (2005).

[79] E. P. Wigner and M. M. Yanase, Proc. Natl. Acad. Sci. U.S.A. **49**, 910 (1963).

[80] D. Girolami, Phys. Rev. Lett. **113**, 170401 (2014).

[81] H. Jeong, Y. Lim, and M. S. Kim, Phys. Rev. Lett. **112**, 010402 (2014).

[82] F. Fröwis, P. Sekatski. and W. Dür, Phys. Rev. Lett. **116**, 090801 (2016).

[83] J. Kofler and Č. Brukner, Phys. Rev. Lett. **99**, 180403 (2007).

[84] F. Hansen and G. K. Pedersen, Bull. London Math. Soc. **35**, 553 (2003).

[85] T. J. Barnea, M.-O. Renou, F. Fröwis, and N. Gisin, arXiv:1605.05956 (2016).

[86] B. Yadin, J. Ma, D. Girolami, M. Gu, and V. Vedral, Phys. Rev. X **6**, 041028 (2016).

[87] D. Markham and V. Vedral, Phys. Rev. A **67** 042113 (2003).

[88] M. C. Tichy, C.-Y. Park, M. Kang, H. Jeong, and K. Mølmer, Phys. Rev. A **93**, 042314 (2016).

[89] L. Mandel, Phys. Scrip **T12**, 34 (1986).

[90] W. H. Zurek, S. Habib, and J. P. Paz, Phys. Rev. Lett. **70**, 1187 (1993).

[91] P. Sekatski, N. Gisin, and N. Sangouard Phys. Rev. Lett. **113**, 090403 (2014).

[92] A. Carlisle, H. Kwon, H. Jeong, A. Ferraro, and M. Paternostro, Phys. Rev. A **92**, 022123 (2015).

[93] M.A. Nielsen and I.L. Chuang, *Quantum Computation and Quantum Information*, (Cambridge University Press, Cambridge, England, 2010).

[94] C. H. Bennett and S. J. Wiesner, Phys. Rev. Lett. **69**, 2881 (1993).

[95] T. K. Chuan and T. Paterek, New J. Phys. **16**, 093063 (2013).

[96] S. Pironio, A. Acin, S. Massar, A. B. de La Giroday, D.N. Matsukevich, P. Maunz, S. Olmschenk, D. Hayes, L. Luo, T. A. Manning, C. Monroe, Nature **464**, 7291 (2010).

[97] R. Raussendorf and H.J. Briegel, Phys. Rev. Lett. **86**, 5188 (2001).

[98] L. Pezzé and A. Smerzi, Phys. Rev. Lett. **100**, 073601 (2008).

[99] P. M. Anisimov, G. M. Raterman, A. Chiruvelli, W. N. Plick, S. D. Huver, H. Lee, and J. P. Dowling, Phys. Rev. Lett. **104**, 103602 (2010).

[100] Y. R. Zhang, G. R. Jin, J. P. Cao, and W. M. Liu, J. Phys. A **46**, 035302 (2013).

[101] P. A. Knott, T. J. Proctor, A. J. Hayes, J. P. Cooling, and J. A. Dunningham, Phys. Rev. A **93**, 033859 (2016).

[102] S.-Y. Lee, C.-W. Lee, J. Lee, and H. Nha, Sci. Rep. **6**, 30306 (2016).

[103] J. Joo, W. J. Munro, and T. P. Spiller, Phys. Rev. Lett. **107**, 083601 (2011).

[104] J. Joo, K. Park, H. Jeong, W. J. Munro, K. Nemoto, and T. P. Spiller, Phys. Rev. A **86**, 043828 (2012).

[105] S.-Y. Lee, C.-W. Lee, H. Nha, and D. Kaszlikowski, J. Opt. Soc. Am. B **32**, 1186 (2015).

[106] C. Oh, S.-Y. Lee, H. Nha, and H. Jeong, Phys. Rev. A **96**, 062304 (2017).

[107] S. L. Braunstein and C. M. Caves, Phys. Rev. Lett. **72**, 3439 (1994).

[108] L. Pezzé, A. Smerzi, Phys. Rev. Lett. **102**, 100401 (2009).

[109] G. Tóth, Phys. Rev. A **85**, 022322 (2012).

[110] P. Hyllus, W. Laskowski, R. Krischek, C. Schwemmer, W. Wieczorek, H. Weinfurter, L. Pezze, and A. Smerzi, Phys. Rev. A **85**, 022321 (2012).

[111] U. M. Titulaer and R. J. Glauber, Phys. Rev. **140**, B676 (1965).

[112] M. Hillery, Phys. Lett. A **111**, 409 (1985).

[113] M. Hillery, Phys. Rev. A **725**, 2 (1987).

[114] P. Marian, T. A. Marian, H. Scutaru, Phys. Rev. Lett. **88**, 153601 (2002).

[115] C. T. Lee, Phys. Rev. A **44**, R2775(R) (1991).

[116] M. S. Kim, W. Son, V. Bužek, and P. L. Knight, Phys. Rev. A **65**, 032323 (2002).

[117] J. K. Asbóth, J. Calsamiglia, and H. Ritsch, Phys. Rev. Lett. **94**, 173602 (2005).

[118] W. Vogel and J. Sperling, Phys. Rev. A **89**, 052302 (2014).

[119] S. Ryl, J. Sperling, and W. Vogel Phys. Rev. A **95**, 053825 (2017).

[120] Á. Rivas and Alfredo Luis, Phys. Rev. Lett. **105**, 010403 (2010).

[121] C. Gehrke, J. Sperling, and W. Vogel, Phys. Rev. A **86**, 052118 (2012).

[122] K. C. Tan, T. Volkoff, H. Kwon, and H. Jeong, Phys. Rev. Lett. **119**, 190405 (2017).

[123] F. Fröwis, J. Phys. A: Math. Theor. **50**, 114003 (2017).

[124] E. Oudot, P. Sekatski, F. Fröwis, N. Gisin, and N. Sangouard, JOSA B **32**, 2190 (2015).

[125] C. K. Law, Phys. Rev. A **51**, 2537 (1995).

[126] M. Aspelmeyer, T. J. Kippenberg, and F. Marquardt, Rev. Mod. Phys. **86**, 1391 (2014).

[127] H. Kwon and H. Jeong, Phys. Rev. A **88**, 052127 (2013).

[128] H. Kwon and H. Jeong, Phys. Rev. A **91**, 012340 (2015).

[129] A. Einstein, B. Podolsky, and N. Rosen, Phys. Rev. **47**, 777 (1935).

[130] J. F. Clauser, M. A. Horne, A. Shimony, and R. A. Holt, Phys. Rev. Lett. **23**, 880 (1969).

[131] N. Gisin and A. Peres, Phys. Lett. A **162**, 15 (1992).

[132] D. Kaszlikowski, P. Gnaciński, M. Żukowski, W. Miklaszewski, and A. Zeilinger, Phys. Rev. Lett. **85**, 4418 (2000).

[133] T. Durt, D. Kaszlikowski, and M. Żukowski, Phys. Rev. A **64**, 024101 (2001).

[134] K. Banaszek and K. Wódkiewicz, Phys. Rev. Lett. **82**, 2009 (1999).

[135] H. Jeong, J. Lee, and M. S. Kim, Phys. Rev. A **61**, 052101 (2000).

[136] T. C. Ralph, W. J. Munro, and R. E. S. Polkinghorne, Phys. Rev. Lett. **85**, 2035 (2000).

[137] Z.-B. Chen, J.-W. Pan, G. Hou, and Y.-D. Zhang, Phys. Rev. Lett. **88**, 040406 (2002).

[138] K. Banaszek, A. Dragan, K. Wódkiewicz, and C. Radzewicz, Phys. Rev. A **66**, 043803 (2002).

[139] H. Jeong, W. Son, M. S. Kim, D. Ahn, and Č. Brukner, Phys. Rev. A **67**, 012106 (2003).

[140] M. A. Rowe, D. Kielpinski, V. Meyer, C. A. Sackett, W. M. Itano, C. Monroe, and D. J. Wineland, Nature (London) **409**, 791 (2001).

[141] M. Ansmann, H. Wang, R. C. Bialczak, M. Hofheinz, E. Lucero, M. Neeley, A. O'Connell, D. Sank, M. Weides, J. Wenner, A. N. Cleland, and J. M. Martinis, Nature (London) **461**, 504 (2009).

[142] J. S. Bell, J. Phys. C **2**, 41 (1981).

[143] E. Santos, Phys. Lett. A **200**, 1 (1995).

[144] S. J. Freedman and J. F. Clauser, Phys. Rev. Lett. **28**, 938 (1972).

[145] A. Aspect, P. Grangier, and G. Roger, Phys. Rev. Lett. **47**, 460 (1981).

[146] W. Tittel, J. Brendel, H. Zbinden, and N. Gisin, Phys. Rev. Lett. **81**, 3563 (1998).

[147] G. Weihs, T. Jennewein, C. Simon, H. Weinfurter, and A. Zeilinger, Phys. Rev. Lett. **81**, 5039 (1998).

[148] P. M. Pearle, Phys. Rev. D **2**, 1418 (1970).

[149] P. H. Eberhard, Phys. Rev. A **47**, R747 (1993).

[150] M. Giustina, A. Mech, S. Ramelow, B. Wittmann, J. Kofler, J. Beyer, A. Lita, B. Calkins, T. Gerrits, S. W. Nam, R. Ursin, and A. Zeilinger, Nature (London) **497**, 7448 (2013).

[151] S. Massar, S. Pironio, J. Roland, and B. Gisin, Phys. Rev. A **66**, 052112 (2002).

[152] M. Genovese, Phys. Rev. A **71**, 052314 (2005).

[153] D. Collins and N. Gisin, J. Phys. A **37**, 1775 (2004).

[154] N. Brunner, N. Gisin, V. Scarani, and C. Simon, Phys. Rev. Lett. **98**, 220403 (2007).

[155] T. Vértesi, S. Pironio, and N. Brunner, Phys. Rev. Lett. **104**, 060401 (2010).

[156] C. Vitelli, M. T. Cunha, N. Spagnolo, F. De Martini, and F. Sciarrino, Phys. Rev. A **85**, 012104 (2012).

[157] Y. Lim, M. Paternostro, M. Kang, J. Lee, and H. Jeong, Phys. Rev. A **85**, 062112 (2012).

[158] R. Chaves and J. B. Brask, Phys. Rev. A **84**, 062110 (2011).

[159] H. Nha and H. J. Carmichael, Phys. Rev. Lett. **93**, 020401 (2004).

[160] R. García-Patrón, J. Fiurášek, N. J. Cerf, J. Wenger, R. Tualle-Brouri, and P. Grangier, Phys. Rev. Lett. **93**, 130409 (2004).

[161] S.-W. Ji, J. Kim, H.-W. Lee, M. S. Zubairy, and H. Nha, Phys. Rev. Lett. **105** 170404 (2010).

[162] J. B. Brask, N. Brunner, D. Cavalcanti, and A. Leverrier, Phys. Rev. A **85**, 042116 (2012).

[163] N. Sangouard, J.-D. Bancal, N. Gisin, W. Rosenfeld, P. Sekatski, M. Weber, and H. Weinfurter, Phys. Rev. A **84**, 052122 (2011).

[164] N. Spagnolo, C. Vitelli, M. Paternostro, F. De Martini, and F. Sciarrino, Phys. Rev. A **84**, 032102 (2011).

[165] C. Simon and W. T. M. Irvine, Phys. Rev. Lett. **91**, 110405 (2003).

[166] J. Park, M. Saunders, Y.-i. Shin, K. An, and H. Jeong, Phys. Rev. A **85**, 022120 (2012).

[167] M. Araújo, M. T. Quintino, D. Cavalcanti, M. F. Santos, A. Cabello, and M. T. Cunha, Phys. Rev. A **86**, 030101(R) (2012).

[168] C. Teo, M. Araújo, M. T. Quintino, J. Minář, D. Cavalcanti, V. Scarani, M. T. Cunha, and M. F. Santos, Nat. Commun. **4**, 2104 (2013).

[169] D. L. Moehring, M. J. Madsen, B. B. Blinov, and C. Monroe, Phys. Rev. Lett. **93**, 090410 (2004).

[170] J. Volz, M. Weber, D. Schlenk, W. Rosenfeld, J. Vrana, K. Saucke, C. Kurtsiefer, and H. Weinfurter, Phys. Rev. Lett. **96**, 030404 (2006).

[171] D. N. Matsukevich, P. Maunz, D. L. Moehring, S. Olmschenk, and C. Monroe, Phys. Rev. Lett. **100**, 150404 (2008).

[172] S.-W. Lee and H. Jeong, Phys. Rev. A **87**, 022326 (2013).

[173] H. Jeong, Phys. Rev. A **72**, 034305 (2005).

[174] C. C. Gerry, Phys. Rev. A **59**, 4095 (1999).

[175] J. H. Shapiro, Phys. Rev. A **73**, 062305 (2006).

[176] J. H. Shapiro and M. Razavi, New J. Phys. **9**, 16 (2007).

[177] B. He, Q. Lin, and C. Simon, Phys. Rev. A **83**, 053826 (2011).

[178] S. R. Mahdi Hosseini, B. M. Sparkes, J. Twamley, B. C. Buchler, and P. K. Lam, Light: Sci. Appl. **1**, e40 (2012).

[179] C. Chudzicki, I. L. Chuang, and J. H. Shapiro, Phys. Rev. A **87**, 042325 (2013).

[180] J. Gea-Banacloche, Phys. Rev. A **81**, 043823 (2010).

[181] B. He and A. Scherer, Phys. Rev. A **85** 033814 (2012).

[182] P. Kok and B. W. Lovett, *Introduction to Optical Quantum Information Processing* (Cambridge University Press, Cambridge, 2010).

[183] W. H. Press, B. P. Flannery, S.A. Teukolsky, and W. T. Vetterling, *Numerical Recipes* (Cambridge University Press, Cambridge, 1988).

[184] F. De Martini, Phys. Rev. Lett. **81**, 2842 (1998).

[185] F. De Martini, F. Sciarrino, C. Vitelli, Phys. Rev. Lett. **100**, 253601 (2008).

[186] P. Sekatski, B. Sanguinetti, E. Pomarico, N. Gisin, C. Simon, Phys. Rev. A **82**, 053814 (2010).

[187] P. Sekatski, N. Sangouard, M. Stobińska, F. Bussieres, M. Afzelius, N. Gisin, Phys. Rev. A **86**, 060301(R) (2012).

[188] U. L. Andersen and J. S. Neergaard-Nielsen, Phys. Rev. A **88**, 022337 (2013).

[189] M. Stobińska, F. Töppel, P. Sekatski, A. Buraczewski, Phys. Rev. A **89**, 022119 (2014).

[190] Y.-B. Sheng, L. Zhou, and G.-L. Long, Phys. Rev. A **88**, 022302 (2013).

[191] A. Ourjoumtsev, R. Tualle-Brouri, J. Laurat, and P. Grangier, Science **312**, 83 (2006).

[192] J.S. Neergaard-Nielsen, B.M. Nielsen, C. Hettich, K. Mølmer, and E.S. Polzik, Phys.Rev. Lett. **97** 083604 (2006).

[193] H. Takahashi, K. Wakui, S. Suzuki, M. Takeoka, K. Hayasaka, A. Furusawa, and M. Sasaki, Phys. Rev. Lett. **101**, 233605 (2008).

[194] T. Gerrits, S. Glancy, T. S. Clement, B. Calkins, A. E. Lita, A. J. Miller, A. L. Migdall, S. W. Nam, R. P. Mirin, and E. Knill, Phys. Rev. A **82**, 031802(R) (2010).

[195] A. P. Lund, H. Jeong, T. C. Ralph, and M. S. Kim, Phys. Rev. A **70**, 020101(R) (2004).

[196] K. Kreis and P. van Loock, Phys. Rev. A **85**, 032307 (2012).

[197] S. Wallentowitz, R. L. de Matos Filho, and W. Vogel, Phys. Rev. A **56**, 1205 (1997).

[198] A photon-subtracted squeezed state and a squeezed single photon are equivalent up to a normalization factor as $\hat{a}\hat{S}(s)\left|0\right\rangle = -\sinh(s)\hat{S}(s)\left|1\right\rangle$ [195, 199].

[199] H. Jeong, A. P. Lund, and T. C. Ralph, Phys. Rev. A **72**, 013801 (2005).

[200] A. Peres, Phys. Rev. Lett. **77**, 1413 (1996).

[201] M. Horodecki, P. Horodecki, and R. Horodecki, Phys. Lett. A **223**, 1 (1996).

[202] J. Lee, M. S. Kim, Y. J. Park, and S. Lee, J. Mod. Opt. **47**, 2151 (2000).

[203] M. Akiba, K. Tsujino, K. Sato, and M. Sasaki, Opt. Express **17**, 16885 (2009).

[204] L. Zhang, L. Kang, J. Chen, Y. Zhong, Q. Zhao, T. Jia, C. Cao, B. Jin, W. Xu, G. Sun, and P. Wu, Appl. Phys. B **102**, 867 (2011).

[205] C. Schuck, W. Pernice, and H. Tang, Sci. Rep. **3**, 1893 (2013).

[206] H. Shibata, K. Shimizu, H. Takesue, and Y. Tokura, Applied Physics Express **6**, 072801 (2013).

[207] C. M. Natarajan, M. G. Tanner, and R. H. Hadfield, Supercond. Sci. Technol. **25**, 063001 (2012).

[208] A. E. Lita, A. J. Miller, and S. W. Nam, Opt. Express **16**, 3032 (2008).

[209] R. H. Hadfield, Nat. Photonics **3**, 696 (2009).

[210] F. Marsili, V. Verma, J. Stern, S. Harrington, A. Lita, T. Gerrits, I. Vayshenker, B. Baek, M. Shaw, R. Mirin, and S. W. Nam, Nat. Photonics **7**, 210 (2013).

[211] J. Fiurášek, S. Massar, and N. J. Cerf, Phys. Rev. A **68**, 042325 (2003).

[212] A. Zavatta, S. Viciani, and M. Bellini, Science **306**, 660 (2004).

[213] J. Wenger, R. Tualle-Brouri, and P. Grangier, Phys. Rev. Lett. **92**, 153601 (2004).

[214] V. Parigi, A. Zavatta, M. S. Kim, and M. Bellini, Science **317**, 1890 (2007); R. W. Boyd, K. W. Chan, and M. N. O'sullivan, ibid. **317**, 1874 (2007).

[215] M. S. Kim, H. Jeong, A. Zavatta, V. Parigi, and M. Bellini, Phys. Rev. Lett. **101**, 260401 (2008).

[216] P. Marek, H. Jeong, and M. S. Kim, Phys. Rev. A **78**, 063811 (2008).

[217] C.-W. Lee, J. Lee, H. Nha, and H. Jeong, Phys. Rev. A **85**, 063815 (2012).

[218]] S.-Y. Lee, J. Park, H.-W. Lee, and H. Nha, Opt. Express **20**, 14221 (2012).

[219] H. Jeong, M. Paternostro, and T. C. Ralph, Phys. Rev. Lett. **102**, 060403 (2009).

[220] P. Sekatski, N. Brunner, C. Branciard, N. Gisin, and C. Simon, Phys. Rev. Lett. **103**, 113601 (2009).

[221] H. Kwon, H. Jeong, D. Jennings, B. Yadin, and M. S. Kim, arXiv: 1711.03395 (2017).

[222] J. Åberg, Phys. Rev. Lett. **113**, 150402 (2014).

[223] P. Skrzypczyk, A. J. Short, and S. Popescu, arXiv:1302.2811.

[224] P. Skrzypczyk, A. J. Short, and S. Popescu, Nat. Commun. **5**, 4185 (2014).

[225] R. Uzdin, A. Levy, and R. Kosloff, Phys. Rev. X **5**, 031044 (2015).

[226] K. Korzekwa, M. Lostaglio, J. Oppenheim, and D. Jennings, New J. Phys. **18**, 023045 (2016).

[227] B. Groisman, S. Popescu, and A. Winter, Phys. Rev. A **72**, 032317 (2005).

[228] D. Jennings and T. Rudolph, Phys. Rev. E **81**, 061130 (2010).

[229] J. J. Park, K.-H. Kim, T. Sagawa, and S. W. Kim, Phys. Rev. Lett. **111**, 230402 (2013).

[230] D. Reeb and M. M. Wolf, New J. Phys. **16**, 103011 (2014).

[231] D. E. Bruschi, M. Perarnau-Llobet, N Friis, K V. Hovhannisyan, and M Huber, Phys. Rev. E **91**, 032118 (2015).

[232] M Huber, M. Perarnau-Llobet, K. V. Hovhannisyan, P. Skrzypczyk, Claude Klöckl, N. Brunner, and A. Acín, New J. Phys. **17** 065008 (2015).

[233] M. Perarnau-Llobet, K. V. Hovhannisyan, M. Huber, P. Skrzypczyk, N. Brunner, and A. Acín, Phys. Rev. X **5**, 041011 (2015).

[234] P. Ćwikliński, M. Studziński, M. Horodecki, and J. Oppenheim, Phys. Rev. Lett. **115**, 210403 (2015).

[235] M. Lostaglio. D. Jennings, and T. Rudolph, Nat. Commun. **6**, 6383 (2015).

[236] M. Lostaglio, K. Korzekwa, D. Jennings, and T. Rudolph, Phys. Rev. X **5**, 021001 (2015).

[237] F. Brandão, M. Horodecki, J. Oppenheim, J. M. Renses, and R. W. Spekkens, Phys. Rev. Lett. **111**, 250404 (2013).

[238] F. G. S. L. Brandão, M. Horodecki, N. H. Y. Ng, J. Oppenheim, and S. Wehner, Proc. Natl. Acad. Sci. U.S.A. **112**, 3275 (2015).

[239] D. Janzing, P. Wocjan, R. Zeier, R. Geiss, and T. Beth, Int. J. Theor. Phys. **39**, 2717 (2000).

[240] G. Gour, D. Jennings, F. Buscemi, R. Duan, and I. Marvian, arXiv:1708.04302.

[241] M. Horodecki and J. Oppenheim, Nat. Commun. **4**, 2059 (2013).

[242] M Lostaglio, M. P. Müller, and M. Pastena, Phys. Rev. Lett. **115**, 150402 (2015).

[243] J. Goold, M. Huber, A. Riera, L. del Rio, and P. Skrzypczyk, J. Phys. A **49**, 143001 (2016).

[244] M. N. Bera, A. Riera, M. Lewenstein, A. Winter, arXiv:1612.04779.

[245] H. Wilming, R. Gallego, and J. Eisert, Phys. Rev. E **93**, 042126 (2016).

[246] M. P. Müller, arXiv:1707.03451.

[247] S. D. Bartlett, T. Rudolph, and R. W. Spekkens, Rev. Mod. Phys. **79**, 555 (2007).

[248] S. Lloyd, Phys. Rev. A **56**, 3374 (1997).

[249] W. H. Zurek, Phys. Rev. A **67**, 012320 (2003).

[250] P. Chen and S. Luo, Theor. Math. Phys. **165**, 1552 (2010).

[251] P. Kómár, E. M. Kessler, M. Bishof, L. Jiang, A. S. Sørensen, J. Ye, and M. D. Lukin, Nat. Phys. **10**, 582 (2014).

[252] D. Petz and C. Ghinea, *Introduction to Quantum Fisher Information*, QP-PQ: Quantum Probability and White Noise Analysis. Vol. 27, edited by R. Rebolledo and M. Orszag (World Scientific, Singapore, 2011), pp. 261–281.

[253] F. Hansen, Proc. Natl. Acad. Sci. U.S.A. **105**, 9909 (2008).

[254] W. Hoeffding, J. Am. Stat. Assoc. **58**, 13 (1963).

국문초록

양자역학이 정립된 이래로, 거시적인 계에서도 양자 중첩이 존재할 수 있는지에 대한 의문은 계속되어 왔다. 고전적인 상태들의 양자 중첩은 슈뢰딩거 고양이 역설에서 잘 나타나듯이 일상적으로 이해하긴 힘든 현상을 유발하며, 이는 이론적 실험적인 관점 모두에서 큰 주목을 이끌어 왔다. 최근 양자 정보 분야의 발전으로 양자 중첩 혹은 결맞음을 비고전적인 작업을 수행하는데 필수적인 자원으로 이해할 수 있게 되었지만, 거시적 양자 결맞음을 비롯한 다른 양자 자원들 간의 정확한 연관 관계들은 아직 밝혀지지 않았다. 본 논문에서는 다양한 물리계에서의 거시적 양자 중첩을 정량화하는 방법을 소개하고 이를 자연법칙의 기본을 탐구하는 기초 학문적인 측면과 훗날 양자 기술에 활용될 수 있는 기술적인 측면에서 어떻게 적용될 수 있는지 살펴본다.

거시적 양자 중첩을 정량화하기 위해서는 물리계의 크기와 결맞음의 정도 두 가지가 한꺼번에 고려되어야 한다. 이를 위해 우리는 양자 상태들 사이의 물리적 거리에 기초하여 결맞음의 정도에 가중치를 둔 척도를 제시하는 한편, 미시적인 양자 중첩에 의한 효과를 배제하기 위한 차단 함수를 도입하여 거시적인 양자 중첩만을 측정하는 방법을 제시한다. 더 나아가, 부정확한 측정에 의한 양자 상태의 변동이 거시적 양자 결맞음을 측정하는 다른 척도가 되며, 이를 통해 왜 우리가 일상생활에서 거시적인 물체의 양자 중첩을 보기 힘든지를 설명하고자 한다. 두 가지의 접근 방법은 모두 비대칭성의 자원이론을 통하여 설명할 수 있으며, 대칭성을 보존하는 작용으로는 거시적인 양자 중첩을 증가시킬 수 없다는 사실을 보이고, 이 두 접근 방법 사이의 근본적인 공통점이 있음을 증명한다. 이

러한 이론적 토대를 바탕으로, 거시적 양자 결맞음의 정도를 임의의 계에 대해서 측정할 수 있으며, 언제 양자 상태가 비고전적인 성질을 잃고 양자-고전 전이를 일으키는지에 대한 지식을 얻을 수 있음을 본 논문을 통하여 논의한다.

거시적 양자 결맞음의 기술적 응용 중 하나로, 양자 정밀측정이라고 알려진 정밀한 변수 추정 작업을 들 수 있다. 본 논문에서는 다중 모드의 광학적 계에서 거시적인 양자 중첩이 광학적 결맞음 상태들 사이의 결맞음의 정도로 볼 수 있으며, 이를 다중 모드 변이 변수를 정밀 추정하는 데에 필요한 자원이 됨을 밝혀낸다. 이러한 발견을 토대로, 글라우버-수다르샨 함수의 음의 값으로 표현되는 빛의 비고전적인 상태를 양자 정밀측정을 위한 자원의 측면에서 이해할 수 있으며, 빔스플리터, 위상변화계, 변이 작용으로 대표될 수 있는 선형 광학적 작용을 통해서는 증가할 수 없는 자원임을 알아본다. 한편, 기초 학문적인 관점에서는 빛의 (양자역학적) 입자성을 띠는 상태와 (고전역학적) 파동성을 가지는 상태 사이의 양자 얽힘은 양자이론의 비국소성을 보이는데 응용될 수 있다는 사실을 탐구한다. 우리는 빛의 편광상태와 연속적인 결맞음 상태의 이종 얽힘 상태를 사용한다면 부정확한 광자측정만 가능한 상황에서도 허점 없는 벨 부등식 위배 될 수 있음을 살펴본다. 또한, 이러한 이종 얽힘 상태를 실제로 구현하는 방법을 구체적인 실험적 수치와 함께 제시한다.

마지막으로, 거시적 양자 결맞음의 또 다른 측면으로 많은 입자 계에서의 결맞음이 양자 열역학에서 어떠한 역할을 하는지 알아본다. 많은 입자 계의 결맞음은 일을 할 수 있는 자원과 시간을 측정하는데 쓸 수 있는 시계 자원 두 가지 종류로 분류될 수 있다. 흥미롭게도 본 논문에서는 이 두 일/시계 자원에 대한 교환관계를 밝혀내었으며, 이는 양자 열역학의

근본적인 에너지-시간의 불확정성을 제시한다고 볼 수 있다.

주요어 : 거시 양자성, 양자 결맞음, 양자 정밀측정, 비국소성, 비고전성, 양자 열역학

학번 : 2012-20355